1-1-2005

Pressure effects on entropically driven phase transitions in block copolymers.

Kristopher A. Lavery
University of Massachusetts Amherst

PRESSURE EFFECTS ON ENTROPICALLY DRIVEN PHASE TRANSITIONS IN BLOCK COPOLYMERS

A Dissertation Presented

by

KRISTOPHER A. LAVERY

Submitted to the Graduate School of the
University of Massachusetts Amherst in partial fulfillment
of the requirements for the degree of

DOCTOR OF PHILOSOPHY

September 2005

Polymer Science and Engineering

PRESSURE EFFECTS ON ENTROPICALLY DRIVEN PHASE TRANSITIONS IN BLOCK COPOLYMERS

A Dissertation Presented

by

KRISTOPHER A. LAVERY

Approved as to style and content by:

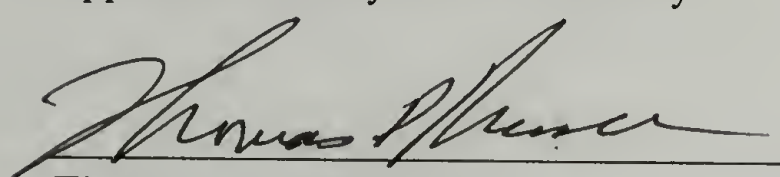

Thomas P. Russell, Chair

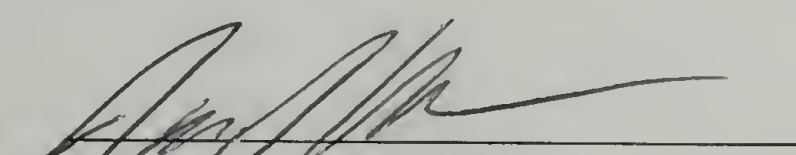

James J. Watkins, Member

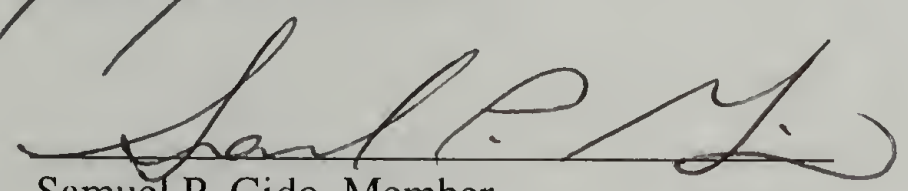

Samuel P. Gido, Member

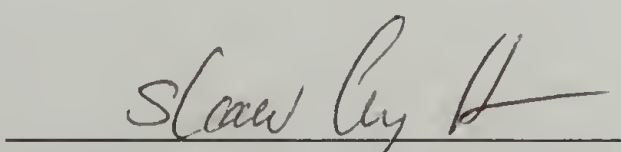

Shaw Ling Hsu, Department Head
Polymer Science and Engineering

DEDICATION

To my parents, who always told me to work hard, and my grandfather, who always told me to just have fun.

ACKNOWLEDGMENTS

First and foremost I must thank my thesis advisor, Professor Tom Russell, for his patience and guidance over the past five years. His dedication to his students is unmatched and he has provided a rich scientific environment that truly allows a graduate student to thrive. I would also like to thank Professor Jim Watkins, who not only served as a member of my committee but also as a mentor in my early experiments. He was gracious enough to allow a relatively inexperienced graduate student work with compressed carbon dioxide in his laboratories, and I have greatly benefited from my exchanges with him over the years. I also thank Professor Sam Gido for serving on my committee and providing valuable insight on my work throughout its evolution.

Addtionally, the friends and collaborators I have met over my graduate career are some of the best I could have imagined. Matt Misner and I have been working together, both in the PSE and in the bars of Amherst, for my entire graduate career. Our discussions have been invaluable and he remains good friend. Amanda Leach has been wonderful, both as a stabilizing force in the Russell Group and in helping maintain perspective outside of the lab. Duyeol Ryu has been one of my closest collaborators, and has imparted a great deal of practical polymer knowledge to me over the years. My other coworkers, both on the beam line and in our home laboratories include James Sievert, Brian Vogt, Jim Goldbach, Ravi Gupta, and Tim Francis. All have been invaluable in shaping the work presented in this thesis. I also wish to thank my good friends Bill Peters, Brad Lewis, and Donna Wrublewski for keeping me in line.

Certainly, none of this would have doable without the love and support of my family. My mom and dad have always stressed the importance of education, and the values they imparted to me underlie any success I've had as a graduate student. I've been lucky to have my sister, Kathy, and my brother-in-law Phil so close during my time in Amherst. I'll miss having the chance to hop in the car grab some Blue Ribbon with my sis on the weekends! Finally, I would like to thank Theodora, whose love has made everything worthwhile.

ABSTRACT

PRESSURE EFFECTS ON ENTROPICALLY DRIVEN PHASE TRANSITIONS IN BLOCK COPOLYMERS

SEPTEMBER 2005

KRISTOPHER A. LAVERY, B.S., CARNEGIE MELLON UNIVERSITY

M.S., UNIVERSITY OF MASSACHUSETTS AMHERST

Ph.D., UNIVERSITY OF MASSACHUSETTS AMHERST

Directed by: Professor Thomas P. Russell

The binary polymer system of polystyrene and poly(n-pentyl methacrylate) was recently found to exhibit closed-loop type phase behavior. This is the first known example of a weakly interacting system exhibiting such a phase diagram. At atmospheric pressure the block copolymer displays both a lower disorder-to-order and upper order-to-disorder transition, representing the lower and upper bounds of the closed-loop phase diagram. The application of hydrostatic pressure served to shrink the closed-loop, yielding pressure coefficients of the lower disorder-to-order and upper order-to-disorder transitions of 725°C/kbar and –725°C/kbar respectively. These pressure coefficients were consistent with those calculated from the Clausius-Clapeyron equation, using the experimentally determined $\Delta H_{disorder}$ and $\Delta V_{disorder}$ for each transition. The χ_{eff} determined from small angle neutron scattering (SANS) was found to decrease, pass through a minimum, increase to a maximum, and then decrease with increasing temperature. Swelling the system with carbon dioxide served to promote an expansion of the closed-loop. This was due to the entropic nature of both transitions, with differential dilation of

the copolymer domains resulting in dissimilar compressibilities of the blocks. In addition to influencing block copolymer phase behavior, carbon dioxide can have a profound impact on resulting morphological structure. A 42/58 PS-*b*-PnPMA diblock copolymer was found to exhibit lamellar morphology at ambient pressures. With the application of 2500 psi carbon dioxide the morphology shifted to hexagonally-packed cylinders due to preferential absorption into the PnPMA block. Furthermore, the influence of carbon dioxide sorption on the morphology of the PS/poly(n-alkyl methacrylate) block copolymer series was studied both in thin films and in the bulk.

TABLE OF CONTENTS

LIST OF TABLES

LIST OF FIGURES

CHAPTER 1

INTRODUCTION AND MOTIVATION

1.1 Thesis Overview

This dissertation focuses on the influence of compressed media on the phase behavior and morphology of block copolymers. The study of compressibility in these systems is essential for the understanding of the thermodynamic driving forces governing phase behavior and morphology[1, 2]. A full understanding of the factors dictating polymer miscibility are of great import in nearly all polymer applications, from mixtures[3] to composites[4, 5] and thin film structures[6]. In this introductory chapter I outline the basics of block copolymer thermodynamics, imparting an understanding of the enthalpic and entropic factors that govern microphase separation. I will also introduce the closed-loop phase diagram, the discovery of which provided the catalyst for much of the work described herein.

In the second chapter I will describe the experimental methods used to investigate block copolymer phase behavior under pressure. This includes the anionic synthesis of model compounds having well-controlled molecular weight and low polydispersity. The quantification of order or disorder was accomplished largely by use of scattering techniques. The theory of small-angle scattering of block copolymers will be described in detail. Additionally, diffraction at large angles will be used to yield information on inter- or intra-chain length scales. The precise determination of the phase boundary in bulk samples was elucidated by use of the depolarization of light by microphase-separated block copolymer grains, the theory of which will be explained. Reflectivity of x-rays or

neutrons was used to non-destructively establish the density profiles of thin films as a function of depth. Spectroscopic methods, including infrared spectroscopy and Raman scattering, were used to probe chain conformation and interactions as a function of temperature. Finally, scanning force microscopy was used to observe the surface structure of block copolymer thin films.

The third chapter will explain experiments utilizing hydrostatic pressure as a means of probing block copolymer phase behavior. This includes the use of the incompressible random phase approximation[7] as a means of extracting the Flory-Huggins pair interaction parameter from scattering data in the disordered state.

The fourth chapter will introduce compressible fluids as a means to differentially dilate components of block copolymers. The consequences of this, both thermodynamically and morphologically, were explored.

The fifth chapter focuses on thin films of block copolymers, and the use of pressure to control morphology and alignment. The use of supercritical carbon dioxide as a means of imparting mobility to high molecular weight copolymers will also be treated.

The final chapter will draw together conclusions from this work, as well as include suggestions for future inquiry.

1.2 Introduction to Block Copolymers

Block copolymers are two chemically distinct polymers covalently joined at one end. These polymers maintain the ability to mix or phase separate as homopolymer mixtures do, however the length scale over which this phase separation occurs is limited by the connectivity of the blocks. Consequently, microphase separation occurs on length

scales comparable to the radius of gyration of the chain[8-11], typically between 10 and 100 nm. Figure 1.1a shows an example of a symmetric AB diblock copolymer.

a.

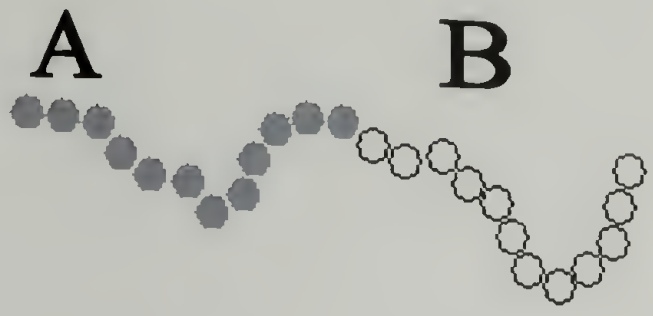

b.

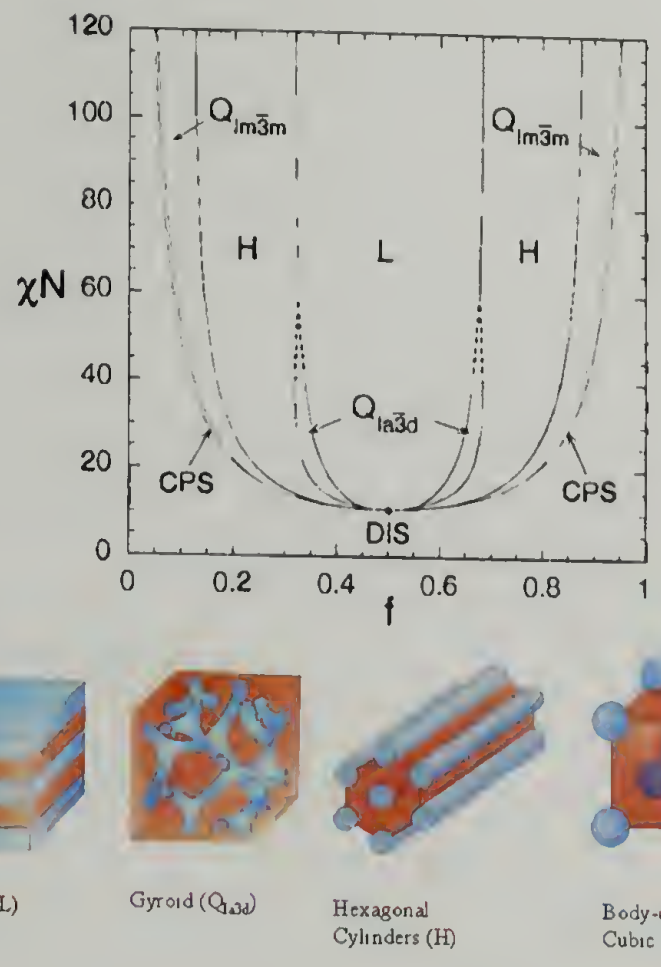

Figure 1.1: a. A symmetric diblock copolymer chain and b. morphologies resulting from the microphase separation of an AB diblock copolymer[12]

Microphase separation in diblock copolymers is dictated by the strength of interactions between the components, the copolymer molecular weight, and the relative volume fractions of the blocks. The microphase-separated copolymer can self-assemble

into a range of morphologies, dictated by the volume fractions of A and B. Microphase-separation is dominated by the desire to diminish the occurrence of unfavorable contacts. However, this enthalpic contribution is counterbalanced by entropic frustration caused by the covalent junction of the components, and manifests in a stretching of the polymer chain from its ideal Gaussian coil conformation. The equilibrium morphologies, then, are a consequence of chain stretching and the desire to keep the junction point near the interface, as well as the energy penalty for creating a curved surface. Examples of the resulting morphologies are shown in Figure 1.1b[12], where the morphology as a function of the volume fraction of block A is illustrated.

The morphologies resulting from microphase separation are used to fabricate materials that combine the properties of the otherwise incompatible component polymers. This is seen in reinforced composite elastomers[13], structured fluids[14], thin film structures[15, 16], and nano-scale templates[17, 18]. In all of these the ability to understand and control the phase diagram plays a key roll in the successful use of block copolymers. In the following sections I will outline the types of phase transitions present in block copolymer systems and address the theoretical treatments developed for use in predicting the types of behavior found in different block copolymer pairs. In so doing I will introduce the closed-loop phase diagram, on which much of the work in this thesis is based.

1.3 The Order-to-Disorder Transition (ODT)

1.3.1 ODT-type Phase Behavior

Polymer systems are for the most part immiscible. Due to the connectivity of the monomer subunits the entropic gain upon mixing is small. Typically, high temperatures, or low polymer molecular weights, are required for mixing to occur. In these cases the entropy of mixing carries a strong enough contribution to the system free energy that it overcomes the unfavorable interactions between dissimilar components. The temperature at which this occurs is termed the upper critical solution temperature (UCST)[19]. The classic picture of block copolymer phase behavior is analogous to the UCST in that, upon heating, the copolymer passes from the ordered state into the disordered state. Many common block copolymer pairs exhibit this sort of behavior, including polystyrene-*block*-poly(methyl methacrylate)[20, 21], polystyrene-*block*-polyisoprene[22], and poly(ethylene propylene)-*block*-poly(dimethyl siloxane).

1.3.2 Thermodynamic Calculation of the ODT

The ODT in block copolymers has been treated in much the same manner as the UCST in polymer blend systems. An incompressible lattice free-energy model was described using the same principles as Flory-Huggins theory[23-25], which is described by equation 1.1.

$$\frac{\Delta G}{RT} = \frac{\phi_A}{N_A} \ln \phi_A + \frac{\phi_B}{N_B} \ln \phi_B + \phi_A \phi_B \chi^{FH} \qquad (1.1)$$

This mean field framework makes use of a rigid lattice of components A and B, where ϕ_i is the volume fraction of component i, N_i is the number of lattice sites occupied by a molecule of component i, and χ^{FH} is the Flory-Huggins interaction parameter. The first two terms on the right of equation 1.1 describe the entropy of mixing A and B, while the third term represents the system enthalpy resulting from contacts between A and B components on the lattice. χ^{FH} is determined from the interaction energy of the different contacts, as per equation 1.2.

$$\chi^{FH} = z\left[\varepsilon_{AB} - \frac{\varepsilon_{AA} + \varepsilon_{BB}}{2}\right] / RT \qquad (1.2)$$

ε_{ij} is the van der Waals attractive energy between segments i and j, while z is the lattice coordination number. This theory, while quite successful in predicting ODT-type phase behavior, suffers from the assumption of incompressibility and, therefore, fails to take into account effects stemming from changes in volume upon mixing.

Despite the shortcomings of an assumed incompressibility, many investigators have used this theory successfully. A number of important relations can be derived from this model. For instance, Flory-Huggins theory predicts that for a symmetric polymer blend spinodal phase separation will occur at a critical product of the degree of polymerization, N, and χ, which for a symmetric blend is when $\chi N = 2$. Leibler extended this to block copolymers[7] and determined that for a symmetric block copolymer the transition occurs when $\chi N = 10.495$, where N is the degree of polymerization of the entire diblock

copolymer. A more detailed discussion of the temperature and pressure dependency of χ, within an incompressible framework, will be discussed in later chapters.

1.4 The Lower Disorder-to-Order Transition

1.4.1 LDOT-type phase behavior

For many diblock copolymers, the ODT description is sufficient to explain the phase behavior observed. For certain block copolymer systems, however, increasing temperature from the disordered state can lead to phase separation. This behavior was first observed by Russell, *et al.* [26 27], in the polystyrene-*block*-poly(n-butyl methacrylate) system, and has since been observed in polystyrene-*block*-poly(vinyl methyl ether) and polystyrene-*block*-poly(ethyl methacrylate), among others. Akin to the lower critical solution behavior of polymer blends, this block copolymer transition was termed the lower disorder-to-order transition (LDOT). In nature this sort of behavior, i.e. phase separation upon heating, can have one of two driving forces. For one, the two components can create a homogeneous phase at low temperatures if A-B contacts are favorable, as in hydrogen bonding or strong dipole interactions. With increasing temperature this interaction weakens until the attractive force is no longer sufficient to overcome repulsive interactions, resulting in phase separation. However, phase separation on heating can occur in weakly interacting systems as well, as in the case of the PS-*b*-PnBMA system, by volume differences upon demixing which can result from a disparity in thermal expansion coefficients. I will describe the thermodynamic arguments used to universally describe this type of phase behavior in such weakly interacting block copolymer systems.

1.4.2 Thermodynamic Calculation of the LDOT

There have been a number of theoretical treatments in recent years to describe the existence of phase separation upon heating a weakly interacting diblock copolymer material. The lattice cluster theory of Dudowicz and Freed[2, 28] uses monomer structure as a way of predicting the importance of chain packing frustration on the system thermodynamics. Ruzzette *et al.*[1, 29] developed regular solution arguments leading to a practical and powerful theory to predict the LDOT simply by knowing a few fundamental properties of the component polymers, such as monomer volume, or density, the solubility parameter, and the thermal expansion coefficient. These volumetric, equation-of-state, considerations were incorporated into a lattice framework.

$$\Delta g_{mix} = kT\left[\frac{\varphi_A\tilde{\rho}_A}{N_A v_A}\ln\phi_A + \frac{\phi_A\tilde{\rho}_B}{N_B v_B}\ln\phi_B\right] + \phi_A\phi_B\tilde{\rho}_A\tilde{\rho}_B\left(\delta_{A,0}-\delta_{B,0}\right)^2 \qquad (1.3)$$
$$+\phi_A\phi_B\left(\tilde{\rho}_A-\tilde{\rho}_B\right)\left(\delta_A^2-\delta_B^2\right)$$

φ_i is the volume fraction of component i, ρ_i is the reduced density, N_i is the degree of polymerization, v_i is the monomer volume, δ_i is the solubility parameter, k is the Boltzmann constant, and T is the absolute temperature. The 0 subscript indicates standard state. As an extension of the Flory-Huggins rigid lattice model this takes the standard expressions for the component interchange energies, and the contribution from combinatorial entropy, and incorporates a dilution factor that comes about due to the thermal expansion of the components. The third term on the right of Equation 1.3 holds the key, as this is the only term that changes sign. As it does so with sufficient magnitude

to overcome the sum of the first two terms, the system undergoes a phase transition. As a result, disparity in thermal expansion can lead to destabilization of the system.

1.5 Closed-Loop Phase Behavior

Recently, this picture of block copolymer phase behavior was expanded to include the existence of a closed-loop type phase diagram. Closed-loop phase behavior has long been observed in small molecule systems, such as in nicotine and water, or more recently in polymer-solvent systems such as poly(ethylene oxide) and water [30]. These systems, however, possess specific interactions, like hydrogen bonding, which weaken upon heating. This leads to phase separation with increased temperature, and further heating leads to phase mixing as combinatorial entropy dominates the free energy. The experimental observations of Ryu *et al.*[31], however, revealed a closed-loop phase diagram in the polystyrene-*block*-poly(n-pentyl methacrylate) system, which possesses no such specific interactions. A schematic of the phase diagram in this system in shown in Figure 1.3a below. The location of the ODT is inaccessible due to its proximity below the glass transition temperature of the block copolymer.

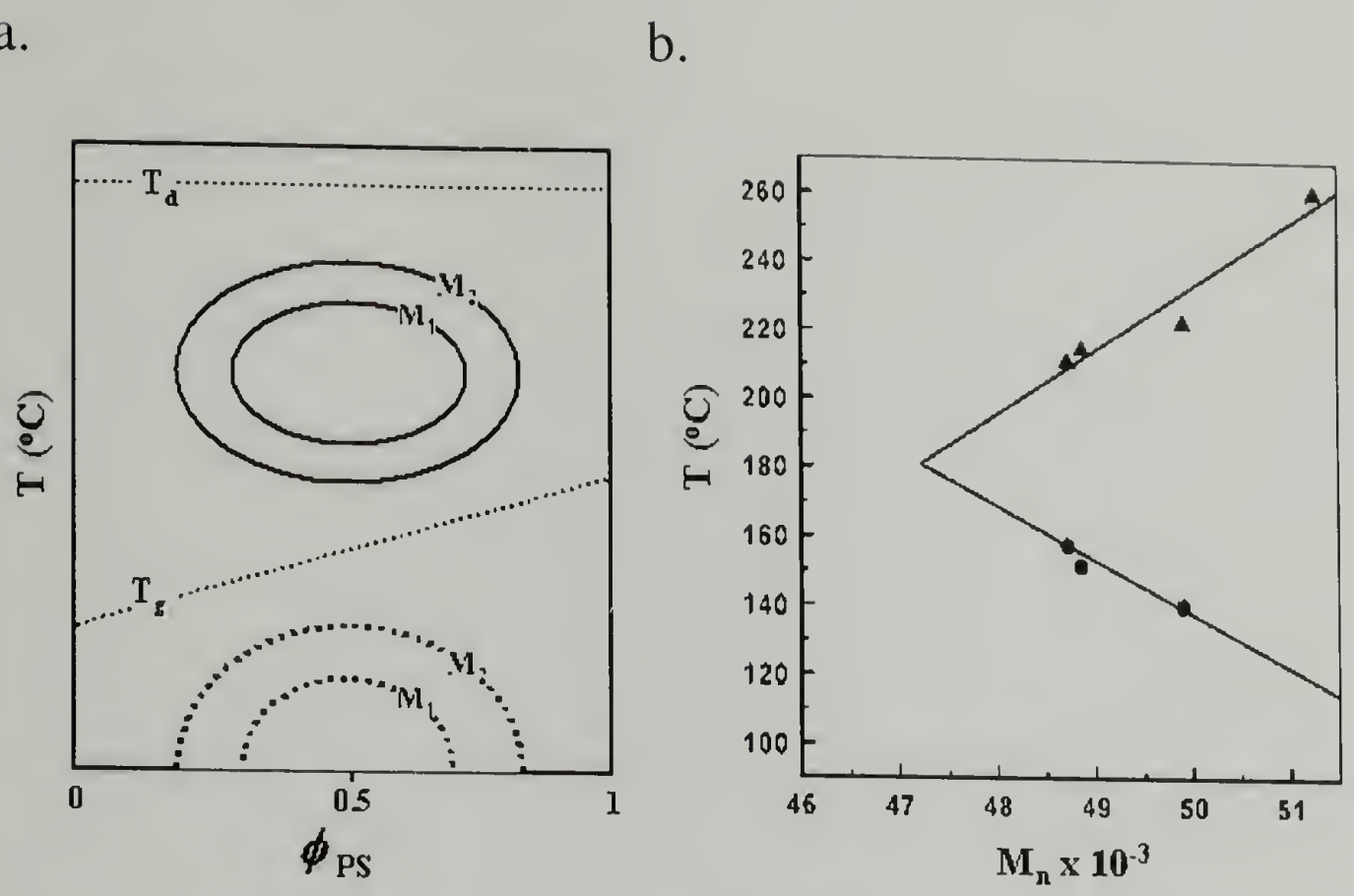

Figure 1.2: a. Schematic of the closed-loop phase diagram in PS-*b*-PnPMA and b. the LDOT and UODT temperatures as a function block copolymer molecular weight for a 50/50 weight fraction block composition[31]

The lower bound of the closed-loop is made up of the LDOT, while the upper bound is termed the upper order-to-disorder transition, or UODT. It is of note that the size of the closed-loop is sensitive to the copolymer molecular weight, as shown in Figure 1.3b. For the symmetric composition the copolymer is fully disordered over the complete temperature range at molecular weights below 47,000 g/mol. Between 47 K and 51 K the closed loop expands as a function of molecular weight, and above 51 K the copolymer is fully ordered over the complete temperature range bounded by the glass transition temperature, T_g, and the polymer degradation temperature, T_d.

Polymers that phase-separate should, also, possess a temperature at which combinatorial entropy drives the system back into the phase-mixed state. Unfortunately, this temperature is usually inaccessible due to T_d. Dudowiscz and Freed predicted the closed-loop in the PS-*b*-PVME[32] system using lattice cluster theory, however experimental evidence showed only the existence of an LCST in the homopolymer blend. PS-*b*-PnPMA, then, is the first known example of a weakly interacting system exhibiting closed-loop phase behavior. In order to study the thermodynamic nature of the closed-loop, experiments using hydrostatic pressure and compressible fluid swelling were undertaken, and will be described in the following chapters. First, however, the experimental techniques used in this study will be explained.

References

1. Ruzette, A.V., et al., A Simple Model for Baroplastic Behavior in Block Copolymer Melts. J. Chem. Phys., 2001. **114**: p. 8205.

2. Dudowicz, J. and K.F. Freed, Explanation for the Unusual Phase Behavior of Polystyrene-b-poly(n-alkyl methacrylate) Diblock Copolymers: Specific Interactions. Macromolecules, 2000. **33**: p. 5292.

3. Hammouda, B. and B.J. Bauer, Compressibility of Two Polymer Blend Mixtures. Macromolecules, 1995. **28**: p. 4505-4508.

4. Beecroft, L.L. and C.K. Ober, Nanocomposite Materials for Optical Applications. Chemistry of Materials, 1997. **9**: p. 1302.

5. Watkins, J.J. and T.J. McCarthy, Polymer/metal nanocomposite synthesis in supercritical CO_2. Chemistry of Materials, 1991. **7**(11).

6. Rockford, L., et al., Polymers on Nanoperiodic, Heterogeneous Surfaces. Physical Review Letters, 1999. **82**(12): p. 2602.

7. Leibler, L., Theory of Microphase Separation in Block Copolymers. Macromolecules, 1980. **13**: p. 1602-1617.

8. Hashimoto, T., et al., Domain Boundary Structure of Styrene-isoprene Block Copolymer Films Cast from Toluene Solutions. Macromolecules, 1974. **7**: p. 364.

9. Hashimoto, T., M. Shibayama, and H. Kawai, Ordered Structure in Block Polymer Solutions. 4. Scaling Rules on Size of Fluctuations with Block Molecular Weight, Concentration, and Temperature in Segregation and Homogeneous Regimes. Macromolecules, 1983. **16**: p. 1093-1101.

10. Bates, F.S. and G.H. Fredrickson, Block Copolymer Thermodynamics: Theory and Experiment. Annual Review of Physical Chemistry, 1990. **41**: p. 525.

11. Hamley, I.W., The Physics of Block Copolymers. 1998, Oxford: Oxford University Press.

12. Bates, F.S. and G.H. Fredrickson, Block Copolymers - Designer Soft Materials. Physics Today, 1999: p. 32.

13. Quirk, R.P. and M. Morton, Research on Anionic Triblock Copolymers, in Thermoplastic Elastomers, G. Holden, et al., Editors. 1996: Munich.

14. Hanley, K.J. and T.P. Lodge, Effect of Dilution on a Block Copolymer in the Complex Phase Window. Journal of Polymer Science: Part B: Polymer Physics, 1998. **36**: p. 3101-3113.

15. Mansky, P., P.M. Chaikin, and E.L. Thomas, Monolayer Films of Diblock Copolymer Microdomains For nanolithographic Applications. J. Mat. Sci., 1995. **30**: p. 1987.

16. Mansky, P., et al., Phase Coherence and Microphase Separation Transitions in Diblock Copolymer Thin Films. Macromolecules, 1999. **32**(15): p. 4832.

17. Huang, E., et al., Nanodomain control in copolymer thin films. Nature, 1998. **395**: p. 757.

18. Park, C., C. De Rosa, and E.L. Thomas, Large Area Orientation of Block Copolymer Microdomains in Thin Films via Directional Crystallization of a Solvent. Macromolecules, 2001. **34**: p. 2602.

19. Utracki, L.A., Polymer Alloys and Blends. 1990.

20. Russell, T.P., R.P. Hjelm, and P.A. Seeger, Temperature Dependence of the Interaction Parameter of Polystrene and Poly(methyl methacrylate). Macromolecules, 1990. **23**: p. 890-893.

21. Menelle, A., et al., Ordering of thin diblock copolymer films. Physical Review Letters, 1992. **68**(1): p. 67.

22. Winey, K.I., et al., Compositional Dependence of the Order-Disorder Transition in Diblock Copolymers. Macromolecules, 1994. **27**: p. 2392-2397.

23. Flory, P.J., Thermodynamics of High Polymer Solutions. Journal of Chemical Physics, 1941. **9**: p. 660.

24. Flory, P.J., Principles of Polymer Chemistry. 1953, Ithaca, NY: Cornell University Press.

25. Huggins, M.L., Solutions of Long Chain Compounds. Journal of Chemical Physics, 1941. **9**: p. 440.

26. Russell, T.P., et al., A lower critical ordering transition in a diblock copolymer melt. Nature, 1994. **368**: p. 729-731.

27. Karis, T.E., et al., Rheology of the Lower Critical Ordering Transition. Macromolecules, 1995. **28**: p. 1129.

28. Dudowicz, J. and K.F. Freed, Effect of Monomer Struture and Compressibility on the Properties of Multicomponent Polymer Blends and Solutions: 1. Lattice Cluster Theory of Compressible Systems. Macromolecules, 1991. **24**: p. 5076.

29. Ruzette, A.V. and A.M. Mayes, A Simple Free Energy Model for Weakly Interacting Polymer Blends. Macromolecules, 2001. **34**: p. 1894.

30. Dormidontova, E.E., Role of Competitive PEO-Water and Water-Water Hydrogen Bonding in Aqueous Solution PEO Behavior. Macro., 2002. **35**(3): p. 987.

31. Ryu, D.Y., et al., Closed-loop phase behaviour in block copolymers. Nat Mat, 2002. **1**(2): p. 114.

32. Dudowicz, J. and K.F. Freed, Relation of Effective Interaction Parameters for Binary Blends and Diblock Copolymers: Lattice Cluster Theory Predictions and Comparisons with Experiment. Macromolecules, 1993. **26**: p. 213-220.

CHAPTER 2

EXPERIMENTAL METHODS

2.1 Anionic Synthesis of Block Copolymers

To study the phase behavior of block copolymer systems the materials require a narrow molecular weight distribution and a high degree of purity. Anionic polymerization techniques can be used to this end. Polymers synthesized via living anionic techniques are more desirable than those synthesized using atom transfer radical polymerization (ATRP) due to the presence of metal impurities, such as copper, used in ATRP which are difficult to remove during the purification steps.

Success of controlled polymerization requires that the initiation be much faster than propagation, and the system must be devoid of impurities that can lead to chain transfer and termination. In anionic polymerization this means that the polymerization system must be devoid of reactive gases, such as carbon dioxide and oxygen, that can lead to termination events such as dimerization. Additionally, the system must extremely dry, for greater than a part per million of water can lead to termination at the negatively charged living end. The materials used in this work were anionically synthesized block copolymers of polystyrene (PS), or deuterated styrene (dPS), and select poly(n-alkyl methacrylates), specifically poly(n-butyl methacrylate) (PnBMA), poly(n-pentyl methacrylate) (PnPMA), poly(n-hexyl methacrylate) (PnHMA), and poly(methyl methacrylate) (PMMA). The PS-*b*-PnBMA, PS-*b*-PnHMA, dPS-*b*-PnPMA, and some of the PS-*b*-PnPMA samples were synthesized by Dr. Du Yeol Ryu in the laboratories of Professor Jin Kon Kim at the Pohang University of Science and Technology in Pohang,

South Korea. Some PS-*b*-PMMA samples were synthesized by Dr. James Goldbach in the laboratories of Professor Jacques Penelle at the University of Massachusetts Amherst. The remaining PS-*b*-PnPMA and PS-*b*-PMMA samples were prepared in house using established techniques[1]. The materials used are summarized in Table 2.1.

Table 2.1: Block copolymer samples used in this work

Sample Description	Mn (g/mol)	Weight Fraction PS	Sample Description	Mn (g/mol)	Weight Fraction PS
PS-*b*-PnPMA L	42,000	0.50	PS-*b*-PnPMA HC1	42,000	0.38
PS-*b*-PnPMA H	52,000	0.50	PS-*b*-PnPMA HC2	52,000	0.41
PS-*b*-PnPMA blend 1	44,500	0.50	PS-*b*-PnPMA LD1	44,500	0.50
PS-*b*-PnPMA blend 2	48,000	0.50	PS-*b*-PnPMA LO1	48,000	0.50
dPS-*b*-PnPMA 45/55	39,000	0.50	PS-*b*-PnPMA LO2	39,000	0.50
dPS-*b*-PnPMA 50/50	42,000	0.50	PS-*b*-PnPMA HD1	42,000	0.41
dPS-*b*-PnPMA 55/45	44,500	0.50	PS-*b*-PnPMA	44,500	0.50
PS-*b*-PnHMA	37,000	0.50	dPS-*b*-PMMA	301,000	0.50
dPS-*b*-PnBMA	30,000	0.50	dPS-*b*-PMMA	500,000	0.50

Anionic block copolymerizations were carried out using the sequential addition of the monomers in tetrahydrofuran (THF) at -78°C in the presence of lithium chloride salt under an inert argon atmosphere. Secondary-butyl lithium was used as an initiator. Lithium chloride (high purity, Aldrich) was dried overnight at 150°C, and dissolved in dried THF. THF was prepared by refluxing over calcium hydride, then stirring over a sodium/benzophenone complex until there was a persistent deep purple color indicative of an oxygen-free, moisture-free environment. The monomers were degassed and the styrene was distilled from dried dibutyl magnesium. The n-alkyl methacrylate monomers were distilled from trioctylaluminum. The styrene or deuterated styrene block took approximately one hour to reach full conversion, at which time an aliquot was extracted and terminated using purified isopropanol for molecular weight analysis. The n-alkyl

methacrylate component was then slowly added and stirred for approximately 5 hours. After the polymerization was completed it was terminated using purified isopropanol and precipitated in a 4: 1 methanol: water mixture.

The total molecular weights were determined using either multi-angle laser light scattering (MALLS), or size exclusion chromatography (SEC) with a polystyrene standard. Molecular weight distributions were determined from SEC. The polystyrene (or deuterated polystyrene)/ poly(n-alkyl methacrylate) block ratios were determined using nuclear magnetic resonance (NMR). Additionally, some of the samples of symmetric PS-*b*-PnPMA and dPS-*b*-PnPMA used were mixtures of higher and lower molecular weights[2-4]. The mixtures were used as a means of probing a series of intermediate molecular weights without the synthetic challenge of preparing a series of precise target molecular weights over a narrow molecular weight range.

2.2 Small Angle Scattering

The use of radiation as a means of probing micro- and nanoscale structures is a well-established characterization method. Referred to as diffraction, or scattering, these events can take place in one of two size regimes; where the wavelength of the incident radiation is large with respect to the structure being explored, or where the radiation is of a much smaller wavelength than the structural features. The former case is useful when exploring the size and shape of structures, for instance in the use of multi-angle laser light scattering for determining of the radius of gyration of a polymer coil in dilute solution. In

studying block copolymer melts, however, the composition fluctuations of the phase mixed state and the evolution of microphase separated structures are of interest. Structural size scales are on the order of tens of nanometers and, therefore, require a probe orders of magnitude smaller. As a result, instead of light, x-rays and neutrons were used.

Scattering can be conceptualized as the deflection of radiation from its incident path due to interactions of the radiation with nuclei or the electron cloud surrounding the atoms. When the energy of the incident radiation is equal to that of the scattered radiation, the scattering is referred to as elastic. The change in the momentum of the incident x-rays or neutrons is described by the vector $\vec{k}$, as shown in schematic in figure 2.1, where $\vec{k} = \vec{k}_i - \vec{k}_s$.

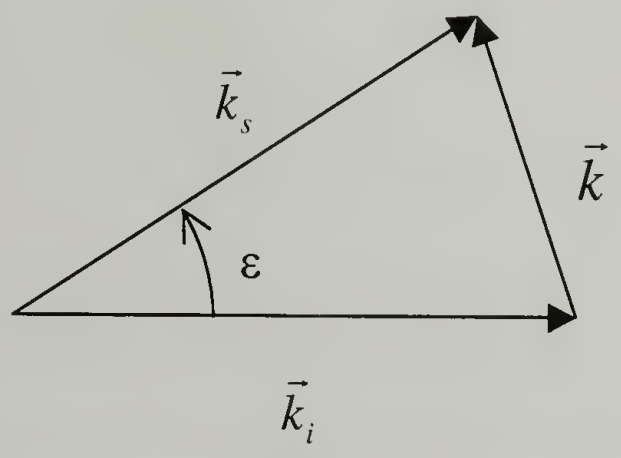

Figure 2.1: Vector construction of the scattering vector $\vec{k}$ from the incident and scattered radiation, $\vec{k}_i$ and $\vec{k}_s$ respectively

The magnitude of the momentum transfer, $\left|\vec{k}\right| = \frac{2\pi}{\lambda}\sin(\varepsilon/2)$. Often, this formula is written in a form describing the magnitude of the scattering vector, $\left|\vec{q}\right| = 2\left|\vec{k}\right|$, and the

angle ε is rewritten to equal twice the scattering angle, θ. $|\vec{q}|$ is often sufficient to describe the scattering vector. This quantity is described in equation 2.1 as a function of the wavelength of the incident radiation, λ, and the scattering angle, θ.

$$|\vec{q}| = \frac{4\pi}{\lambda}\sin\theta \tag{2.1}$$

Constructive and destructive interference of the radiation scattered from the block copolymer result in variations in scattered intensity as a function of scattering angle or scattering vector. This scattered intensity is also dependent upon the contrast between the object and the surrounding medium. The origin of contrast is dependent on the source of radiation, and speaks to the mechanism by which scattering occurs. In the case of x-rays, elastic interactions occur with the electronic clouds surrounding the atoms, and as such contrast arises from differences in the electron densities of the atoms. As for neutrons, scattering occurs at the nuclei and contrast arises from differences in the neutron scattering cross sections of the components. These contribute to an effective refractive index of the material for the wavelength of radiation used. The real component, δ, of the refractive index, n, is determined from the electron densities or atomic scattering cross-sections, by equations 2.2 and 2.3 respectively

$$\delta_X = \lambda^2 \rho_{el} r_0 / 2\pi \tag{2.2}$$

$$\delta_N = \frac{N_A \rho \lambda^2}{2\pi} \frac{b_{mon}}{M_{mon}} \tag{2.3}$$

where N_A is Avogadro's number, ρ_{el} is the electron density, ρ is the mass density, λ is the wavelength of the radiation, r_0 is the classical electron radius (2.82×10^{-13} cm), b is the neutron scattering length, and M is the molecular mass. Organic polymers (containing only carbon, hydrogen, oxygen, and nitrogen) are non-absorbing so the imaginary component to the refractive index is negligible. δ_X and δ_N for common polymers and substrates are shown in table 2.2[5].

Table 2.2: Real component of the refractive index for x-rays and neutrons for materials used in this work

	$10^6 \delta_X$	$10^6 \delta_N$
Polystyrene	3.33	0.509
Deuterated PS	3.38	2.336
Poly(methyl methacrylate)	3.98	0.390
Deuterated PMMA	3.97	2.563
Silicon	7.44	0.791
Silicon Oxide	7.33	1.371

Coherent scattering radiation, contains information describing the spatial correlations between the polymer chains or subunits. For a microphase separated diblock copolymer these correlations give rise to maxima that result from constructive interference between the scattered waves. From the peak shape and periodicity one can extract information on the shape and spatial distribution of microdomains, such as the hexagonal packing of cylinders. For phase-mixed block copolymers, however, a single, broad scattering peak results[6]. Termed the correlation hole scattering[7], this results from the connectivity of the block components. Therefore, there is a characteristic compositional inhomogeneity with a length scale on the order of the radius of gyration, R_g, of the polymer chain. In fact, the correlation hole peak occurs at $q = 2/R_g$ where $R_g^2 = Nl^2$ where l is the length of a statistical segment of the copolymer chain.

The correlation hole scattering yields information on the degree of thermodynamic compatibility between the two phases in the disordered state, and theoretical fits to this type of data will be used to extract an effective Flory-Huggins χ parameter. The intensity of the peak is related to the scattering function, S(q) and the contrast (electron density, ρ, or scattering length, b) between the two components, as by equation 2.4 for neutrons

$$I(q) = v^{-1}(b_1 - b_2)^2 S(q) \qquad (2.4)$$

where v is the segment reference volume. The scattering function was defined by Leibler using the incompressible random phase approximation for an ideal Gaussian polymer coil. This is shown in equation 2.5

$$S(q) = W(q) / \Sigma S_{ii}(q) - 2\chi W(q) \tag{2.5}$$

where W(q) is the determinant of the matrix $||S_{ij}||$, which describes the compositional fluctuations between polymer chains. The components of this matrix are given in equations 2.6a-c.

$$S_{11}(q) = N g_1(f, x) \tag{2.6a}$$

$$S_{22}(q) = N g_1(1-f, x) \tag{2.6b}$$

$$S_{12}(q) = S_{21}(q) = N/2[g_1(1, x) - g_1(f, x) - g_1(1-f, x)] \tag{2.6c}$$

In these equations f is defined as the segment fraction of component 1 (N_1/N where N is the number of statistical segments in the block copolymer). The function $g_1(f,x)$ is the Debye function, defined below as

$$g_1(f,x) = 2[fx + \exp(-fx) - 1]/x^2 \tag{2.7}$$

where x is defined as

$$x = \frac{q^2 N l^2}{6} = q^2 R_g{}^2 \tag{2.8}$$

Equation 2.5 can now be simplified, incorporating the definitions for the Debye function. The scattering function, then, is written in terms of the Flory-Huggins interaction parameter, χ, as follows.

$$S(q) = N/[F(x) - 2\chi N] \tag{2.9}$$

This allows one to extract thermodynamic information from scattering data in the disordered state, as well as the radius of gyration of the polymer coil. The relations outlined above, however, assume the statistical segment lengths are identical for both blocks. Bates modified F(x) to include contributions from dissimilar blocks[8], as shown in equation 2.10 below.

$$F(x_1, x_2) = \frac{f^2 g(x_1) + 2f(1-f)h(x_1)h(x_2) + (1-f)^2 g(x_2)}{f^2(1-f)^2[g(x_1)g(x_2) - h^2(x_1)h^2(x_2)]} \tag{2.10}$$

Here, f is the volume fraction of component 1. The functions $g(x_i)$, $h(x_i)$, and x_i are given below.

$$g(x_i) = 2[x_i + \exp(-x_i) - 1]/x_i^2 \tag{2.11}$$

$$h(x_i) = x_i^{-1}(1 - \exp(-x_i)) \tag{2.12}$$

$$x_i = \frac{q^2 N_i a_i^2}{6} = q^2 R_{gi}^2 \tag{2.13}$$

The relations described here were used to determine important information on the thermodynamics of block copolymers under hydrostatic pressure, as will be described later in this thesis.

2.3 Specular Reflectivity

The reflection of x-rays or neutrons off of a surface has emerged as a powerful means of non-destructively extracting important information on film thickness, interfacial roughness, and the density profile of polymer films[9]. Specular reflectivity, where the angle of incidence equals the angle of reflection, is of particular interest since the momentum transfer, $\vec{k}$, is directed up from reflecting surface, as shown in the vector construction in Figure 2.2. Therefore, this allows one to probe compositional variations in the film along the z-axis of the film. The situation where θ_{in} does not equal θ_{out} is termed off-specular

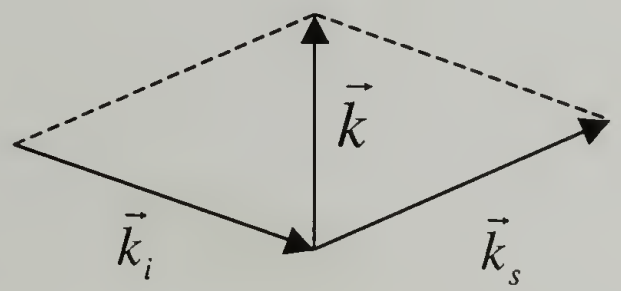

Figure 2.2: Vector construction of the momentum transfer in a specular reflectivity experiment

scattering. This is useful in investigating lateral structural elements, such as correlated roughness or block copolymer domains exhibiting high degrees of long-range lateral order. Off-specular scattering will not be discussed further. Figure 2.3 illustrates a typical experimental geometry known as a "theta-2 theta" system. The sample is rotated in plane with respect to the fixed source of incident radiation. The detector is also rotated with respect to the incident beam by an angle a factor of 2 greater than the sample rotation.

This ensures that the angle of incidence equals the angle of reflection and that the momentum transfer vector remains normal to the reflecting surface.

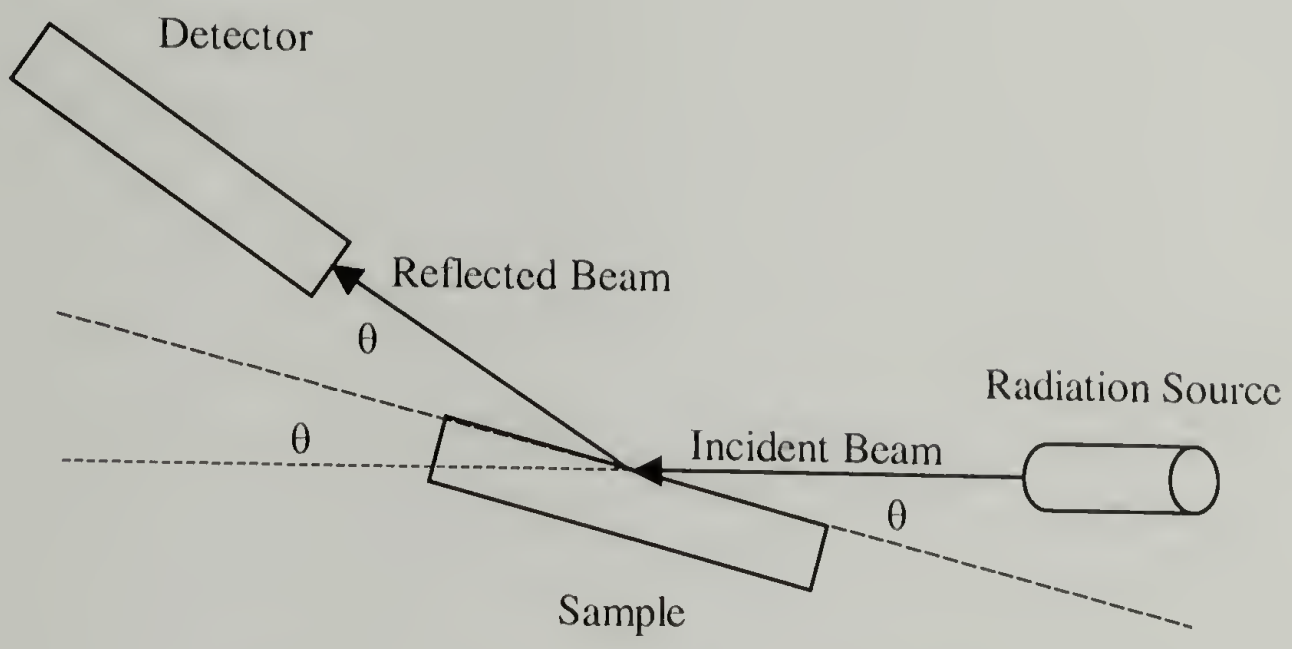

Figure 2.3: Theta-2 theta reflectivity instrumentation

The theory governing reflectivity[10, 11] starts by considering an interface between two media of refractive indices n_1 and n_2. Radiation impinges upon this surface at an angle θ_1, referred to as the grazing angle of incidence, defined with respect to the surface. The angle of refraction, θ_2, is determined from Snell's Law, which states

$$n_1 \cos\theta_1 = n_2 \cos\theta_2 \qquad (2.14)$$

As long as $n_2 > n_1$, $\theta_2 > \theta_1$ and there will exist an angle of refraction. However, if $n_2 < n_1$, as is often the case for neutrons or X-rays in many polymeric, crystalline, and metallic materials, the angle of refraction will only exist at angles of incidence greater than some critical angle, θ_c, at which the angle of refraction equals 0. All incident angles less than the critical angle result in a total external reflection of the incident radiation, with the exception of an evanescent wave that propagates into the film.

As was mentioned earlier, the momentum transfer of the incident radiation at the reflecting interface yields information in the z-axis of the film. That momentum transfer is defined as

$$k_{z,0} = (\frac{2\pi}{\lambda})\sin\theta \tag{2.15}$$

where λ is the wavelength of the radiation, θ is the angle of incidence, and the subscript 0 indicates vacuum. For a medium, i, the momentum transfer is expressed in terms of $k_{z,0}$ and the momentum transfer at the critical angle, $k_{c,i}$ as follows.

$$k_{z,i} = (k_{z,0}^2 - k_{c,i}^2)^{1/2} \tag{2.16}$$

The momentum transfer, then, is used to determine the reflectivity coefficient, r, for an interface between any given media, assuming an infinitely sharp interface. The reflection coefficient between layers i and i+1 is given by

$$r_{i,i+1} = (k_{z,i} - k_{z,i+1})/(k_{z,i} + k_{z,i+1}) \tag{2.17}$$

from which the Fresnel reflectivity, R, is calculated. R is simply the product of the reflectivity coefficient and its complex conjugate, R*. For a vacuum/sample interface the reflectivity is given in equation 2.18.

$$R(k_{z,0}) = \left| \frac{1-[1-(k_{c,1}/k_{z,0})^2]^{1/2}}{1+[1-(k_{c,1}/k_{z,0})^2]^{1/2}} \right|^2 \tag{2.18}$$

In the case of a multi-layered system, the reflectivity coefficient is calculated using an recursive process starting with the bottom-most interface (that between an infinitely thick substrate and a layer of finite thickness) and proceeding up through the film for every interface, using the end result to determine a cumulative reflectivity coefficient. The r for the bottom-most interface is calculated first using equation 2.17. The result is then renamed " $r'_{n,n+1}$ " and used to calculate the reflectivity coefficient for the next interface,

that between layers n and n-1. The reflectivity coefficient for this interface takes the following form, where d_n is the thickness of layer n and layer n+1 is the substrate. The factor $r'_{n,n+1}$ is calculated from equation 2.17.

$$r_{n-1,n} = \frac{r'_{n-1,n} + r'_{n,n+1}\exp(2id_n k_n)}{1 + r'_{n-1,n} r'_{n,n+1}\exp(2id_n k_n)} \tag{2.19}$$

This process in then repeated for the interface between the n and n+1 layers, as per equation 2.20.

$$r_{n-2,n-1} = \frac{r'_{n-2,n-1} + r_{n-1,n}\exp(2id_{n-1} k_{n-1})}{1 + r'_{n-2,n-1} r_{n-1,n}\exp(2id_{n-1} k_{n-1})} \tag{2.20}$$

The recursion is then carried out for every interface in the film, finishing with the interface between the first layer and vacuum. The resulting r is used in the calculation of the Fresnel reflectivity.

An example of a calculated reflectivity curve is shown in Figure 2.4. The inset shows the electron density as a function of film depth. The periodicity of the layered

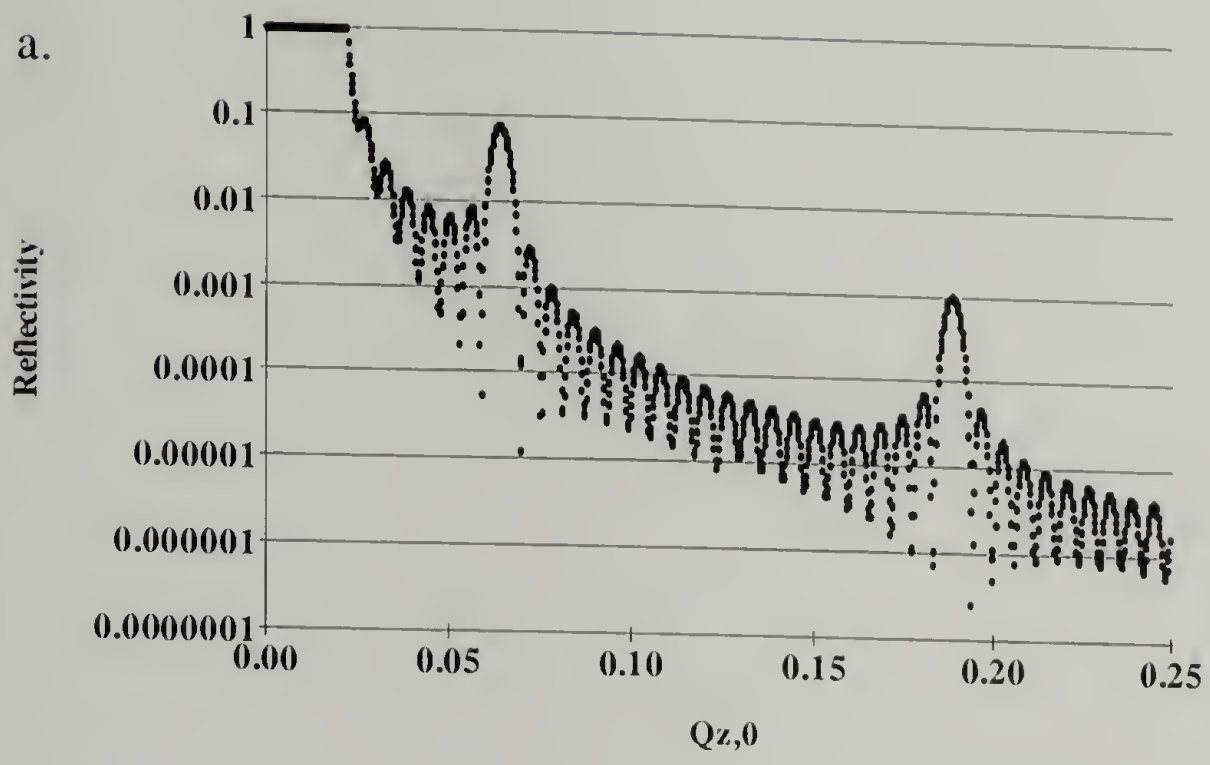

Figure 2.4: a. Reflectivity and b. density profile of a 10-period layered structure on a high-density substrate

structure gives rise to constructive interferences and, therefore, Bragg peaks are observed in the scattering curve. Interferences due to the entire thickenss of the film give rise to oscillations along the curve known as Kiessig fringes. The value of $\Delta k_{z,0}$ as measured

between adjacent troughs can be used to calculate the total film thickness, t, via the relation $t = \pi / \Delta k_{z,0}$.

The incorporation interfacial roughness into reflectivity calculations is accomplished by multiplying the Fresnel reflectivity by $e^{-\sigma^2 q^2}$ where σ describes the roughness of the surface. This results in a decrease in the intensity of the calculated reflectivity curve, while not affecting characteristic features of the curve such as Kiessig fringes or Bragg peaks. Roughness is considered a change in the density of the film as one moves along the z-axis, so the quantity dρ/dz must be evaluated. Assuming a Gaussian form to the density change, with a standard deviation, σ, of the interface from its average, the roughness takes the form in equation 2.21.

$$\frac{R(k_{z,0})}{R_F(k_{z,0})} = \exp(-4k_z^2\sigma^2) \tag{2.21}$$

The quantity $\frac{R(k_{z,0})}{R_F(k_{z,0})}$ illustrates how roughness can be considered as inducing a deviation of the observed reflectivity from the ideal Fresnel reflectivity. For the multilayered case the general form of equation 2.22 is used, where n is the total number of layers, D is the thickness of layer i, and layer 0 is the substrate.

$$\frac{R(k_{z,0})}{R_F(k(_{z,0})} = \left(\sum_{i=0}^{n} \frac{\rho_i - \rho_{i+1}}{\rho_0} \exp(-2ikD_i) \exp(-2k_i k_{i+1} \sigma_{i+1}^2) \right)^2 \qquad (2.22)$$

2.4 Depolarized Light Birefringence

An intrinsic property of microphase separated block copolymer materials is the form birefringence of the domains within each grain of the material. The birefringence, or the existence of slow and fast directions of light propagation, results from the directional stretching of the copolymer chains in the microphase-separated state[12]. Within one copolymer grain the domains of lamellae or cylinders are oriented in the same direction, leading to anisotropy within the material. Spherical and gyroidal morphologies, however, due to the symmetry of the domain arrangement, exhibit no birefringence. Likewise, the phase-mixed state is fully isotropic and, as such, is non-birefringent.

The birefringence of cylinder and lamella-forming block copolymers can be exploited as a means of precisely determining the location of an order-to-disorder transition. Figure 2.5 illustrates an experimental geometry in which laser light at 632.8 nm is directed through an optical polarizer, through the sample polymeric material, then

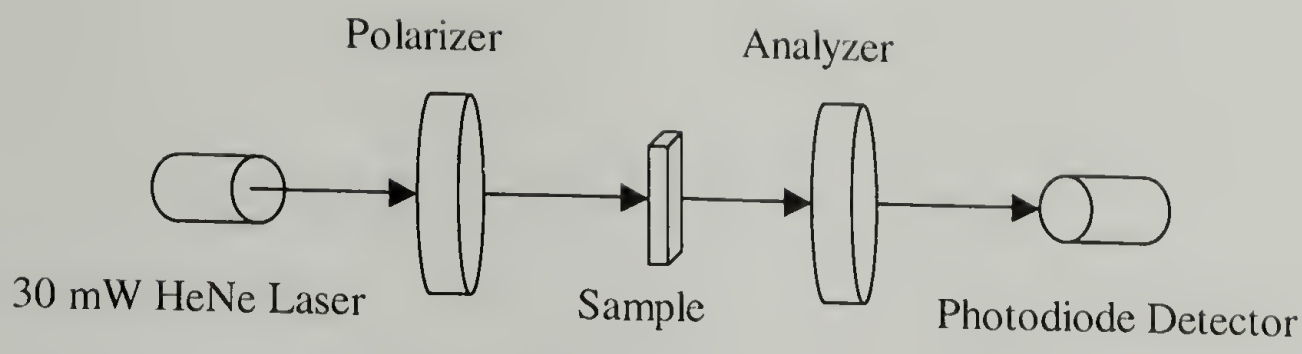

Figure 2.5: Optical birefringence experimental setup for the identification of order-to-disorder transitions in block copolymers

through an analyzer oriented normal to the polarizer. The intensity of the resulting radiation is recorded by a photodiode light detector. A disordered, fully homogenous block copolymer will not depolarize the incident light, and the crossed polars will result in total extinction of the radiation. However, a lamellar or cylinder-forming block copolymer in the ordered state will exhibit anisotropy sufficient to depolarize the incident light, resulting in a detectible intensity. In this way, a crossed-polars arrangement is a powerful tool for precisely detecting the existence of order-to-disorder transitions and grain ripening.

References

1. Allen, R.D., T.E. Long, and J.E. McGrath, *Preparation of High-Purity, Anionic-Polymerization Grade Alkyl Methacrylate Monomer.* Polym. Bul., 1986. **15**: p. 127.

2. Karis, T.E., et al., *Rheology of the Lower Critical Ordering Transition.* Macromolecules, 1995. **28**: p. 1129.

3. Almdal, K., J.H. Roseldale, and F.S. Bates, *Order-Disorder Transition in Binary Mixtures of nearly Symmetric Diblock Copolymers.* Macro., 1992. **23**: p. 4336.

4. Hashimoto, T., et al., *Ordered Structure in Blends of Block Copolymers .1. Miscibility Criterion for Lamellar Block Copolymers.* Macro., 1993. **26**: p. 2895.

5. *Encyclopedia of Polymer Science and Engineering.* 1987, New York: John Wiley & Sons.

6. Leibler, L., *Theory of Microphase Separation in Block Copolymers.* Macromolecules, 1980. **13**: p. 1602-1617.

7. de Gennes, P.-G., *Scaling Concepts in Polymer Physics.* 1979, Ithaca: Cornell University Press.

8. Bates, F.S., J.H. Rosedale, and G.H. Fredrickson, *Fluctuation effects in a symmetric diblock copolymer near the order-disorder transition.* Macromolecules, 1990. **92**(10): p. 6255.

9. Russell, T.P., *X-ray and neutron reflectivity for the investigation of polymers.* Materials Science Reports, 1990. **5**: p. 171.

10. Born, M. and E. Wolf, *Principles of Optics.* 1980, Oxford: Pergamon Press.

11. Felcher, G.P., et al., Rev. Sci. Instr., 1987. **58**: p. 609.

12. Lodge, T.P. and G.H. Fredrickson, *Optical Anisotropy of Tethered Chains.* Macromolecules, 1992. **25**: p. 5643-5650.

CHAPTER 3

BLOCK COPOLYMERS UNDER HYDROSTATIC PRESSURE

3.1 Phase Behavior at High Pressures

As was discussed in Chapter 1, many block copolymer systems pass from the ordered state to the disordered state upon heating. This type of phase behavior is enthalpically driven, as unfavorable interactions between dissimilar segments are overcome with increasing temperature. The temperature at which the transition from microphase separation to homogenization occurs is termed the order-to-disorder transition (ODT) temperature. A few groups have studied ODT block copolymer systems under hydrostatic pressure, often using the incompressible random phase approximation method as a means of extracting an effective χ parameter from SANS data[1]. This has proven to be an invaluable means of extracting important thermodynamic information on polymer systems, such as packing efficiency and molecular compatibility, as well as crucial insight into local chain structure.

The influence of pressure on the location of the ODT is dependent on the sign of the volume change on passing through the transition. The relation in equation 3.1 describes the effect of pressure as one moves along the spinodal[2].

$$\left.\frac{\delta T}{\delta P}\right|_x = \frac{v_{xx}}{s_{xx}} = \frac{T_s v_{xx}}{h_{xx}} \tag{3.1}$$

Here, T_s is the spinodal temperature, and v_{xx}, s_{xx}, and h_{xx} are the second derivatives of the volume, entropy, and enthalpy with respect to composition. A more familiar form of this relation is the Clausius-Clapeyron equation, given in equation 3.2.

$$\left.\frac{dT_{ODT}}{dP}\right|_x \cong \Delta V_{dis} / \Delta S_{dis} = T_{ODT} \Delta V_{dis} / \Delta H_{dis} \qquad (3.2)$$

This directly relates the pressure coefficient, dT_{ODT}/dP, at constant composition to the temperature of the transition, the volume change on disordering, ΔV_{dis}, and the enthalpy of disorder, ΔH_{dis}. For ODT systems ΔH_{dis} is always positive, so the sign of the pressure coefficient is exclusively dependent on the sign of ΔV_{dis}. In either case, the application of pressure favors the denser state. For instance, if the system densifies upon disordering, as is the case when $\Delta V_{dis} > 0$, dT_{ODT}/dP will be positive. This is, in fact, the general case for ODT systems.

3.2 ODT-Type Block Copolymers

A number of studies have investigated ODT-type systems and, in many cases, dT_{ODT}/dP was found to be positive. For example, Ruzette and coworkers studied the effect of pressure on the phase behavior of polystyrene-*block*-poly(methyl methacrylate)[3], a well-studied system exhibiting an ODT[4]. They found a pressure coefficient of 23˚C/kbar, which is consistent with the positive volume change on mixing in this system. The application of hydrostatic pressure reduces the volume of the system, thereby forcing the densification of unfavorable contacts between dissimilar segments. This results in an

increase in system immiscibility, as predicted by Clausius-Clapeyron. Hajduk, *et al.*, observed a pressure coefficient of around 20°C/kbar for PS-*b*-polyisoprene[5, 6], and Stühn and coworkers observed a pressure coefficient of 19°C/kbar for the same system at larger pressures[7, 8]. Schwann *et al.* studied the poly(ethylene-*alt*-propylene)-*block*-polydimethlsiloxane system and uncovered an interesting result[9]. Figure 3.1 illustrates the location of the phase boundary as a function of temperature and pressure. At pressures below 0.4 kbar dT/dP is negative, being around -20°C/kbar at 0.05 kbar and decreasing in magnitude with increasing pressure.

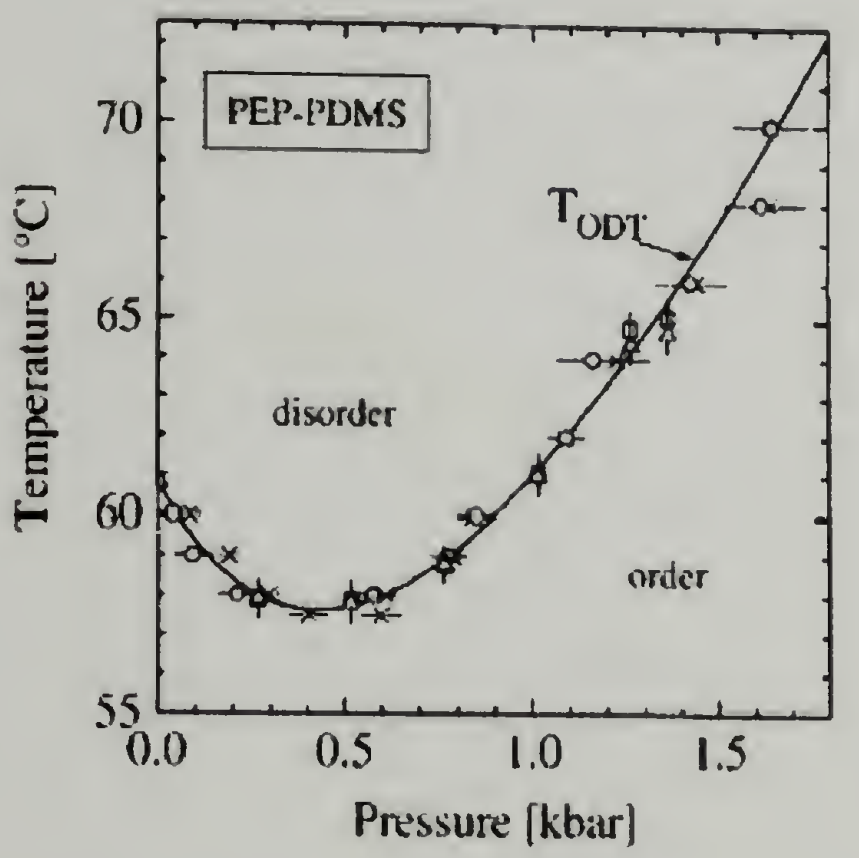

Figure 3.1: Location of the ODT as a function of hydrostatic pressure in PEP-*b*-PDMS[9]

At pressures above 0.5 kbar dT/dP becomes positive, increasing in magnitude with increasing pressure up to a pressure coefficient of around 20°C/kbar. The behavior at low pressures can be attributed to the negative volume change on disordering in the system,

with pressure favoring the denser, disordered state. With increasing pressure, however, the excess volume is squeezed out and the density of unfavorable contacts increases. This leads to the positive pressure coefficient observed at higher pressures. This effect was also observed by Ruzette and coworkers in PS-*b*-poly(n-octyl methacrylate)[3]. Interestingly, the reduction in magnitude of negative pressure coefficients with increasing pressure is not a general phenomenon. Frielinghaus *et al.* found a constant pressure coefficient of -20°C/kbar over the entire experimental pressure range in poly(ethylene propylene)-*b*-poly(ethyl ethylene)[10]. Ruzette and coworkers observed a constant dT/dP of -60°C/kbar for PS-*b*-poly(n-hexyl methacrylate) for pressures up to 1 kbar. This system has a particularly large negative pressure coefficient, and will be further discussed later in this work.

3.3 LDOT-Type Block Copolymers

The LDOT is characterized by a negative volume change on passing into the disordered state. As such, the pressure coefficient will always be positive and serve to drive the system towards homogeneity. Two characteristic LDOT systems illustrate this effect. Pollard, *et al.*, determined the impact of hydrostatic pressure on dPS-*b*-poly(n-butyl methacrylate) block copolymers[11], finding a large dT_{LDOT}/dP of 147°C/kbar. The magnitude of this pressure coefficient opened up the possibility of designing a new class of materials, termed "baroplastics", in which pressure is used to enhance flow properties, thus aiding in low temperature material processing. The work of Gonzalez and Mayes[12] has expanded upon this idea. PS-*b*-PVME, another LDOT-type system, has not been studied under hydrostatic pressure due to synthetic challenges. However, PS/PVME

blends were investigated by Hammouda, *et al.*, and found to have a pressure coefficient of 20°C/kbar for asymmetric compositions[13], while Janssen and coworkers[14] determined a dT_{LDOT}/dP of 12°C/kbar for the symmetric composition.

3.4 Polystyrene-*block*-poly(n-alkyl methacrylate)s

It was mentioned above that while PS-*b*-PMMA is an ODT-type system, PS-*b*-PnBMA exhibits an LDOT. These two materials are examples of the range of phase behaviors exhibited by the series of block copolymers termed the PS-*b*-poly(n-alkyl methacrylate)s. The work of Ruzette and coworkers uncovered the trend that with increasing methacrylate alkyl side-chain length the phase behavior of these copolymers changed markedly[3, 4]. As alkyl chain length increased from methyl methacrylate to ethyl methacrylate the compatibility behavior with polystyrene changed from an ODT to an LDOT system. Ethyl, n-propyl, and n-butyl methacrylate displayed LDOTs, however increasing the side-chain to further to n-hexyl methacrylate led to an ODT-type system. These materials were studied under hydrostatic pressure, and the sign of the volume change on disordering were noted. These results are summarized in Table 3.1.

Table 3.1: Pressure coefficients in PS-*b*-PnAMAs[3]

Copolymer	Transition Type	Sign of ΔV_{dis}	Pressure coefficient (°C/kbar)
PS-*b*-PMMA	ODT	+	23
PS-*b*-PEMA	LDOT	-	100
PS-*b*-PnPrPMA	LDOT	-	90
PS-*b*-PnBMA	LDOT	-	140
PS-*b*-PnHMA	ODT	-	-60
PS-*b*-PnOMA	ODT	-	-5
PS-*b*-PnLMA	ODT	+	13

These trends show that intermediate length alkyl side-chains (2-4 carbons) display LDOT phase behavior. This was explained by examining the χ_{eff} for the PS-*b*-PnAMAs as a function of alkyl side-chain length, as shown in Figure 3.2.

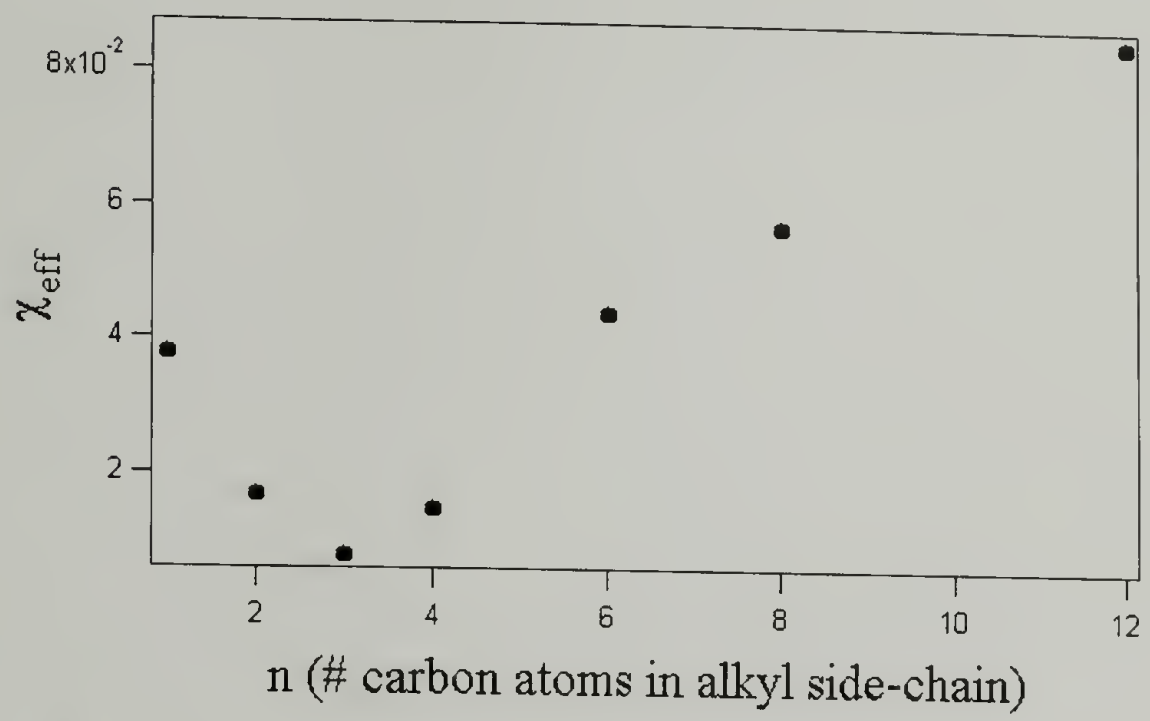

Figure 3.2: χ_{eff} as a function of alkyl side-chain length at 150°C[4]

It was observed that these intermediate side-chain methacrylates had the greatest degree of thermodynamic compatibility with polystyrene; χ_{eff} was lowest for these block copolymers. Analysis of the solubility parameters and molar volumes for PS and the PnAMAs illustrates this trend as well. Methods for calculating these quantities, as well as comparisons with other systems of interest, will be discussed later in this chapter. As a consequence of the high degree of thermodynamic compatibility, the small volumetric difference induced by disparate thermal expansion coefficients was sufficient to destabilize the system at high temperatures.

Ruzette and coworkers did not include PS-*b*-poly(n-pentyl methacrylate) block copolymers in their experiments due to the lack of nPMA monomer availability at the time

of the study. Ryu *et al.* were able to synthesize this block copolymer and fill in this gap in the knowledge of the PS-*b*-PnAMA series[15]. This proved to be an important endeavor as this block copolymer was the first weakly interacting system known to exhibit closed-loop phase behavior. Hydrostatic pressure was utilized to gain an understanding of the thermodynamic driving force for this unusual phase behavior.

3.5 Polystyrene-*block*-poly(n-pentyl methacrylate)

The Clausius-Clapeyron relation was used in order to predict the effect of hydrostatic pressure on the LDOT and UODT temperatures. Three quantities were required in order to calculate the pressure coefficient, $dT_{transition}/dP$; the temperature of the transition, the changes in volume and enthalpy in passing to the disordered state. The transition temperatures were determined accurately using birefringence techniques. Birefringence traces illustrating the location of the LDOT and UODT temperatures as a function of copolymer molecular weight are shown in Figure 3.3.

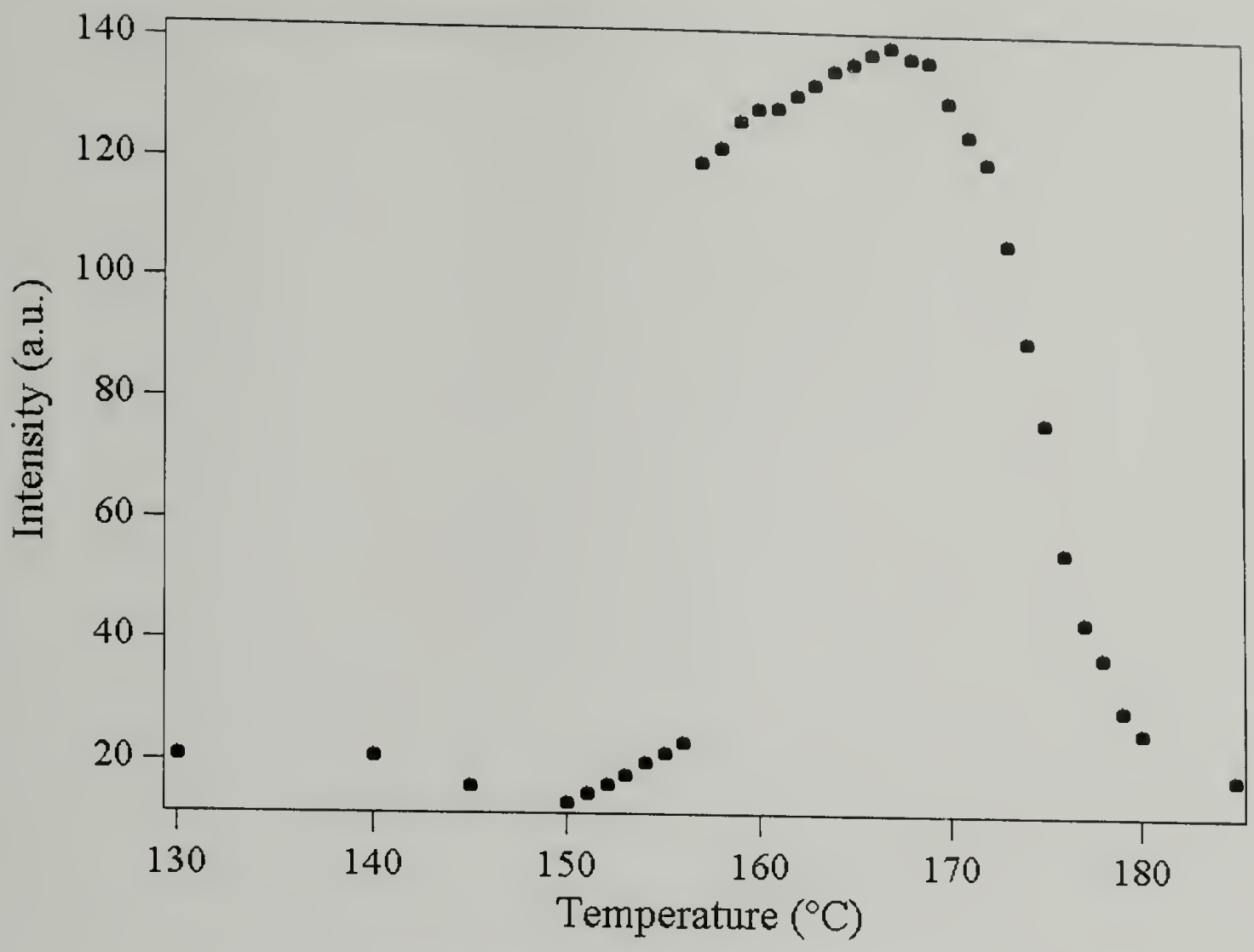

Figure 3.3: Birefringence of 47K 50/50 PS-*b*-PnPMA

The volume change on mixing was determined using two different methods. Dilatometry was used as a means of measuring the volume change of the bulk material. This was volumetric data at ambient pressure was measured by Dr. Du Yeol Ryu at POSTECH using a dilatometer (DIL402, Netzsch Co.) at a heating rate of 0.5°C/min in a He atmosphere[16]. The aluminum oxide cell contained 0.4 g of the block copolymer. These data allow the calculation of the thermal expansion coefficients in both the ordered and disordered states, as well as the volume changes on passing through the LDOT and UODT. Dilatometry results are shown in Figure 3.4 below.

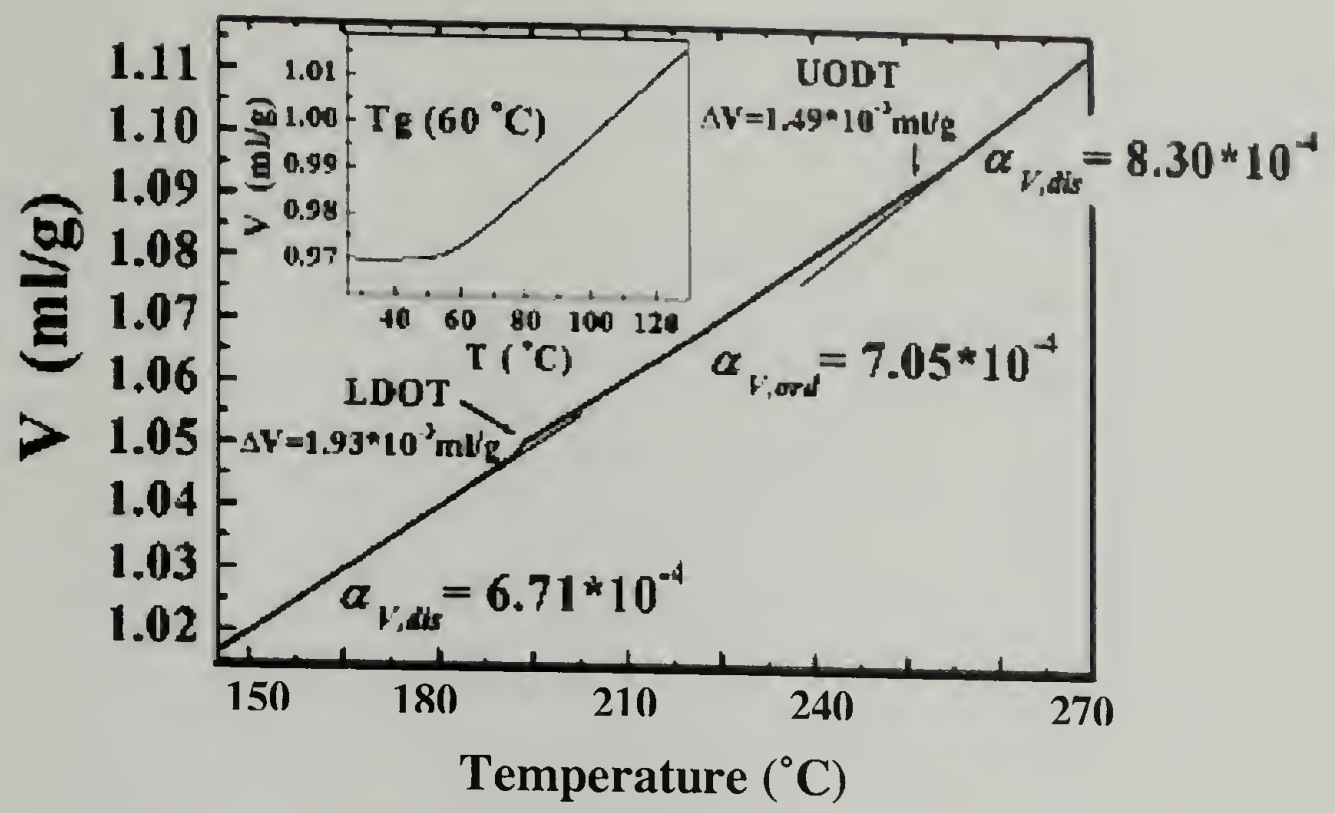

Figure 3.4: Dilatometry of 50K 50/50 dPS-*b*-PnPMA[16]

In thin films, the use of x-ray reflectivity was employed. The spacing of the Kiessig fringe minima was measured as a function of temperature, giving a value for the total film thickness. The thickness was carefully determined so as to prevent the formation of islands and holes in the microphase-separated state. Note that a slightly lower molecular weight (30K) was used to allow the observation of the LDOT and UODT temperatures in the thin film. The low surface energy of PS, combined with the preferential interaction of PnPMA with the native oxide layer of the silicon wafer, led to a surface-induced LDOT depression and UODT elevation. Once the thickness change with temperature was determined, the volume change was calculated by multiplying the sample dimensions by the total film thickness. This was possible due to the two-dimensional confinement of the polymer film on the silicon substrate[17]. As a result, the change in film thickness captures

the total volume change of the system. Figure 3.5 shows a representative reflectivity curve used in these experiments.

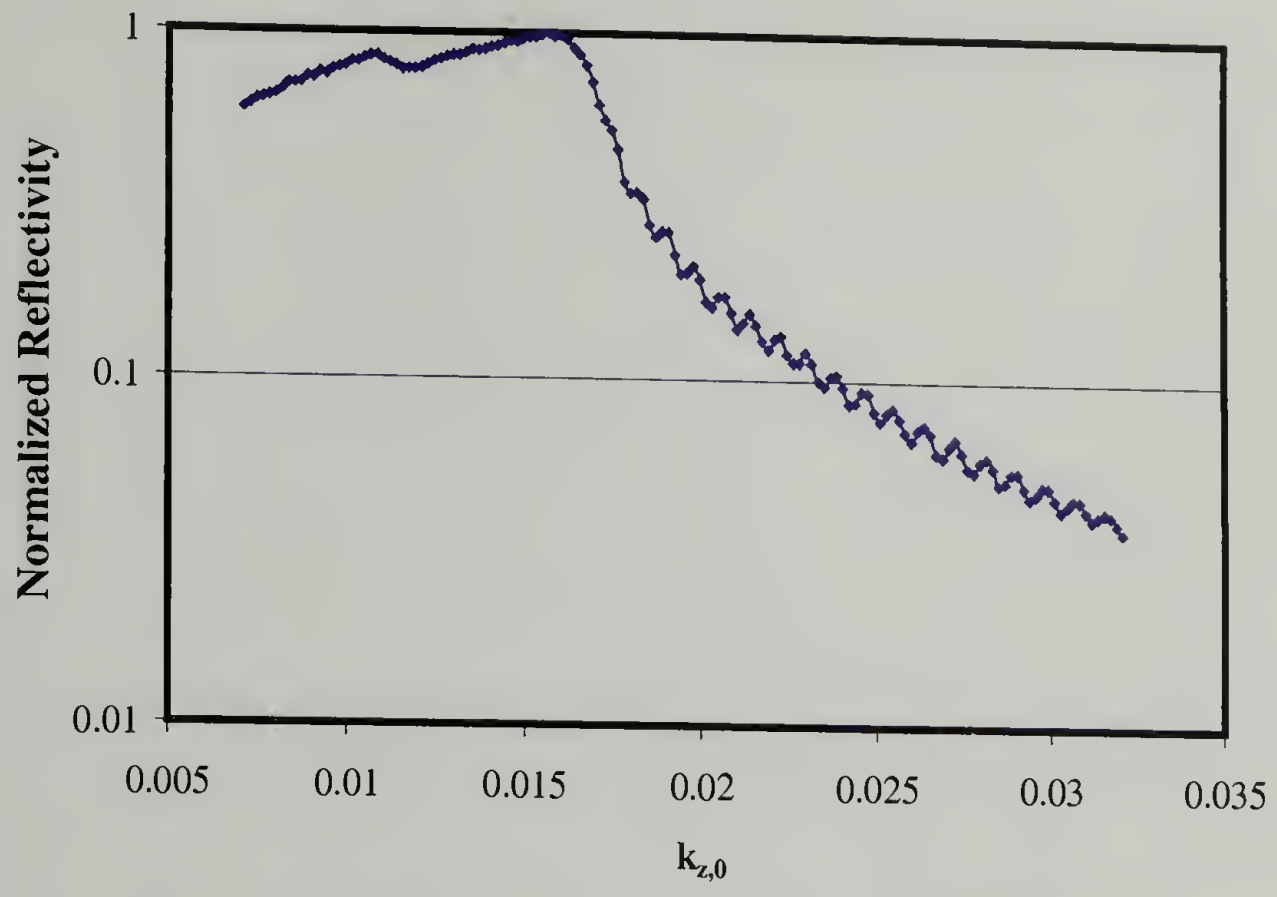

Figure 3.5: X-ray reflectivity for 50/50 35K PS-*b*-PnPMA

Film thickness, calculated by $\pi/\Delta k_{z,0}$, as a function of temperature is plotted in Figure 3.6. While the precise $\Delta k_{z,0}$ was difficult to resolve for each individual fringe spacing, over the sum of several fringes small changes in $\Delta k_{z,0}$ become apparent, allowing angstrom resolution in film thickness. In this way, fits to the reflectivity curve allowed the precise determination of the film thickness as a function of temperature.

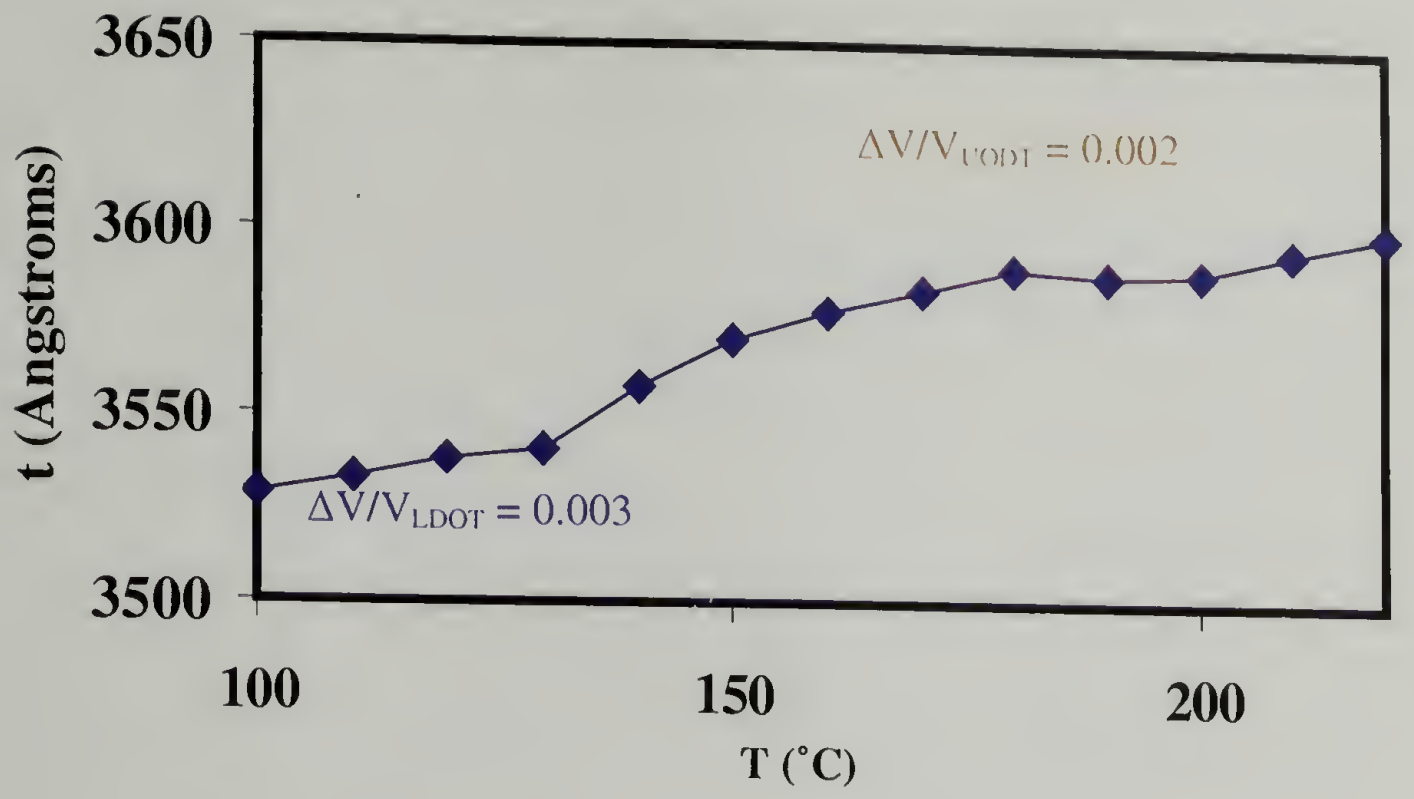

Figure 3.6: Film thickness as a function of temperature for 50/50 35K PS-*b*-PnPMA

The volume changes obtained by dilatometry are comparable with the results obtained using x-ray reflectivity. The values for the thermal expansion coefficients of the ordered and disordered states, as well as the volume changes on disordering, are given in Table 3.2.

Table 3.2: Summary of measurements of the thermal expansion in PS-*b*-PnPMA

	Thermal expansion coefficient (T < LDOT)	Thermal expansion coefficient (T > UODT)	Thermal expansion coefficient (ordered)	ΔV_{dis} LDOT	ΔV_{dis} UODT
Dilatometry	6.71×10^{-4}	8.30×10^{-4}	7.05×10^{-4}	-1.93×10^{-3}	-1.49×10^{-3}
Reflectivity	5.0×10^{-4}	6.5×10^{-4}	6.0×10^{-4}	-2.0×10^{-3}	-1.5×10^{-3}

The final piece of data required to estimate the pressure coefficient was the enthalpy change on disordering for the LDOT and UODT. Excellent DSC data was collected by Dr. Du Yeol Ryu at POSTECH. Calorimetric measurements were made using a Perkin-Elmer DSC 7 differential scanning calorimeter. The DSC thermograms were obtained during the first heating run at a rate of 10°C/min. In order to enhance the signal-to-noise ratio, a DSC pan accommodating 50 mg of sample was used. This data is given in Figure 3.7.

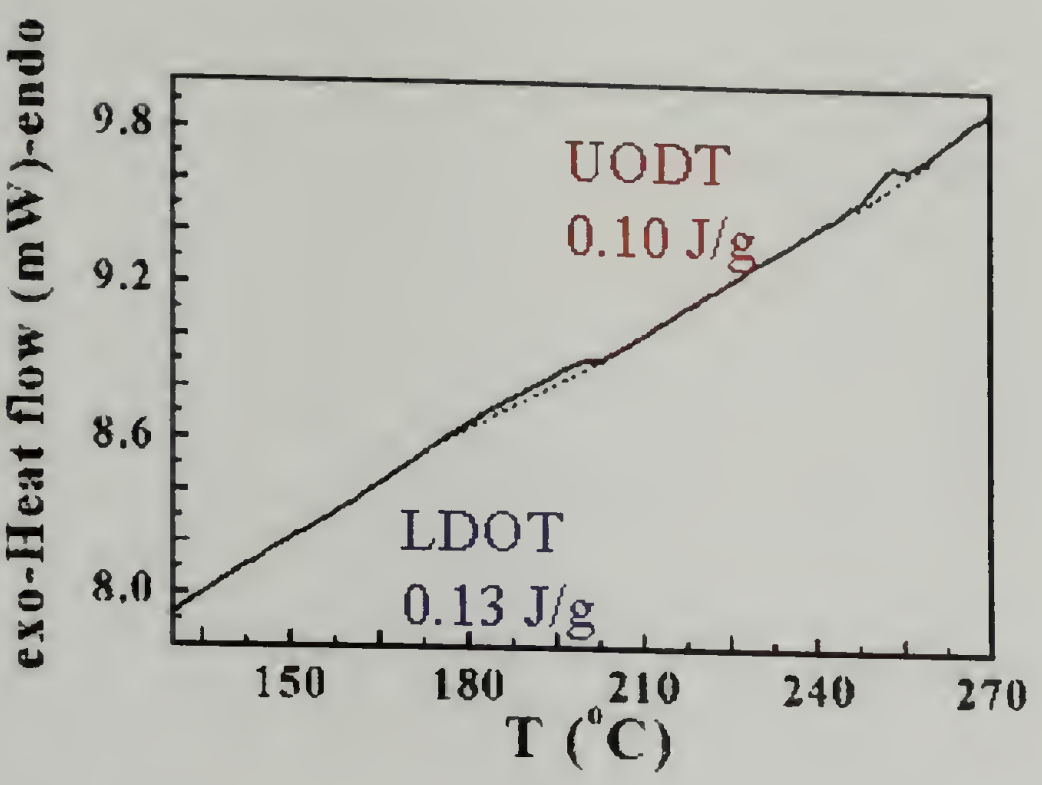

Figure 3.7: DSC measurement of PS-*b*-PnPMA

The $\Delta H_{dis,LDOT}$ was 0.13 J/g, and $\Delta H_{dis,UODT}$ was 0.10 J/g. Inserting these values into Equation 3.2, along with ΔV_{dis} and $T_{transition}$ determined above, yields a pressure coefficient, dT/dP, of 660°C/kbar for the LDOT and -780°C/kbar for the UODT.

SANS was employed as a means to measure the pressure coefficient experimentally. SANS measurements were performed on the Small Angle Neutron Diffraction line at the Intense Pulsed Neutron Source at Argonne National Laboratory. The success of the experiments was indebted to the efforts of the beam line scientists, P. Thiyagarajan and Denis Wosniak. Experiments were performed at constant temperature while stepping up in pressure from atmospheric to 1 kbar in 100 bar increments. The same set of pressures was checked for temperatures between 140°C to 260°C in 15°C increments. All measurements were checked for reversibility in pressure and temperature. Data were then reduced to absolute scale using a deuterated polystyrene standard. A representative set of SANS curves is shown in Figure 3.8, taken at 170°C.

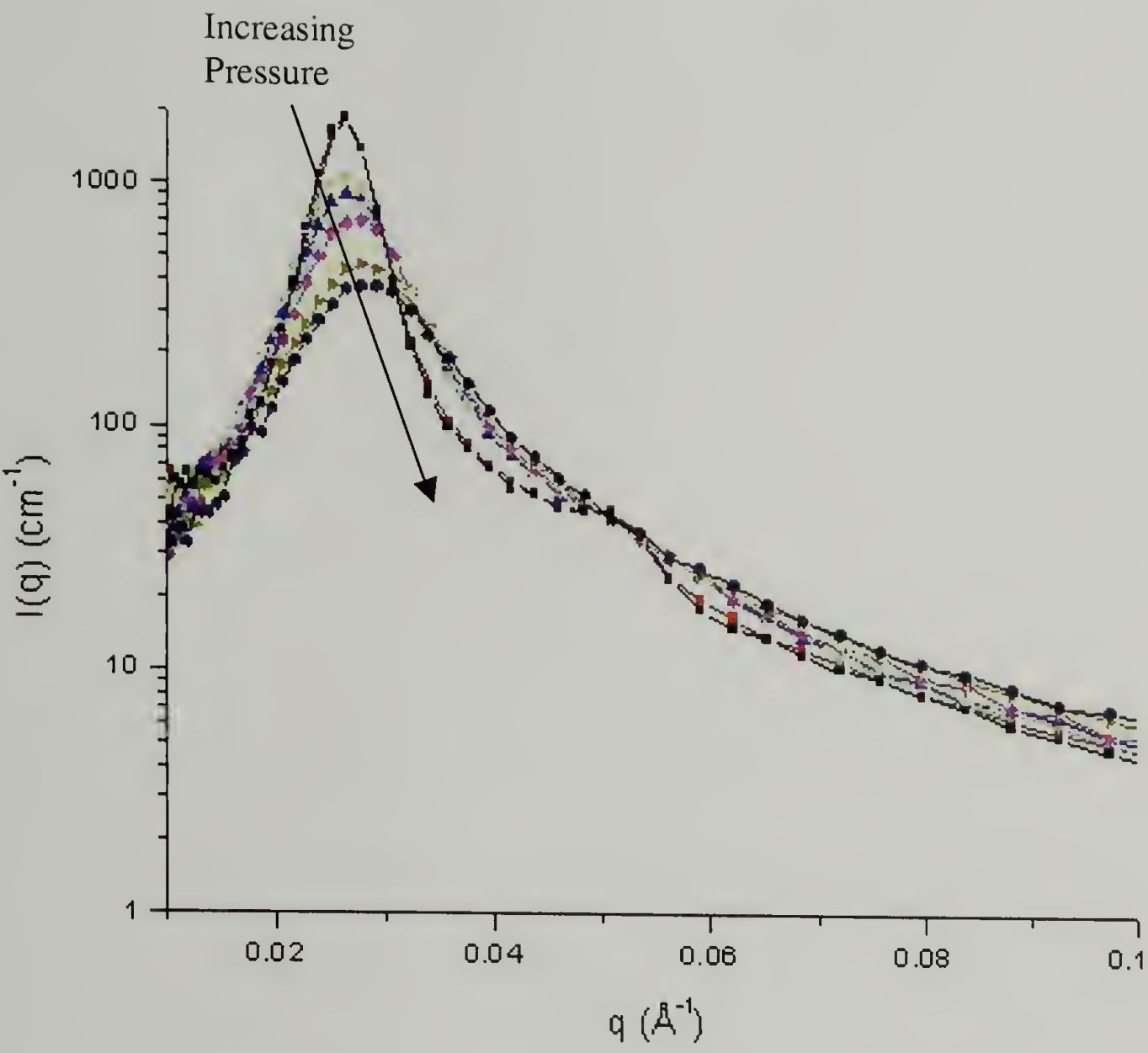

Figure 3.8: SANS of 50K dPS-*b*-PnPMA at 170˚C at pressures of 0.05 to 1 kbar

There are several features of note in these scattering curves. The first is the transition from the ordered state into the disordered state with the application of only 100 bar. The location of this transition is identifiable by the abrupt change in the shape of the first order scattering peak. At atmospheric pressure it has a high intensity and a narrow width, characteristic of the ordered state. Additionally, the presence of a second order scattering peak illustrates the existence of long-range order in the system, characteristic of a well-

ordered block copolymer melt. At 100 bar, however, the first order scattering peak drastically decreases in intensity and broadens. The second order peak disappears entirely. This is characteristic of the transition from the ordered to the disordered state. This shows that the phase behavior of this system is highly sensitive to the application of pressure, with a $P_{c,LDOT}$ between 50 and 100 bar. At pressures above 100 bar only the correlation hole scattering maximum is observable.

The shape and location of the correlation hole scattering at high pressures reveals a great deal about the thermodynamics of the system, as well as providing clues on the chain packing efficiency and segment compatibility[1]. In particular, three features of this scattering maximum are of note; it's height, width, and position. The maximum scattering intensity, I_{max}, is plotted as a function of temperature for a series of pressures in Figure 3.9.

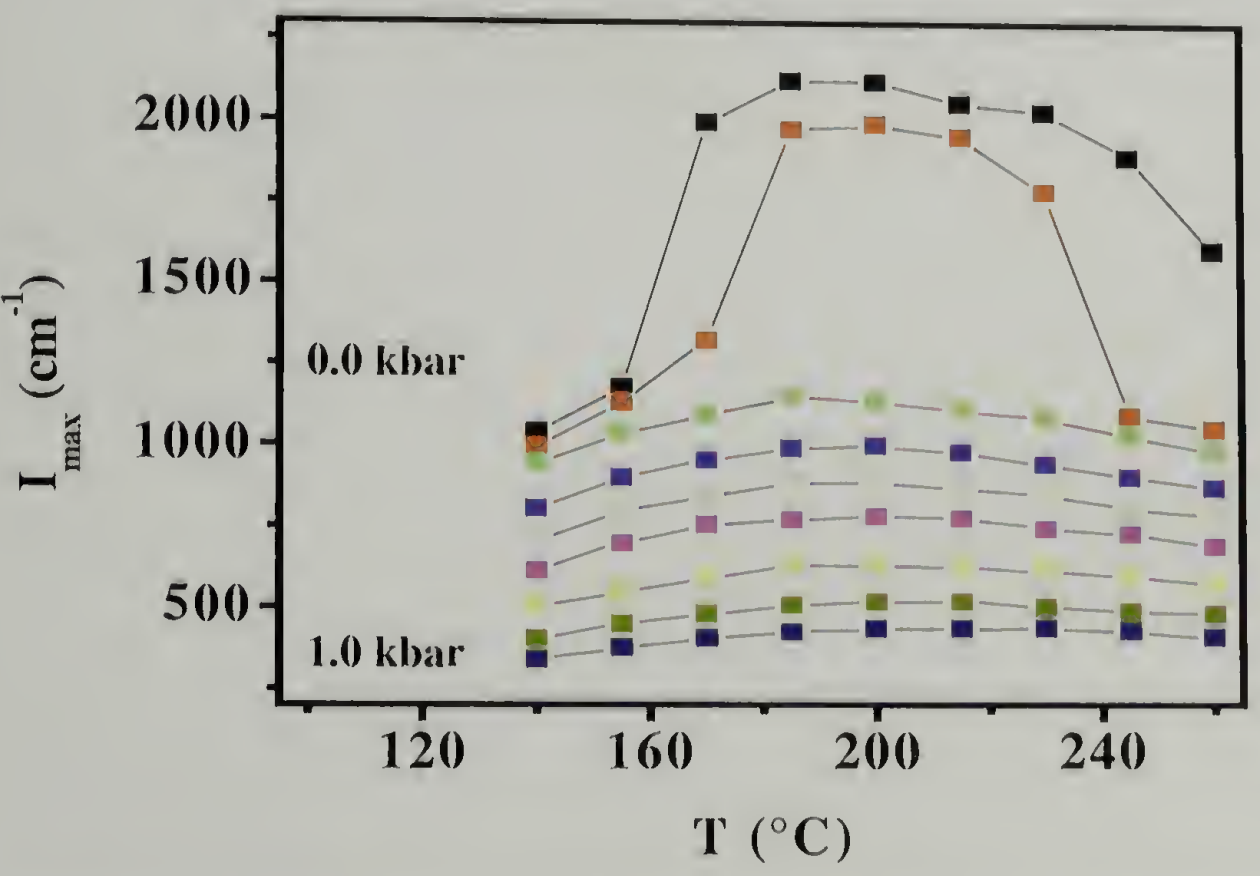

Figure 3.9: SANS maximum intensity as a function of temperature for pressures up to 1 kbar

At atmospheric pressure the system underwent an LDOT between 160 and 175°C, as evidenced by the sharp increase in peak intensity. At higher temperatures this intensity started to decrease, although a UODT was not observable. At 50 bar (the red data points) both an LDOT and UODT were observed. At higher pressures the system was fully disordered over the complete temperature range. With increasing pressure the intensity systemically decreased as the system was driven further into a fully homogenous state. At constant pressure the correlation hole intensity was observed to increase slightly to a maximum, then decrease with increasing temperature. This behavior is reminiscent of the closed loop, where the temperature of maximum intensity corresponds to the center of the closed loop. This represents the temperature at which density fluctuations are highest in magnitude. As a function of temperature, the location of this maximum shifts to higher temperatures. This behavior is a consequence of the pressure sensitivities of the enthalpic and entropic contributions to the system free energy, and its possible thermodynamic origins will be discussed later in this chapter.

The SANS data were then utilized to determine the pressure coefficient of the block copolymer. Ruzette and coworkers made use of the thermodynamic equivalence of temperature and pressure to shift SANS intensity, q*, and full-width at half maximum (FWHM) data along the temperature axis[3], using Equation 3.3

$$\Delta T = -\frac{dT}{dP}(P - P_0) \tag{3.3}$$

where ΔT is the temperature shift, P is the experimental pressure, and P_0 is the reference pressure, taken here to be atmospheric pressure. The data in Figure 3.9 were, then shifted in both the LODT and UODT regions along the temperature axis. The break point between the transitions was taken as the temperature of maximum intensity for each isobar. As long as the data points being shifted are close to the transition temperature, Equation 3.3 remains valid. The shifted data are shown in Figure 3.10.

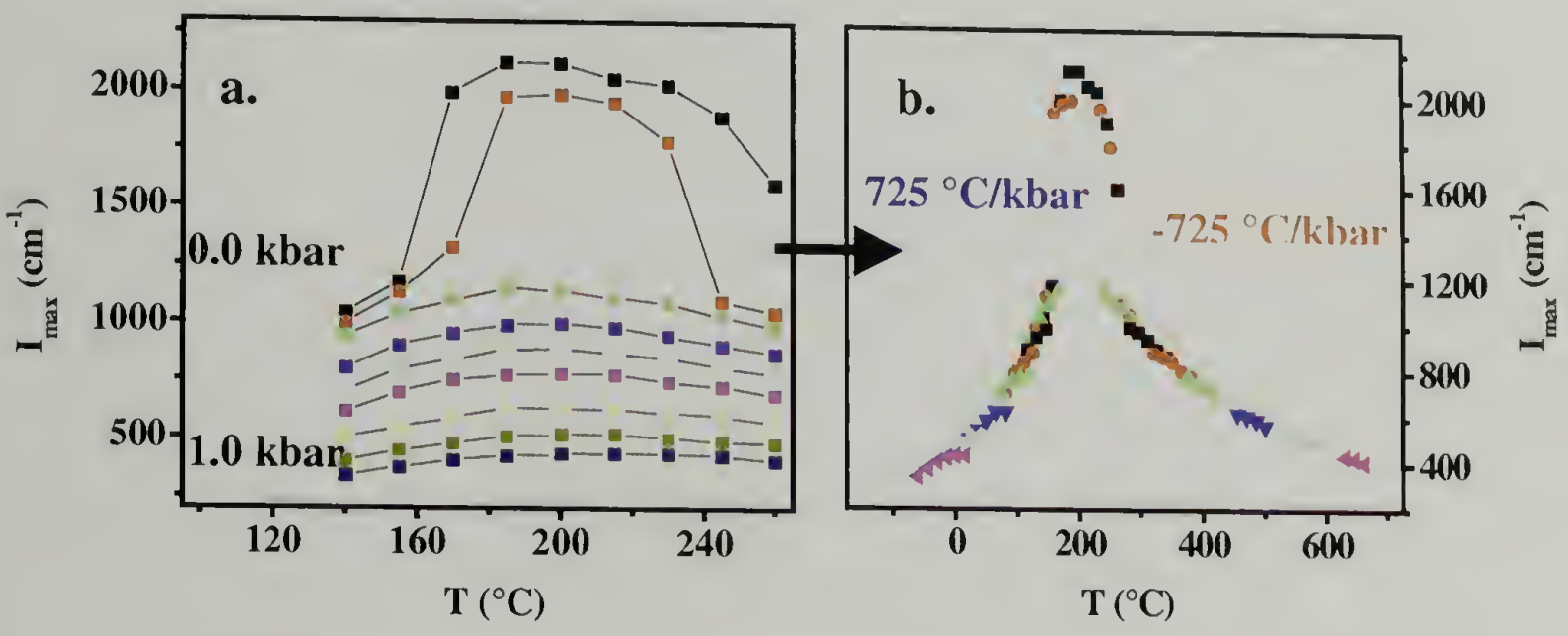

Figure 3.10: a. Maximum SANS intensity and b. the data shifted along the temperature axis by the pressure coefficients listed on the plot

As seen in Figure 3.10b, the data collapse onto a smooth curve when a pressure coefficient of 725°C/kbar is applied to the LDOT and a pressure coefficient of -725°C/kbar/kbar. These pressure coefficients are the largest determined for any block copolymer system to date, due to the large volume change on mixing in this sytem. Both values are also compatible with the predictions of Clausius-Clapeyron. The dT_{LDOT}/dP

determined via SANS of 725°C/kbar is similar in magnitude to the predicted 660°C/kbar, as is the dT_{UODT}/dP of -725°C/kbar close to the predicted -780°C/kbar.

In addition to the maximum scattering intensity, the width of the primary scattering peak is also of importance when evaluating the thermodynamic state of the block copolymer melt. In Figure 3.11 the full width at half maximum is plotted as a function of temperature for the series of pressures studied.

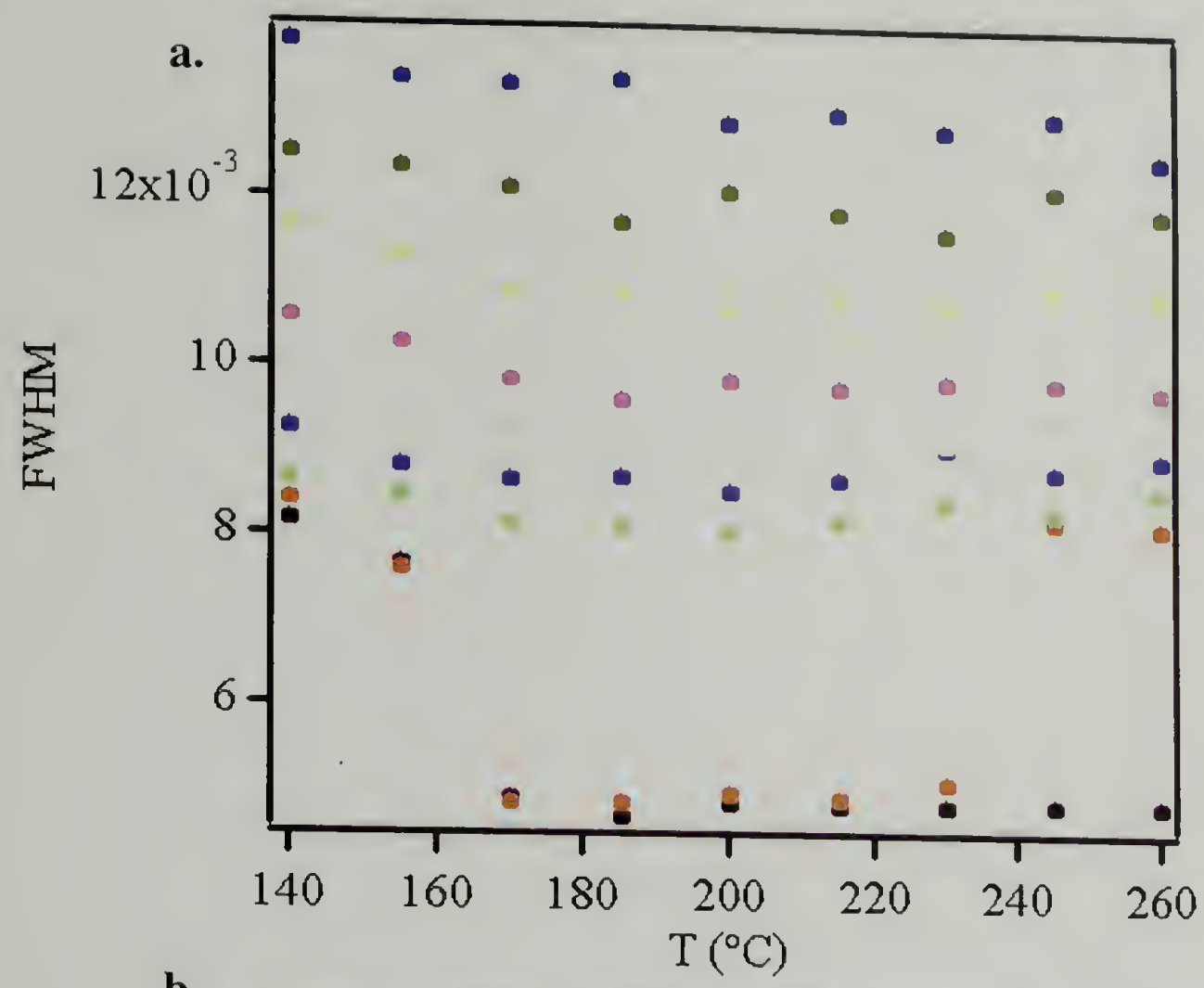

Figure 3.11: a. FWHM as a function of temperature at various pressures and b. shifted along the temperature axis

The pressure coefficients used to shift the data along the temperature axis were the same as those determined from the maximum intensity data. In the disordered state, the correlation hole scattering intensity at q* and FWHM can be used to determine an effective χ parameter from the incompressible random phase approximation described in Chapter 2. The iRPA formalism describes a system that is devoid of compressibility effects, that is the system volume should not change with pressure. We have shown that dPS-*b*-PnPMA is in fact highly sensitive to pressure. However, the χ_{eff} determined from fits to correlation hole scattering data can still be used to gain qualitative insight into the system thermodynamics, such as information on the pressure and temperature dependence of the enthalpic and entropic contributions to χ. Fits to dPS-*b*-PnPMA correlation hole scattering data were performed using the formalism set by Leibler, with modifications by Bates for polydispersity and dissimilar block Kuhn lengths[18, 19]. The polymer coils were assumed to obey Gaussian statistics, as described by the Debye function, g(x). Recall Equation 2.9, which related the block copolymer scattering function to the Flory-Huggins interaction parameter, χ. Fits to correlation hole scattering data were determined using only three independent variables; χ, the average statistical segment length $a_{avg} = a_i(V_i / V_0)^{1/2}$, and a pressure-independent scaling factor. Constant factors used in the fitting procedure include scattering lengths $b_{dPS} = 1.0656 \times 10^{-11}$ cm and $b_{PnPMA} = 1.493 \times 10^{-12}$ cm, $v_{ref} = \sqrt{(v_{dPS} * v_{PnPMA})} = 1.79 \times 10^{-22}$ cm^3, and the copolymer degree of polymerization, N = 368 with an $f_{PS} = 0.5$. A representative fit is given in Figure 3.12, where the independent variables were adjusted to maximize the statistical r^2 value.

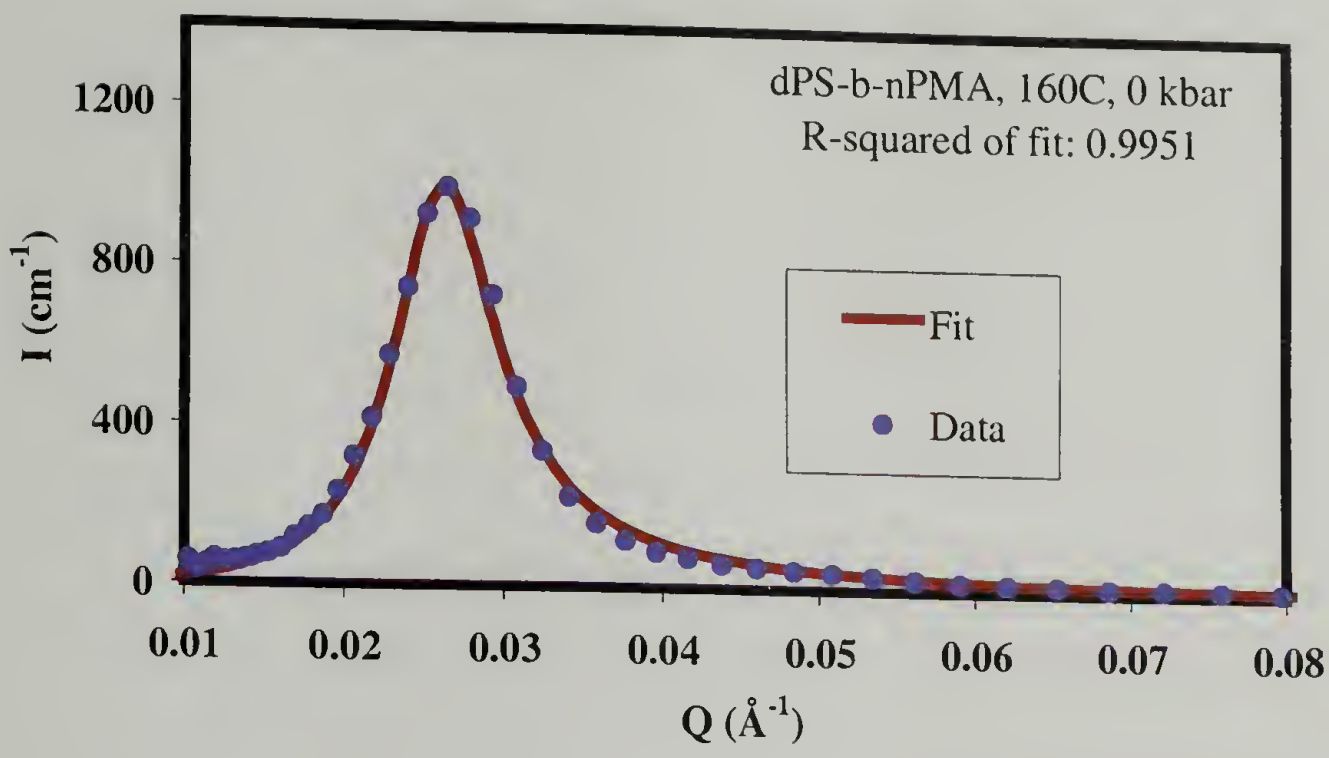

Figure 3.12: SANS data and theoretical fit using the iRPA theory

The χ_{eff} values determined from the above fits are plotted below in Figure 3.13 as a function of temperature for the pressure range studied, again shifted along the temperature axis by the pressure coefficients determined above. This placed all of the data on the same temperature scale, using atmospheric pressure as the reference pressure.

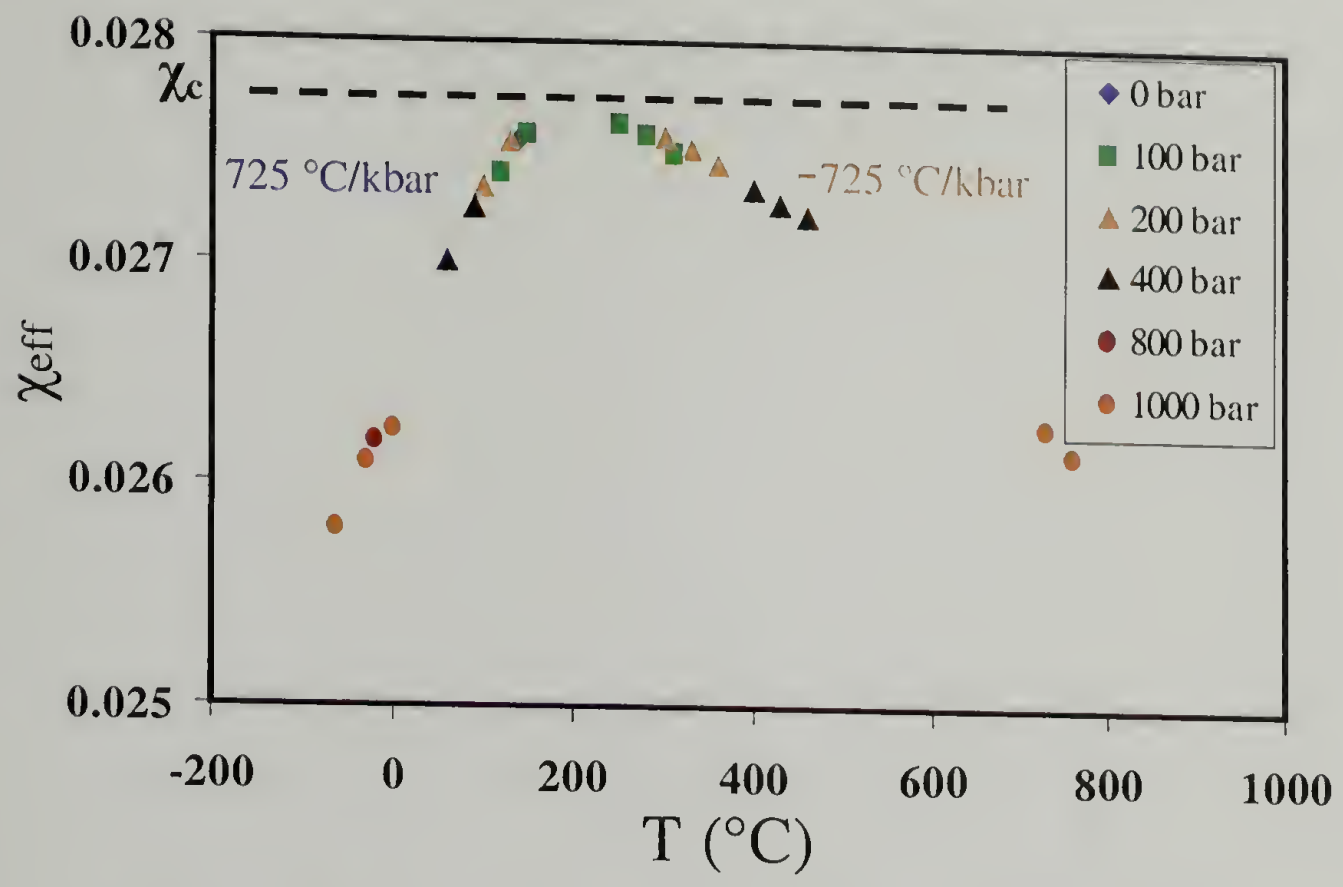

Figure 3.13: χ_{eff} as a function of temperature, shifted along the temperature axis using the pressure coefficients listed on the graph

This figure illustrates the unique χ behavior of the PS-*b*-PnPMA block copolymers. χ_{eff} increases with increasing temperature, up to χ_c where the system undergoes microphase separation (the LDOT). At higher temperatures, above the UODT where $\chi_{eff} < \chi_c$, the system χ_{eff} decreases with increasing temperature.

A common method of evaluating the entropic and enthalpic contributions to χ is through the form $\chi = A + B/T$ where A represents the enthalpic contribution and B represents the entropic contribution. A will always be positive, as enthalpic, repulsive interactions favor phase separation. B, however, can be either negative or positive depending on the nature of the entropic contribution. For instance, ODT systems will

have $B > 0$ because thermodynamic compatibility increases with increasing temperature. Likewise, LDOT systems will have a $B < 0$ such that χ increases with increasing temperature. This formalism, however, is insufficient to differentiate between the ODT and UODT, as the entropic contribution in both cases is positive. Therefore, we must evaluate the different contributions to the system entropy to get at the true nature of the UODT.

For the purpose of evaluating the phase behavior of weakly interacting systems Ruzette and Mayes[20, 21] developed a compressible modification to regular solution theory (Equation 1.3). This has proven to be a powerful tool for experimentalists for, despite its simplicity, it predicts phase behavior trends with great accuracy. All of the system-dependent parameters contained therein were either determinable by PVT experiments, or are easily calculated using group contribution methods[22]. In addition, the system free energy was written such that the contributions from segmental interactions, combinatorial entropy, and differential free volume were easily discernable. Table 3.3 lists the parameters used in the calculation of the phase behavior in PS-*b*-PnPMA block copolymers.

Table 3.3: Equation of state parameters used in the compressible regular solution theory calculations

Parameter	Polystyrene	Poly(n-pentyl methacrylate)
Hard core cohesive energy density $\delta^2_{i,0}$ (J cm^{-3})	385.54	394.32
Monomer molecular weight m_i (g mol^{-1})	104	156
Hard core segmental volume v_i (cm^3 mol^{-1})	83.96	124.64
Hard core density ρ_i^* (g cm^{-3})	1.24	1.23
Thermal expansion coefficient α_i (K^{-1})	5.13×10^{-4}	~7.6×10^{-4} and see below
Density at 298 K $\rho_{i,298}$ (g cm^{-3})	1.06	1.03
Reduced Density at 298 K $\tilde{\rho}_{i,298}$	0.855	0.813
Solubility parameter at 298 K $\delta_{i,298}$ ($J^{0.5}$ $cm^{-1.5}$)	18.19	18.14

The density measurements were carried out using dilatometry. The thermal expansion behavior of the polymer was assumed to take the form of Equation 3.4, where ρ^* is the hard core density of the polymer, extrapolated from dilatometry data to 0 K, and α is the thermal expansion coefficient.

$$\rho_i(T) = \rho_i * \exp(-\alpha_i T) \tag{3.4}$$

While styrene density data was described using this formalism, the density behavior of the poly(n-pentyl methacrylate) homopolymer deviated slightly from the ideal case. This data is shown in Figure 3.14.

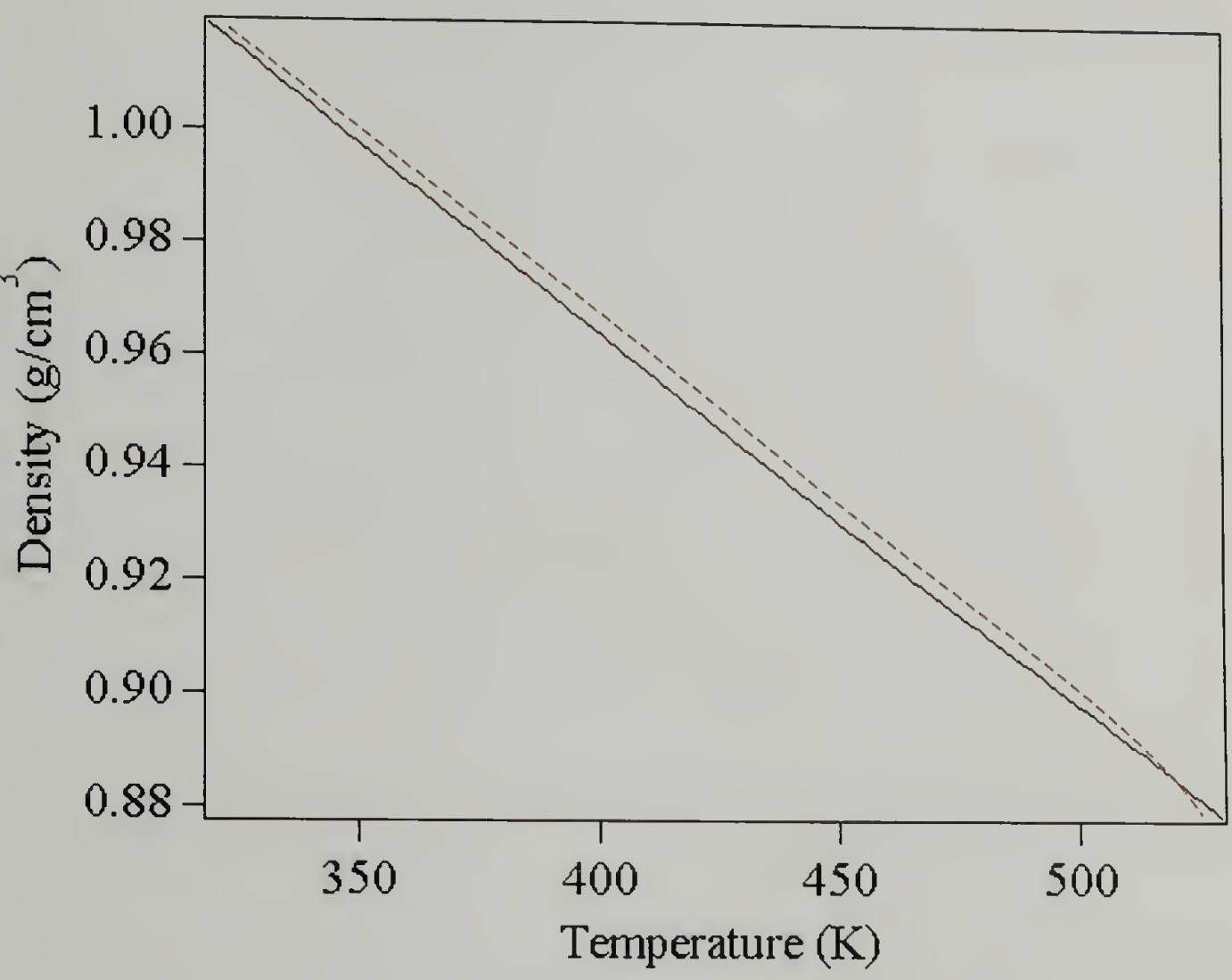

Figure 3.14: Density of 35K PnPMA as a function of temperature, determined using dilatometry (black) and a fit to this line using the form $\rho_i(T) = \rho_i * \exp(-\alpha_i T)$

Upon close inspection, the density data (black) does not follow the form in Equation 3.4, shown in red. At low temperatures (below 350 K) and at high temperatures (above 500 K) the change in density variation follows the fit closely. At intermediate temperatures,

however, the density variation deviates slightly from the fit. This small change in the system volume can have profound effects on the phase behavior of a system, especially in this system where the reduced volume and solubility parameters are so closely matched. In order to extract the thermal expansion coefficient as a function of temperature, a plot of the $-\ln(\rho_i(T)/\rho^*)$ versus temperature was constructed, as shown in Figure 3.15. This yields a plot with a slope of α. Differentiation of this data, then, gave the value of the thermal expansion coefficient as a function of temperature, which was used in the compressible RPA equations to predict the system phase behavior.

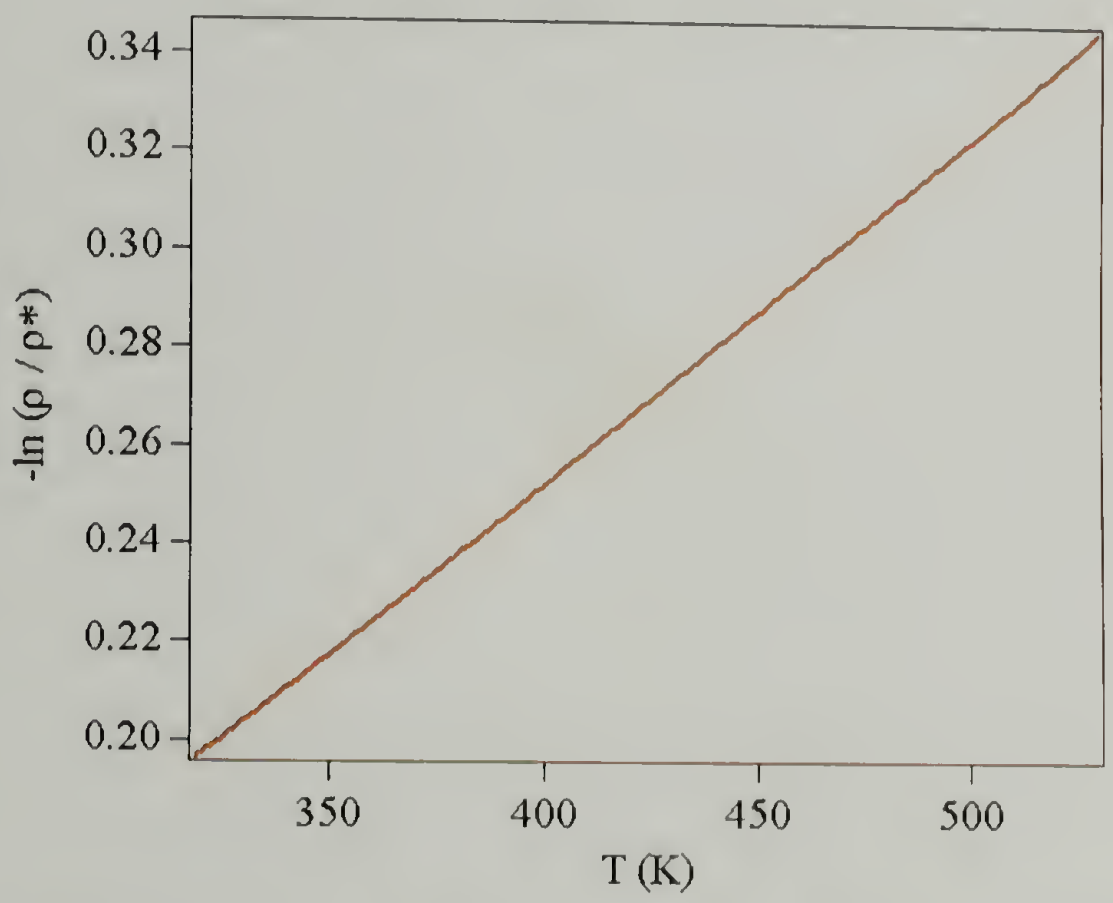

Figure 3.15: Plot for the determination of the thermal expansion coefficient variation as a function of temperature

The solubility parameters were determined from group contribution calculations, described by van Krevelen, where each functional group of the monomer subunit

contributes to the overall degree of dispersive, dipole-dipole, and hydrogen bonding forces exerted by the monomer. These contributions were determined for the styrene and n-pentyl methacrylate units at 298 K. Extrapolations to other temperatures, including the hard core cohesive energy density at 0 K, were carried out using Equation 3.5.

$$\delta_i^2(T) = -\frac{1}{2}\frac{z\varepsilon_{ii}\rho_i(T)}{M_w^i} = \delta_i^2(298)\left(\frac{\rho_i(T)}{\rho_i(298)}\right) = \delta_i^2(298)\left(\frac{\tilde{\rho}_i(T)}{\tilde{\rho}_i(298)}\right) \tag{3.5}$$

It is worth noting that PnPMA has an unusually high degree of thermodynamic compatibility with PS, both volumetrically (similar hard core density) and energetically (similar solubility parameters at 298 K). Of all the alkyl methacrylates, PnPMA has the closest solubility parameter to PS at 298 K, as shown in Figure 3.16. As a result the impact of volume, as affected by the thermal expansion behavior, may have a particularly magnified effect on the phase behavior of this system.

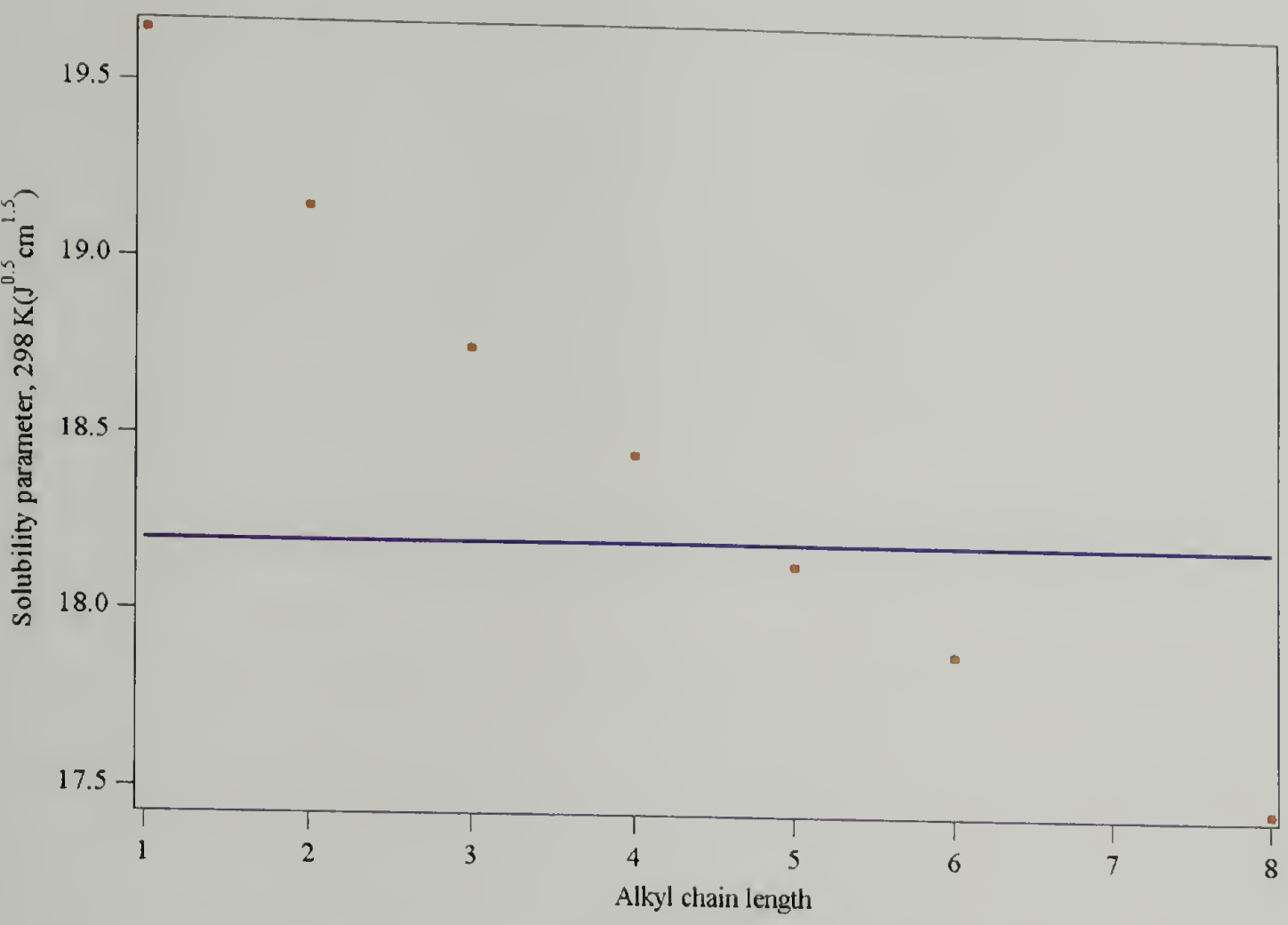

Figure 3.16: Solubility parameter at 298 K as a function of n-alkyl methacrylate side chain length compared to that of PS

Calculation of the PS-*b*-PnPMA phase behavior was carried out using the parameters determined above, using the relation for the second derivative of the free energy expression with respect to composition, as shown in Equation 3.6.

$$\left.\frac{\partial^2 \Delta g_{mix}}{\partial \phi_A{}^2}\right|_{T,P} \approx \left.\frac{\partial^2 \Delta g_{mix}}{\partial \phi_A{}^2}\right|_{T,P,\tilde{\rho}} = kT\left[\frac{\tilde{\rho}_A}{\phi_A N_A v_A} + \frac{\tilde{\rho}_B}{\phi_B N_B v_B}\right] - 2\tilde{\rho}_A\tilde{\rho}_B(\delta_{A,0} - \delta_{B,0})^2 - 2(\tilde{\rho}_A - \tilde{\rho}_B)(\delta_A{}^2 - \delta_B{}^2) \quad (3.6)$$

The stability criterion is $g_{\phi\phi} > 0$. The three contributions to the system phase behavior are neatly broken down into separate terms. The first term represents combinatorial entropy, the second the exchange interaction energy, and the third the differential free volume effects. Figure 3.17 shows the second derivative of the system free energy as a function of absolute temperature, determined from Equation 3.6.

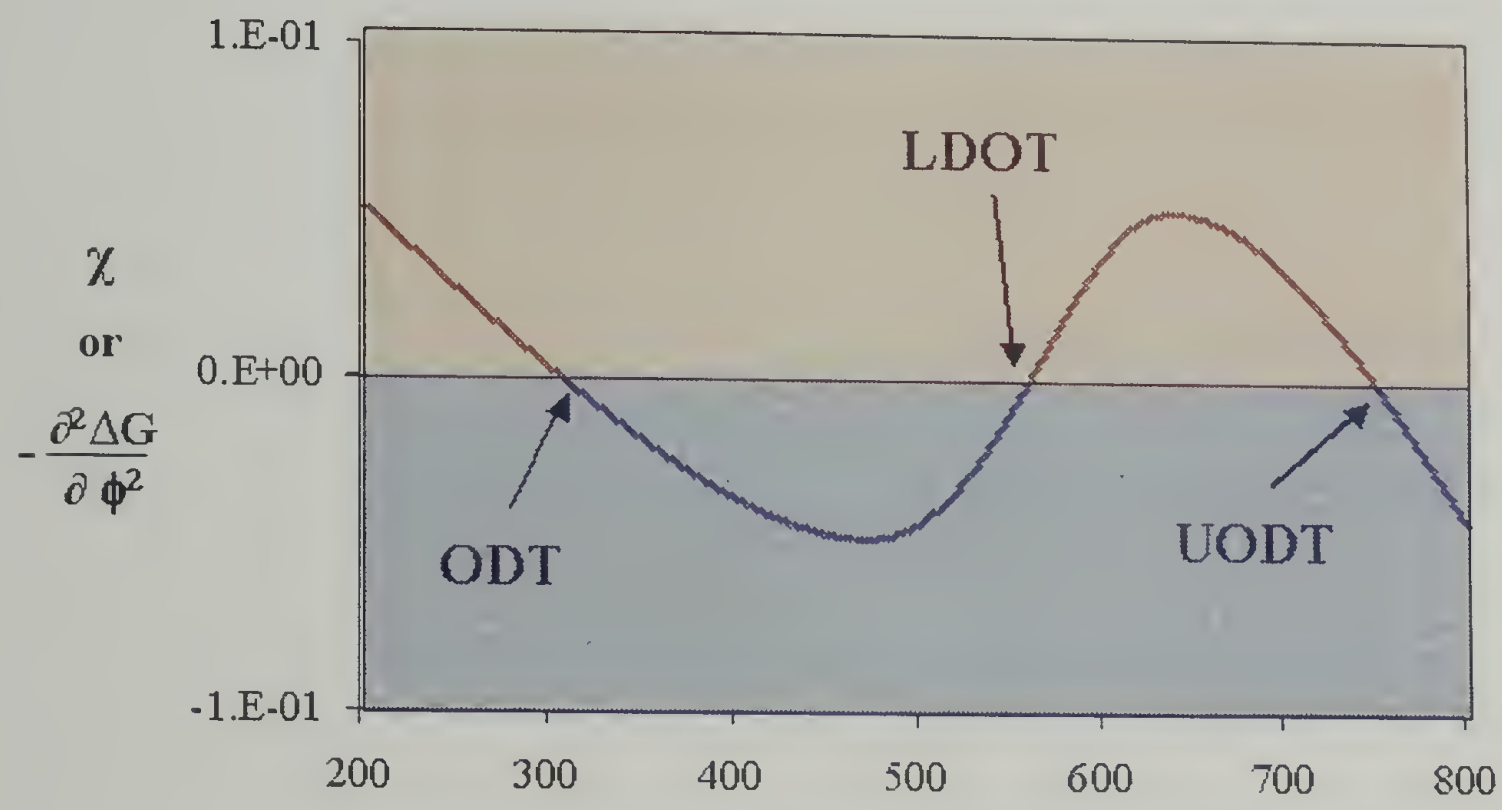

Figure 3.17: Calculated stability curve for 42K symmetric PS-*b*-PnPMA, where the red region indicated microphase separated and the blue phase mixed

In order to better understand to origins this phase behavior, the different contributions to the system free energy are drawn in Figure 3.18.

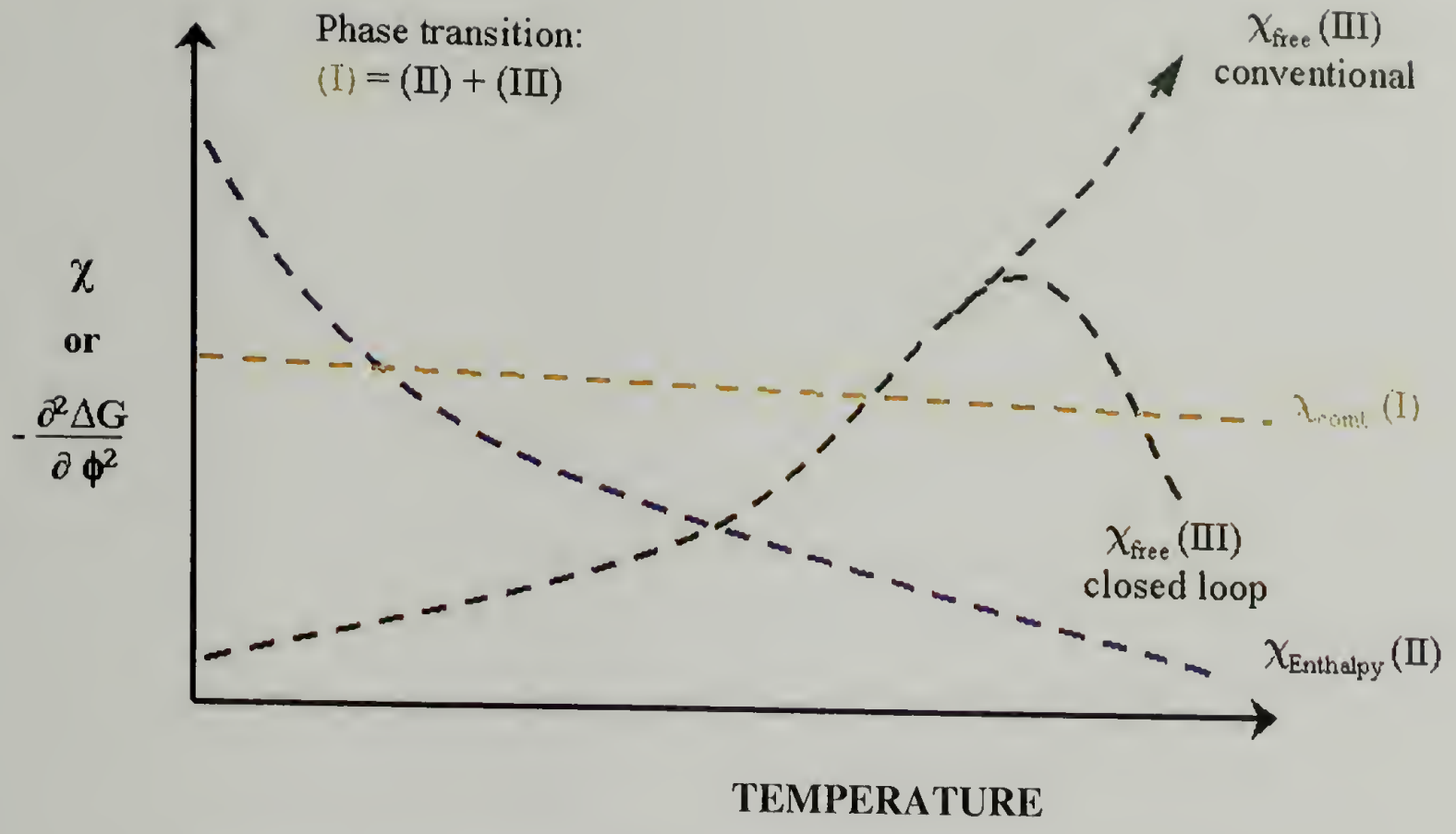

Figure 3.18: Schematic of the contributions to the system free energy

The orange curve represents the contribution from combinatorial entropy. This always favors mixing and is therefore always positive in sign. Its magnitude decreases slightly with temperature due to the effect of thermal expansion. The blue curve represents the contribution from enthalpy. This always favors microphase separation, and is therefore negative in sign. This decreases in magnitude with temperature due to the dilution of unfavorable interactions with thermal expansion. The third term is represented by the green curve. These contributions, due to differences in free volume and the changes in cohesive energy density with increasing dilation, tend to favor phase separation with increasing temperature. These terms contain the subtle effects necessary to describe LDOT and UODT behavior. If the two components of interest are similar in density and solubility parameter, yet have disparate thermal expansion behavior, this term will increase

in magnitude with increasing temperature, diverging and leading to LDOT behavior at elevated temperatures. This is shown in the green "conventional" curve. Once the sum of terms 2 and 3 are sufficient to overcome combinatorial entropy an LDOT will be observed. This is the case in systems such as PS-*b*-PnBMA and PS-*b*-PnOMA. In the case of PS-*b*-PnPMA, however, the situation is slightly more complicated. The temperature-dependent thermal expansion behavior caused the reduced densities of PS and PnPMA to approach one another at temperatures above the LDOT. Therefore, the magnitude of the free volume contribution decreases as shown in the green "closed loop" curve. Combinatorial entropy becomes larger in magnitude than the sum of terms 2 and 3, and this mixing term dominates the system free energy. This creates a UODT; the upper bound of the closed-loop phase diagram.

It should be noted that the UODT is a general case for block copolymers exhibiting LDOT-type phase behavior. There will be a temperature at which combinatorial entropy eventually overcomes differences in component free volume. This temperature, however, is extremely large and lies far above the degradation temperature of the polymers. The unique thermal expansion behavior of the PS-b-PnPMA system, combined with the extraordinary thermodynamic compatibility of these systems, lead to the observation of the closed-loop in an experimentally accessible temperature regime.

3.6 PnPMA Side-Chain Conformation

In order to predict the existence of the closed-loop an unusual form for the thermal expansion coefficient was used. While experimentally verified using dilatometry, the origins of this behavior were still unknown. One possible explanation lies with the five carbon side-chain. The work of Beiner *et al.* has illustrated that the length of acrylate or methacrylate side-chains has a marked effect on the polymer relaxation behavior[23]. They attributed this to a sort of "nanophase separation", where the longer ($C \geq 5$) alkyl side-chains are locally concentrated away from the polar acrylic COO unit. They observed this interchain spacing using WAXD, as shown in Figure 3.19.

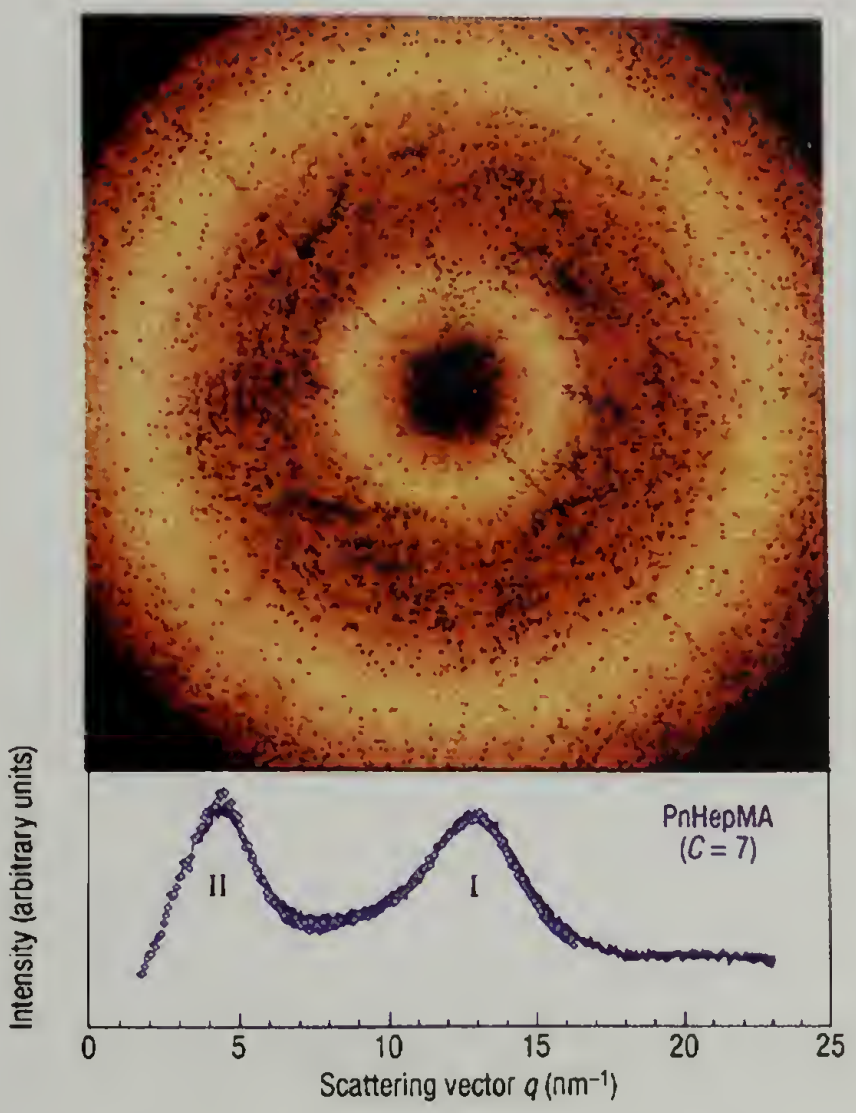

Figure 3.19: WAXD of PnHepMA at room temperature[23]

The wide-angle scattering trace shows two broad intensity regions. Peak I, at 13 nm^{-1}, was attributed to intramolecular van der Waals forces, while Peak II, at ~4 nm^{-1}, was attributed to the interchain spacing. This interchain spacing offered a potential means of observing the interchain distance, and possible changes in the side-chain length, upon heating. The results of this experiment are given in Figure 3.20.

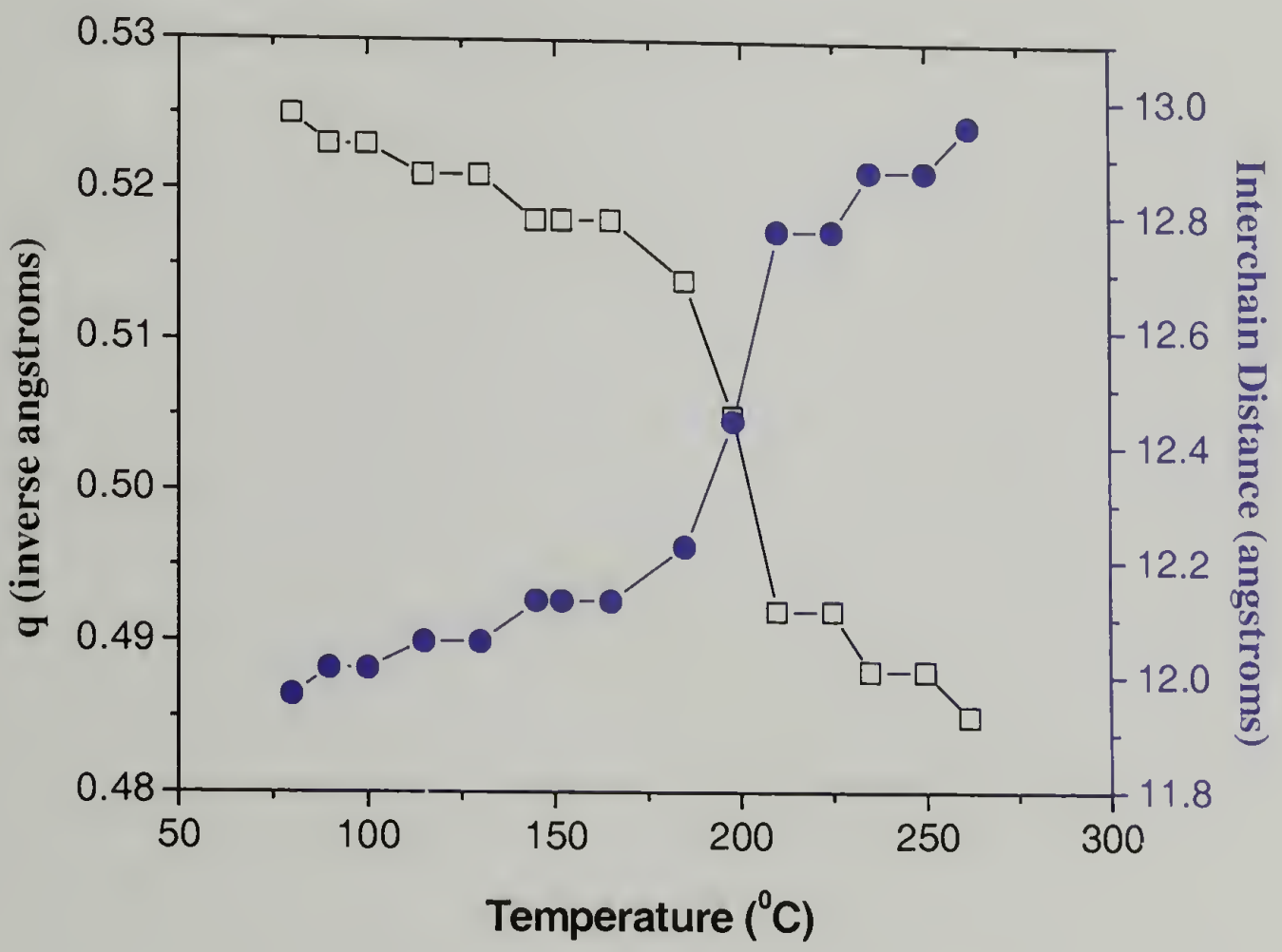

Figure 3.20: Interchain spacing as a function of temperature as determined from WAXD measurements

It should be noted that the block copolymer used to obtain the data in Figure 3.20 had an LDOT at 156°C and an UODT at 188°C. The WAXD measurements show a jump of ~ 0.5 nm, or 4%, in the interchain distance on passing through the ordered state near the

UODT. This increase in the interchain distance is likely indicative of the overall volume change of the block copolymer, which is known to decrease on passing from the disordered state through the LDOT. The experiments did not reach a large enough temperature to observe the UODT. The jump in interchain spacing, then, was attributed to the volume expansion on passing through the LDOT, which can be traced to the packing efficiency between the PS and PnPMA blocks in the homogeneous state.

Since interchain spacing via WAXD did not detetect any densification of the alkyl side-chain, other techniques needed to be employed. NMR would have been ideal for examining the conformation of the alkyl side-chain, but no high temperature NMR instruments were available that were able to reach 250°C. Raman scattering was then employed in order to examine the conformation of the alkyl side-chain at high temperatures. These data are shown in Figure 3.21.

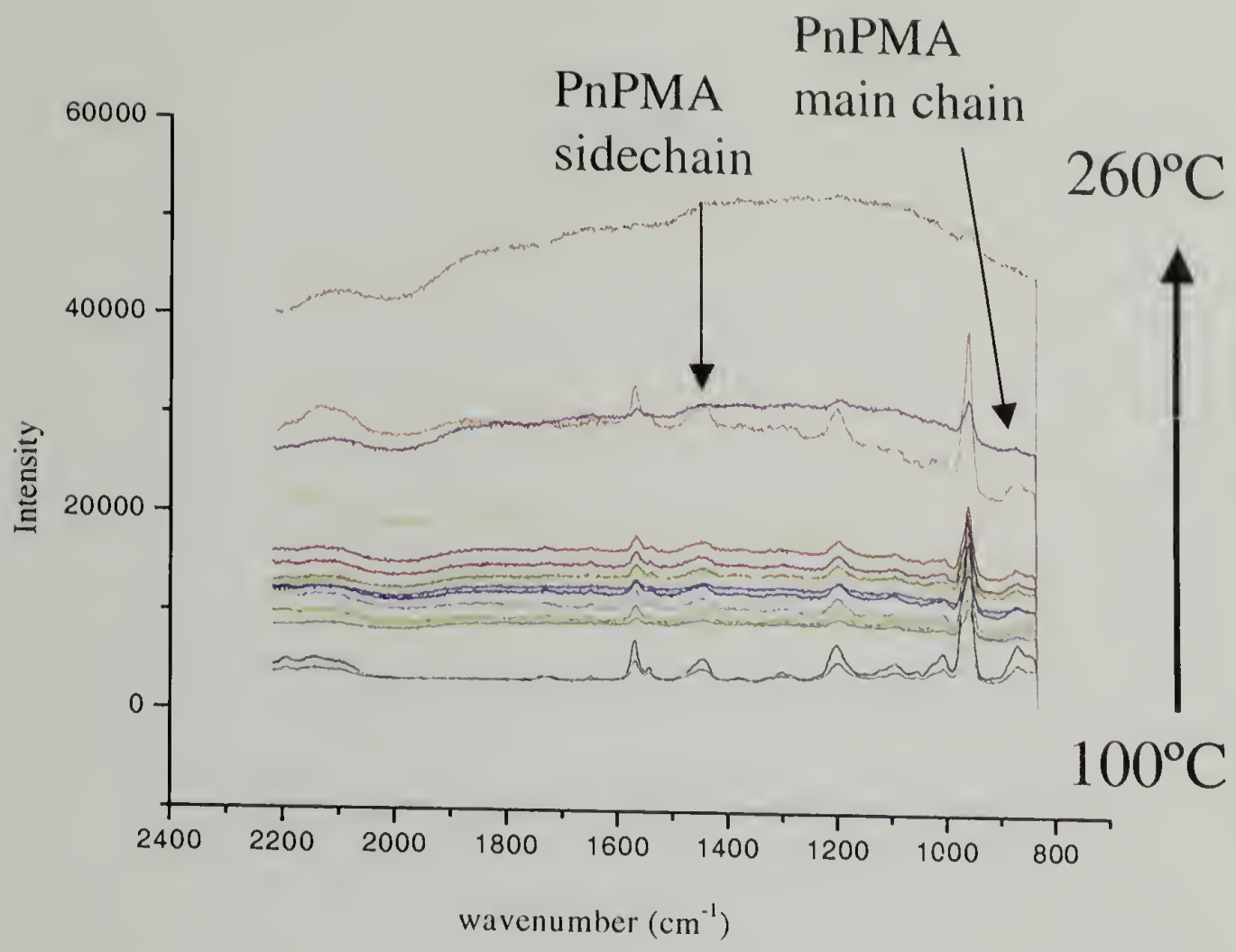

Figure 3.21: High temperature Raman scattering of PnPMA

There are two important peaks to note in this figure. The first is the C-C deformation along the PnPMA backbone, which occurs ~880 cm^{-1}. The second is the sidechain deformation, which occurs at ~1450 cm^{-1}. Shifts in the locations of these peaks indicate a change in the distribution of conformations of the C-C chains, for example a change in the relative numbers of trans to gauche conformations. An increased number of gauche conformations would be accompanied by a slight increase in the deformation energy. As observed in Figure 3.21, the main chain conformation did not change over the entire temperature range. However, the sidechain peak did experience a slight shift in the energy of the deformation.

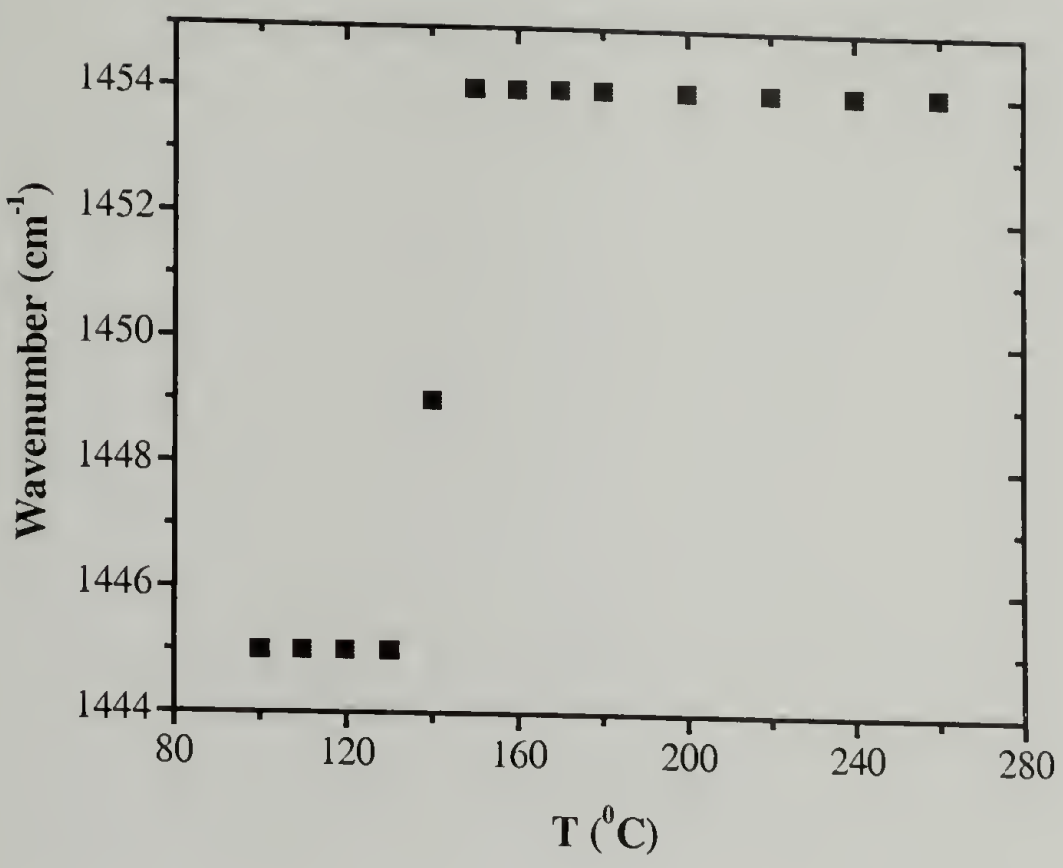

Figure 3.22: Raman sidechain deformation wavenumber as a function of temperature in PnPMA

This change, occurring at approximately 130°C, was attributed to a relative increase in the number of gauche conformations on the PnPMA sidechain. This may help explain the slight hitch in the thermal expansion curve. The sidechain undergoes a conformational transition from fully extended to the incorporation of gauche states. The thermal expansion coefficient, then, decreases slightly at the temperature of this transition, namely ~130°C. This may account for the deviation from ideal thermal expansion behavior observed in Figure 3.14. The thermal expansion curve, however, hints that the change in the sidechain conformational distribution may be more gradual than what is observed in the Raman peak shift. Other experimental techniques, such as NMR or SANS, may reveal more concrete information as to the state of the sidechain.

3.7 Conclusions

SANS was utilized as a means of uncovering the entropic origins of the closed-loop phase behavior observed in PS-*b*-PnPMA block copolymers. The pressure coefficients observed were the largest of any block copolymer studied to date. The existence of the closed-loop was explained using straightforward volumetric arguments obtained using a compressible modification to regular solution theory. Unusual thermal expansion behavior of the PnPMA homopolymer was observed, which allowed prediction of the closed-loop at experimentally accessible temperatures. The thermal expansion behavior was possibly due to a change in the side chain conformation.

References

1. Leibler, L., *Theory of Microphase Separation in Block Copolymers.* Macromolecules, 1980. **13**: p. 1602-1617.

2. Sanchez, I.C. and C.G. Panayiotou, *Equation of State Thermodynamics of Polymer and Related Solutions*, in *Models for Thermodynamic and Phase Equilibria Calculations*. 1994, Marcel Dekker, Inc.: New York. p. 187.

3. Ruzette, A.V., et al., *Pressure Effects on the Phase Behavior of Styrene/n-Alkyl Methacrylate Block Copolymers.* Macro., 2003. **36**(9): p. 3351-3356.

4. Ruzette, A.-V.G., et al., *Phase Behavior of Diblock Copolymers between Styrene and n-Alkyl Methacrylates.* Macromolecules, 1998. **31**(24): p. 8509-8516.

5. Hajduk, D.A., et al., *High-Pressure Effects on the Disordered Phase of Block Copolymer Melts.* Macromolecules, 1995. **28**: p. 7148-7156.

6. Hajduk, D.A., et al., *High-Pressure Effects on the Order-Disorder Transition in Block Copolymer Melts.* Macromolecules, 1996. **29**: p. 1473-1481.

7. Stuhn, B., *The Relation Between the Microphase Separation Transition and the Glass Transition in Diblock Copolymers.* Journal of Polymer Science:Part B:Polymer Physics, 1992. **30**: p. 1013.

8. Kasten, H. and B. Stuhn, *Density Discontinuity at the Microphase Separation Transition of a Symmetric Diblock Copolymer.* Macro., 1995. **28**: p. 4777.

9. Schwahn, D., et al., *Temperature and Pressure Dependence of the Order Parameter Fluctuations, Conformational Compressibility, and the Phase Diagram of the PEP-PDMS Diblock Copolymer.* Physical Review Letters, 1996. **77**(15): p. 3153.

10. Frielinghaus, H., et al., *Composition Fluctuations and Coil Conformation in a Poly(ethylene-propylene)-Poly(ethylethylene) Diblock Copolymer as a Function of Temperature and Pressure.* Macromolecules, 1996. **29**: p. 3263.

11. Pollard, M., et al., *The Effect of Hydrostatic Pressure on Lower Critical Ordering Transition in Diblock Copolymers.* Macromolecules, 1998. **31**(19): p. 6493-6498.

12. Gonzalez-Leon, J.A., et al., *Low-Temperature Processing of 'Baroplastics' by Pressure-Induced Flow.* Nature, 2003. **426**: p. 424.

13. Hammouda, B. and B.J. Bauer, *Compressibility of Two Polymer Blend Mixtures.* Macromolecules, 1995. **28**: p. 4505-4508.

14. Janssen, S., et al., *Pressure Dependence of the Flory-Huggins Interaction Parameter in Polymer Blends: A SANS Study and a Comparison to the Flory-Orwoll-Vrij Equation of State.* Macro., 1993. **26**: p. 5587.

15. Ryu, D.Y., et al., *Closed-loop phase behaviour in block copolymers.* Nat Mat, 2002. **1**(2): p. 114.

16. Ryu, D.Y., et al., *Effect of Hydrostatic Pressure on Closed-Loop Phase Behavior of Block Copolymers.* Physical Review Letters, 2003. **90**: p. 235501.

17. Pollard, M., et al., *Some Thermodynamic Considerations of the Lower Disorder to Order Transition of Diblock Copolymers*, in *Scattering from Polymers, ACS Symposium Series*, B.S. Hsiao, D.J. Lohse, and P. Cebe, Editors. 2000, American Chemical Society. p. 261.

18. Bates, F.S., J.H. Rosedale, and G.H. Fredrickson, *Fluctuation effects in a symmetric diblock copolymer near the order-disorder transition.* Macromolecules, 1990. **92**(10): p. 6255.

19. Bates, F.S., et al., *Fluctuations, Conformational Asymmetry and Block Copolymer Phase Behavior.* Faraday Discuss., 1994. **98**: p. 7.

20. Ruzette, A.V. and A.M. Mayes, *A Simple Free Energy Model for Weakly Interacting Polymer Blends.* Macromolecules, 2001. **34**: p. 1894.

21. Ruzette, A.V., et al., *A Simple Model for Baroplastic Behavior in Block Copolymer Melts.* J. Chem. Phys., 2001. **114**: p. 8205.

22. van Krevelen, D.W. and P.J. Hoftyzer, *Preperties of Polymers. Correlation with Chemical Structure.* 1972, New York: Elsevie Publishing Co.

23. Beiner, M. and H. Huth, *Nanophase separation and hindered glass transition in side-chain polymers.* Nat. Mat., 2003. **2**(9): p. 595.

CHAPTER 4

BLOCK COPOLYMERS SWOLLEN WITH COMPRESSED CARBON DIOXIDE

4.1 Supercritical Carbon Dioxide

Supercritical carbon dioxide has been an integral part of engineering and materials research for decades. Numerous technologies make use of the unique properties of supercritical fluids, namely the transport properties of a gas combined with the solution properties of a liquid, to perform unique chemistries, processes, and separations. Carbon dioxide has proven to be particularly advantageous in these applications due to an easily accessible critical point (T_c = 31°C, P_c = 74 bar), low cost, and safety of handling. An additional advantage arises from the tunable fluid density, which is plotted in Figure 4.1 as a function of pressure for a variety of temperatures.

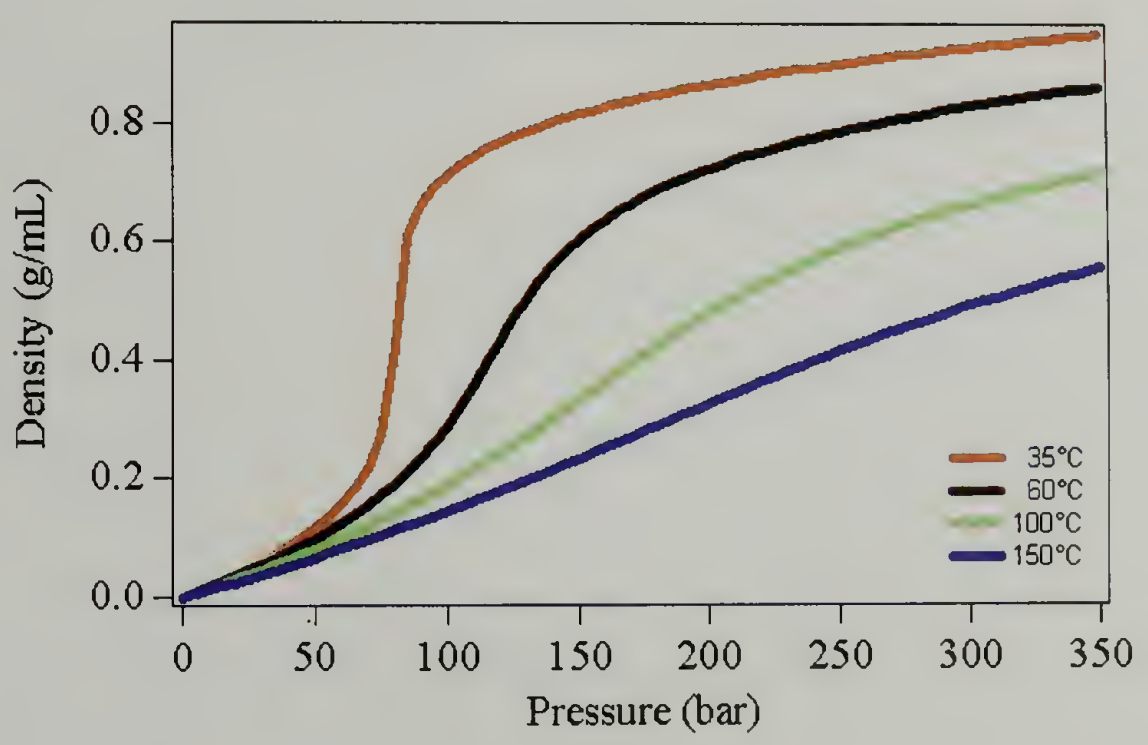

Figure 4.1: Carbon dioxide density as a function of pressure for a variety of temperatures[1]

As observed here, there is a continuous variation in system density as pressure increases, with a jump in density at the critical point[2]. At higher temperatures the density variation at the critical point becomes less severe. The consequence of this fact is that the solution properties of carbon dioxide, i.e. the solvent activity, can be dialed in by varying the system temperature and pressure. This facilitates control over the amount of solute dissolved in the fluid phase. This has been used to great advantage in extraction processes[2], where high fluid densities result in high solvent strength, and with a rise in temperature the solvent strength drops accordingly allowing precipitation of the solute.

Supercritical carbon dioxide is a solvent for many small molecules. This fact, combined with gas-like transport properties and low surface tension, has been used to great advantage to perform many interesting chemistries[3], including nanocrystal and nanoparticle synthesis[4], surface modifications[5], and high aspect ratio nanostructure growth[6]. Most macromolecules, however, are insoluble in supercritical carbon dioxide. The exceptions to this rule are many fluoropolymers, such as Teflon, polysiloxanes, such as PDMS, and poly(ether-*block*-carbonate) copolymers[7, 8]. While other classes of polymers fail to dissolve in carbon dioxide, they can absorb appreciable amounts of the fluid[9]. Carbon dioxide absorption has a substantial effect on the properties of the absorbing polymer, the most notable of these being the depression of T_g[10]. Figure 4.2 shows a plot of T_g as a function of carbon dioxide sorption in PS and PMMA.

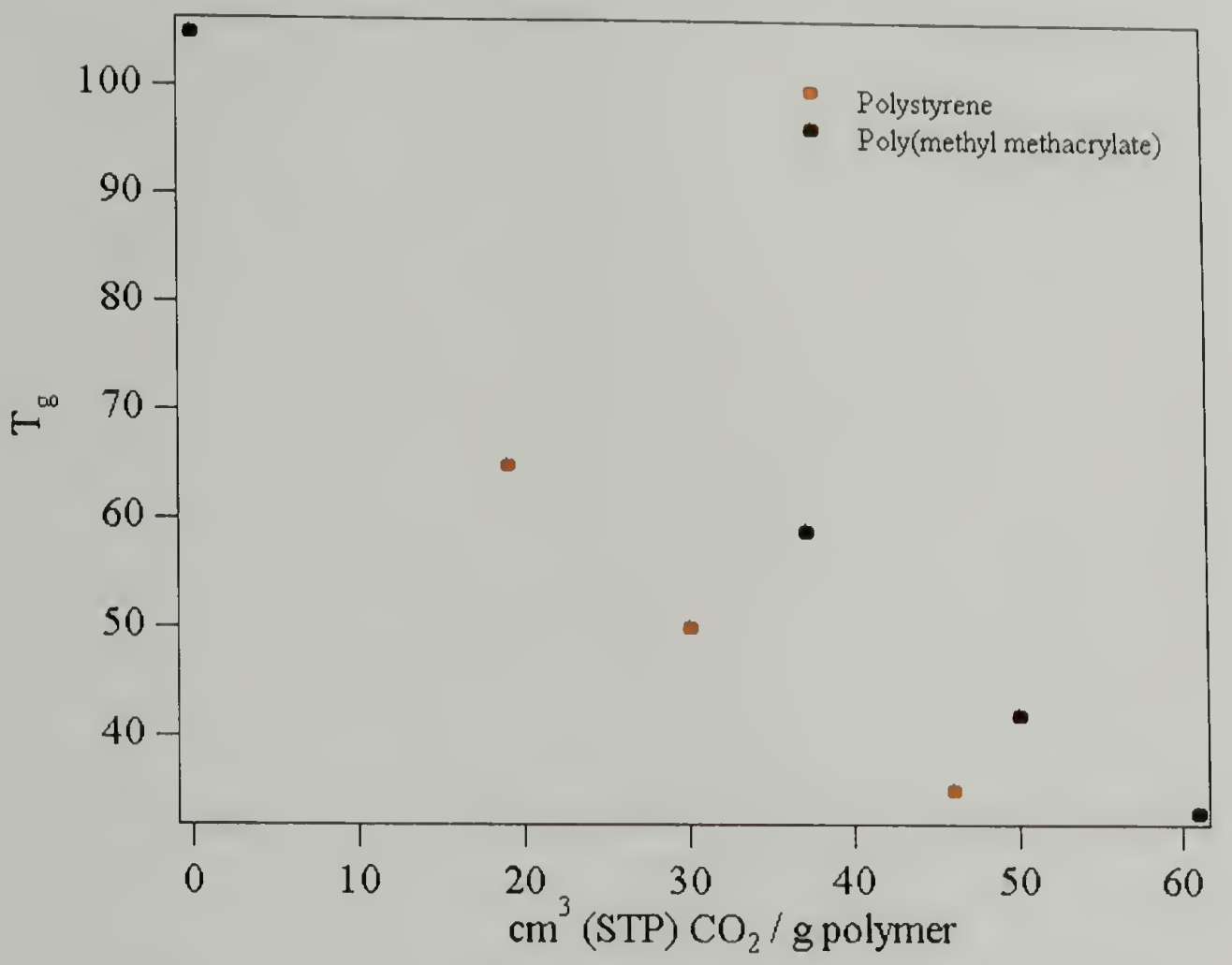

Figure 4.2: Glass transition temperature as a function of carbon dioxide sorption in PS and PMMA[10]

The decrease in T_g upon CO_2 sorption strongly enhances the transport properties of the swollen polymer, leading to increased self-diffusion coefficients. This will be discussed in greater detail in Chapter 5. In addition to the transport properties, carbon dioxide sorption increases the free volume of the swollen polymer[11]. As was discussed previously, polymer free volume has profound importance in the determination of the compatibility behavior of polymer systems. This is the subject of the current chapter, in which the use carbon dioxide sorption will be used to further understand and control the closed-loop phase behavior of the PS-*b*-PnPMA system. First will be an outline of the impact of carbon dioxide on other types of block copolymer phase transitions.

4.2 ODT-Type Block Copolymers

Order-to-disorder transitions in block copolymers result when the unfavorable interactions between dissimilar segments are overcome with increasing temperature. The influence of carbon dioxide sorption on the location of the ODT was explored by Vogt *et al.* using PS-*b*-PI[12] and PS-*b*-PnHMA[13] copolymers. This work showed that carbon dioxide promotes system miscibility, similar to the influence of liquid solvents. The location of the transition temperature as a function of CO_2 density is shown in Figure 4.3.

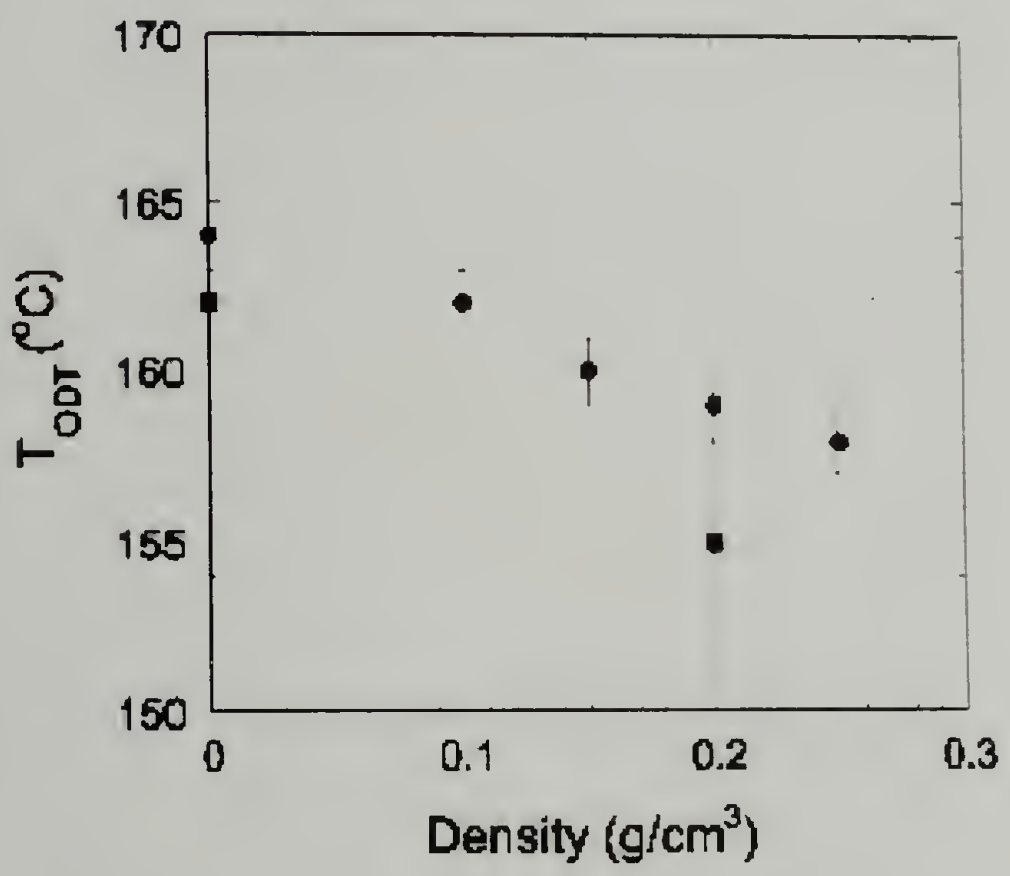

Figure 4.3: ODT temperature in PS-*b*-PnHMA as determined by birefringence (●) and SANS (■)[13]

Carbon dioxide effectively shielded the unfavorable interactions between components, decreasing their number density. As a result, the ODT was depressed by as much as 10°C at large carbon dioxide densities. As was mentioned above, this was similar to the

observation for liquid diluents. The work of Lodge *et al.* illustrated a depression in the ODT in PS-*b*-PI upon swelling with the neutral solvent dioctyl phthalate (DOP)[14]. They found that the dilution approximation, which assumes the solvent is evenly distributed throughout the block copolymer, did not hold as predicted by an ODT scaling ~ ϕ^{-1}. Instead, they found that the lamellar copolymer ODT ~ $\phi^{-1.6}$, and the cylindrical phase ODT ~ $\phi^{-1.4}$. The underestimation of the solvent-induced ODT depression was due to a preferential segregation of the solvent to the microdomain interface[15, 16]. This served to further mediate interactions, favoring homogenization at lower temperatures. Similarly, the lamellar PS-*b*-PI materials used by Vogt displayed a scaling of $\varphi^{-1.33}$ for similar molecular weights at large polymer volume fraction.

4.3 LDOT-Type Block Copolymers

Lower disorder-to-order transitions in block copolymers are driven by volumetric disparity between the blocks. As such, the increase in free volume imparted to the polymer through CO_2 sorption has a pronounced influence on the system compatibility. The first LDOT system studied under compressible fluids was PS-*b*-PnBMA, as investigated by Watkins and Russell[17]. It was found that CO_2 significantly depressed the LDOT temperature, promoting microphase separation. While the ODT-type system, PS-*b*-PnHMA exhibited an ODT depression of 7°C at 7% volume dilation, PS-*b*-PnBMA displayed an LDOT depression of 70°C at a dilation of only 3%[13]. This result is shown in Figure 4.4. It should be noted that there is a hysteresis on heating and cooling, likely due to the difference in CO_2 sorption in the ordered and disordered states. Carbon dioxide had

to be expelled from the polymer in passing from the ordered to the disordered state, thus depressing the transition temperatures upon cooling.

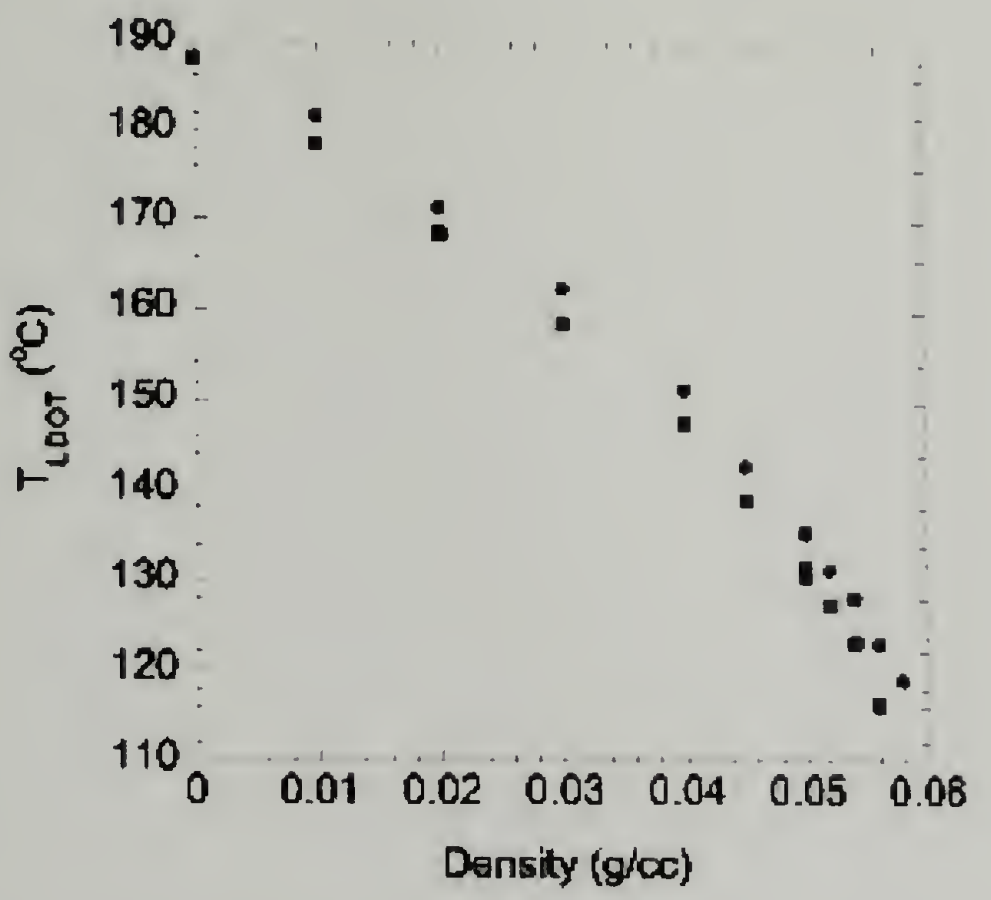

Figure 4.4: LDOT depression in PS-*b*-PnBMA on heating (●) and cooling (■)[13]

Additionally, the PS/ PVME homopolymer blend was explored by RamachandraRao *et al.* revealing a depression in the analogous LCST with carbon dioxide sorption[11].

4.4 PS-*block*-PnPMA

In Chapter 3 the origins of the closed-loop phase diagram in PS-*b*-PnPMA block copolymers were investigated using hydrostatic pressure. It was suggested that the closed-loop was volumetric in origin, and that miniscule changes in the thermal expansion coefficient had a profound influence on the microphase separation behavior. Carbon dioxide, being a compressible fluid, imparts free volume to the sorbing polymer. As such,

the volumetrically-driven phase transitions in PS-*b*-PnPMA should be highly sensitive to carbon dioxide swelling.

4.4.1 Preferential Swelling

In order to assess the influence of carbon dioxide on this block copolymer system the CO_2 absorption of the component materials must be determined. This was accomplished using equilibrium pressure decay sorption measurements as described in Chapter 2. 25K PS and 20K PnPMA were the molecular weights used in these measurements. The data are shown in Figure 4.5, in which the volume fraction of polymer after sorption is plotted as a function of solvent strength, or activity, of carbon dioxide.

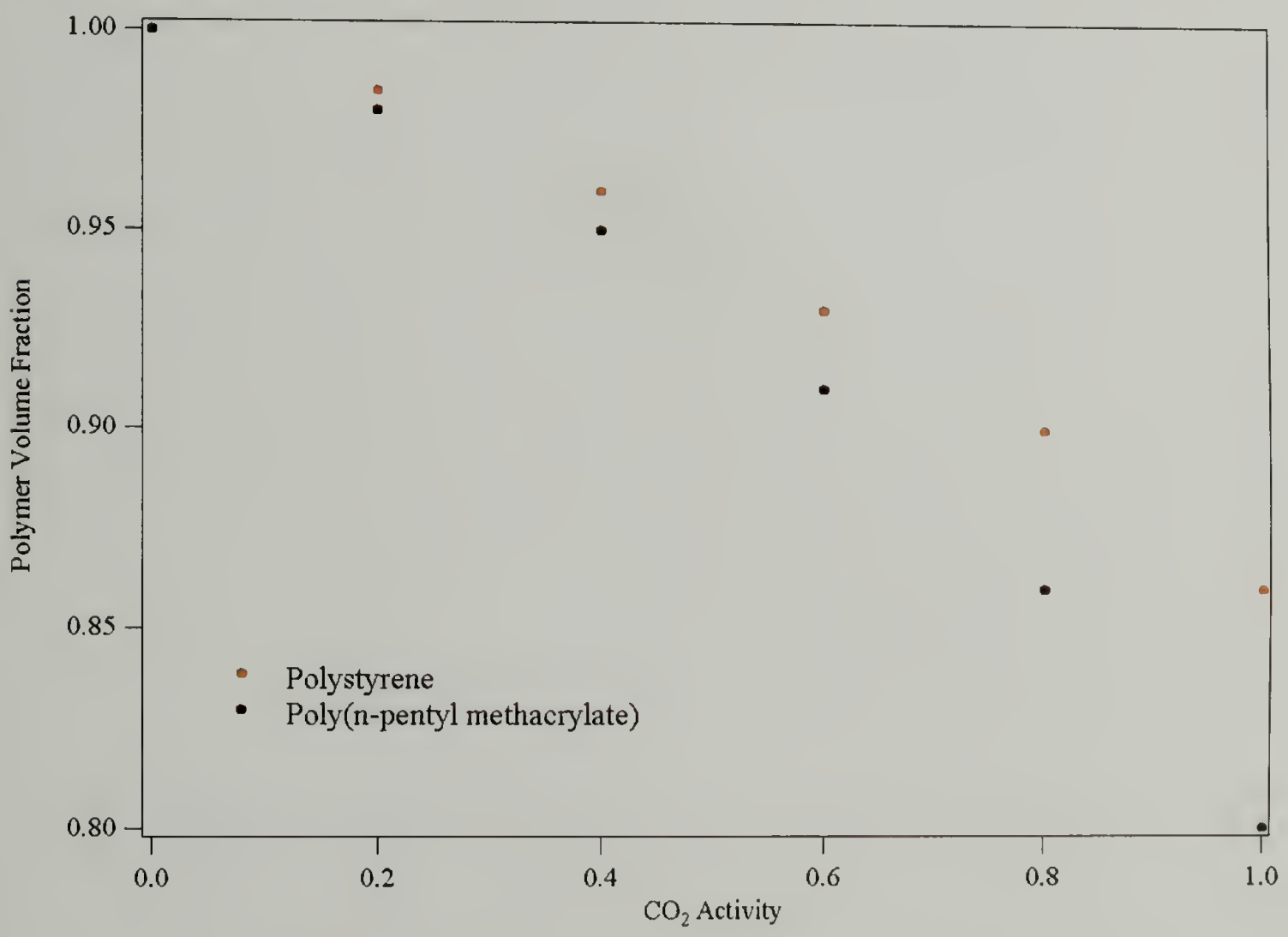

Figure 4.5: Polymer volume fraction as a function of CO_2 activity for 20K PS and 22K PnPMA

The experiments were carried out isothermally at 160°, varying activity through a variation in pressure. It has been shown previously that swelling isotherms for a given homopolymer collapse if all data are plotted on a volume fraction versus activity scale[18], so measurements were only carried out at one temperature. This adequately represented the influence of CO_2 solvent strength on homopolymer sorption.

The activity of carbon dioxide was calculated using Equation 4.1, given below.

$$A = \frac{P(T,V)\phi(T,V)}{P^{sat}(T,V^{sat})\exp\left(\frac{\overline{V}_R}{RT}(P - P^{sat})\right)} \tag{4.1}$$

Here, $\phi(T,V)$ is the fugacity coefficient, calculated using the Peng-Robinson equation of state, $\overline{V}_R$ is the specific volume of sorbed carbon dioxide, and the *sat* superscript represents the saturation value[11, 13]. The Antoine equation was used to extrapolate the vapor pressure, chosen for its relative accuracy near the critical point. This equation, including the Antoine coefficients for CO_2, is given in Equation 4.2.

$$\log P_{vap} = 7.046268249 - \frac{597.5752878}{T + 227.6017026} \tag{4.2}$$

The specific volume of CO_2 in the sorbed polymer was assumed to be 46.2 mL/mol in both homopolymers, as determined in the literature[19]. The Peng-Robinson EOS parameters, a and b, were calculated using Equations 4.3a and b, given below.

$$a = \left(\frac{0.45724 \cdot R^2 \cdot T_c^{\,2}}{P_c} \right) \left(1 + k \left(1 - \left(\frac{T}{T_c} \right)^{0.5} \right) \right)^2 \tag{4.3a}$$

$$b = \frac{0.07780 \cdot R \cdot T_c}{P_c} \tag{4.3b}$$

where

$$k = 0.37464 + 1.54226w - 0.026992w^2 \tag{4.3c}$$

using the CO_2 accentric factor, w, of 0.225. The carbon dioxide volumes were then calculated in both the fluid and sorbed phases by solving Equation 4.4 for V.

$$P_i = \frac{RT}{V - b} + \frac{a}{V(V + b) + b(V - b)} \tag{4.4}$$

The activity calculation in Equation 4.1 requires knowledge of the fugacity coefficients, ϕ_i, which are calculated using an isothermal Gibbs departure function, as given in Equation 4.5.

$$\phi_i = \exp\left[(z_i - 1) - \ln\left(z_i - b \cdot \frac{P_i}{RT}\right) - \frac{a}{2^{1.5} bRT} \ln\left(\frac{V_i + (1+2^{0.5})b}{V_i + (1-2^{0.5})b}\right)\right] \qquad (4.5)$$

where z_i is the compressibility factor, which describes the system deviation from ideal PVT behavior $z_i = P_i V_i / R T$.

It has been shown that carbon dioxide activity accurately quantifies the degree of swelling of a given homopolymer. These data can be used to accurately describe the swelling in the microphase separated state, where the total extent of swelling is the arithmetic mean of swelling from each component weighted by the component volume fraction. These calculated activities, then, were used in quantifying the effect of carbon dioxide sorption on the closed-loop phase behavior of PS-*b*-PnPMA block copolymers. The closed-loop is composed of the LDOT as the lower bound, and the UODT as the upper bound. In Chapter 3 it was shown that volumetric disparity between the components gave rise to this miscibility gap, which was overcome by combinatorial entropy at higher temperatures. In order to confirm these entropic origins, the impact of differential dilation with carbon dioxide was explored.

4.4.2 Birefringence Measurements

High-pressure birefringence measurements were undertaken as a means of determining the locations of the UODT and LDOT temperatures as a function of carbon dioxide activity. The pressure cell used, designed by the Watkins group at the University of Massachusetts Chemical Engineering Department, was stainless steel with sapphire windows and an allowable pressure range of atmospheric to 4500 psi. Figure 4.6 shows a

representative birefringence trace under carbon dioxide pressure. All measurements were performed at constant CO_2 activity, increasing temperature at 0.1°C/minute intervals near the transition temperatures. The sharp increase in detected light intensity indicated the location of a microphase separation transition. These measurements were performed using both lamellar (50/50 volume fraction) and cylindrical (41/59) block copolymers of 49 KDa molecular weight. Figure 4.7 shows the location of the LDOT and UODT as a function of carbon dioxide activity for these two block copolymers.

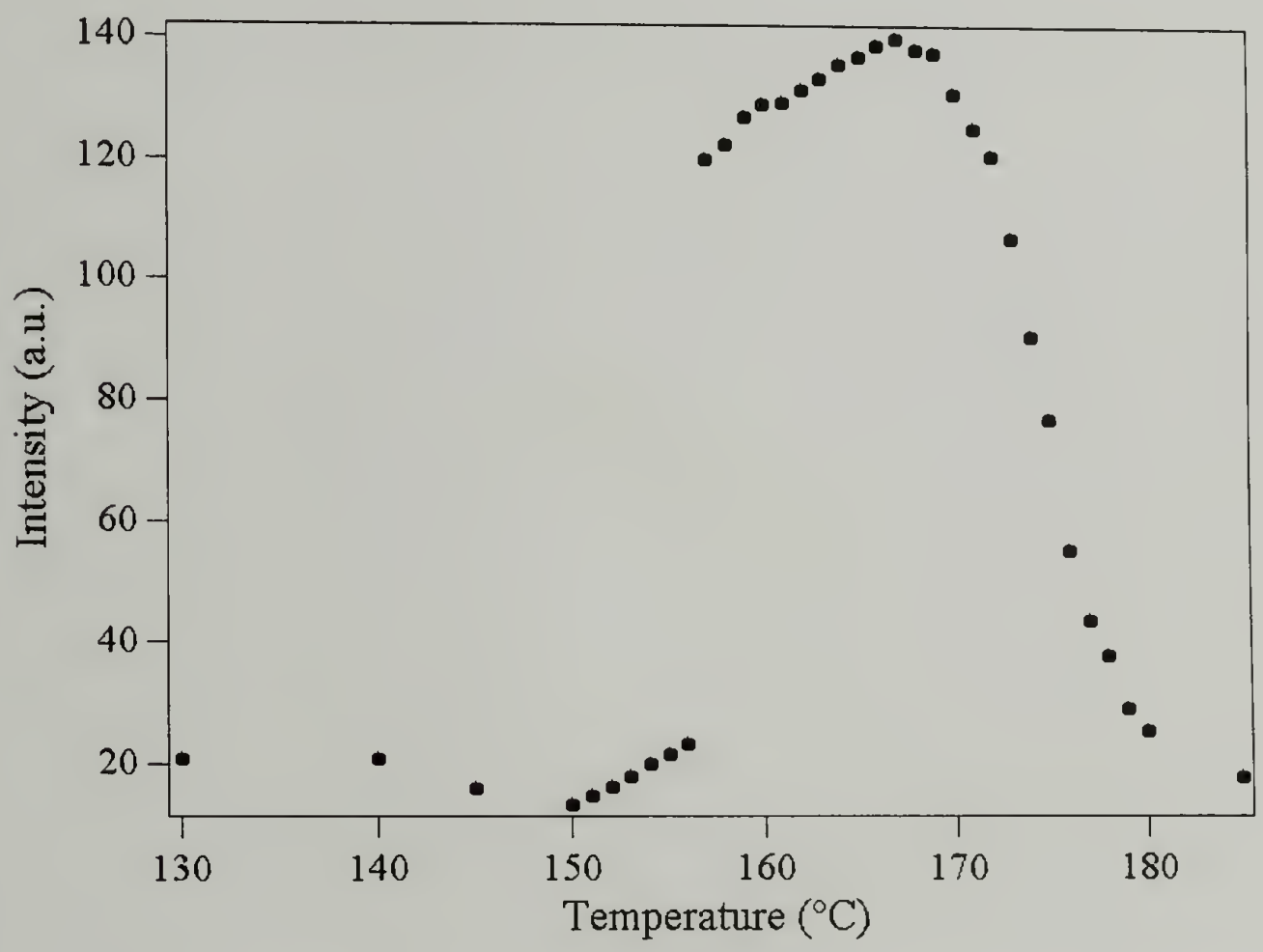

Figure 4.6: Representative birefringence trace for 41/59 PS-*b*-PnPMA at CO_2 activity of 0.1

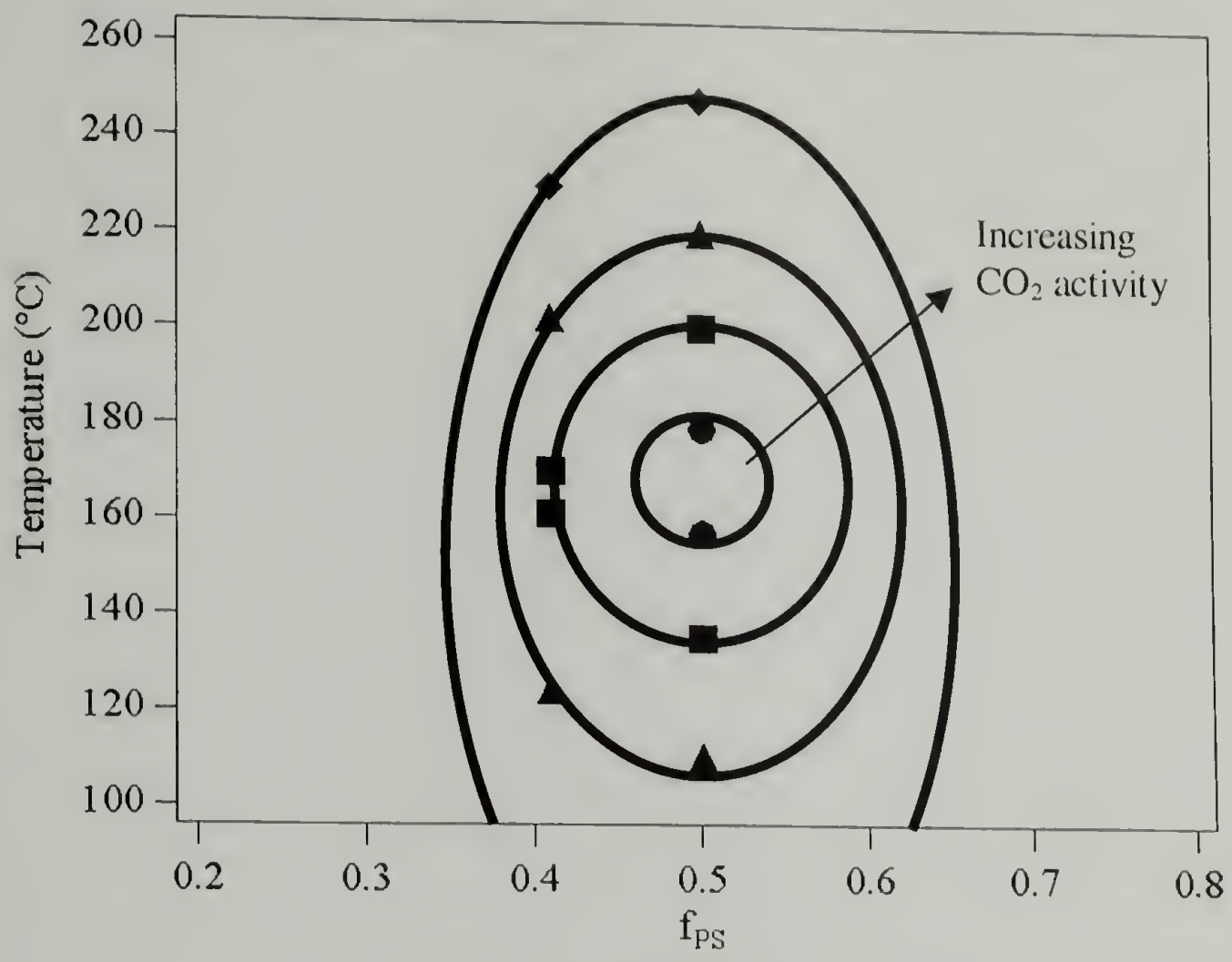

Figure 4.7 Closed-loop expansion in 49 K PS-*b*-PnPMA

As seen in Figure 4.7, the size of the closed-loop is appreciably increased at higher carbon dioxide activities. For the symmetric composition, the closed-loop was accessible at atmospheric pressure with the LODT at 157°C and the UODT at 179°C. The application of a small amount of carbon dioxide, having an activity of 0.1, affected an appreciable UODT elevation and LDOT depression. This increase in the size of the immiscibility window was due to the differential dilation of the system when swollen with carbon dioxide. As a slightly selective solvent for PnPMA, carbon dioxide swelling exacerbated the volumetric disparity in the system, driving the block copolymer further into the microphase separated state. Transition temperatures higher than 250°C were not observed due to polymer degradation and pressure cell o-ring limitations. Temperatures below 100°C were likewise unattainable due to slow polymer kinetics near T_g. Within the

experimentally-accessible temperature range the closed-loop expansion was roughly symmetric, with the UODT increasing at 23.0°C/0.1 activity unit, and the LDOT decreasing at 23.5°C/0.1 activity unit. Additionally, the asymmetric block copolymer studied was fully disordered over the complete temperature range at atmospheric pressure. However, at 0.1 carbon dioxide activity the copolymer was driven into the microphase separated state, displaying both LDOT and UODT temperatures. At larger activity the closed-loop expanded, although the expansion was greater in magnitude in the asymmetric material, being 30.0°C/0.1 activity unit for both the UODT and LDOT. This was thought to be a function of increased CO_2 loading, as this copolymer had PnPMA as a major component. This led to larger volumetric disparity than in the symmetric material at the same CO_2 activity.

It should be noted that all transitions measured were corrected for hydrostatic pressure. As was shown previously, hydrostatic pressure has an appreciable impact on the phase behavior of PS-*b*-PnPMA block copolymers. When measuring the effect of carbon dioxide dilation on closed-loop expansion, the tendency of hydrostatic pressure to miscibilize the system needed to be accounted for. The pressure coefficients of 725°C/kbar and -725°C/kbar for the LDOT and UODT were applied at each data point in Figure 4.7 such that the only effect illustrated was that from preferential swelling. To illustrate the effect of this correction, Figures 4.8a and b are plots of the location of the UODT in 42K, 50/50 PS-*b*-PnPMA. At atmospheric pressure this copolymer is fully disordered, however at activities above 0.20 the closed-loop is observed.

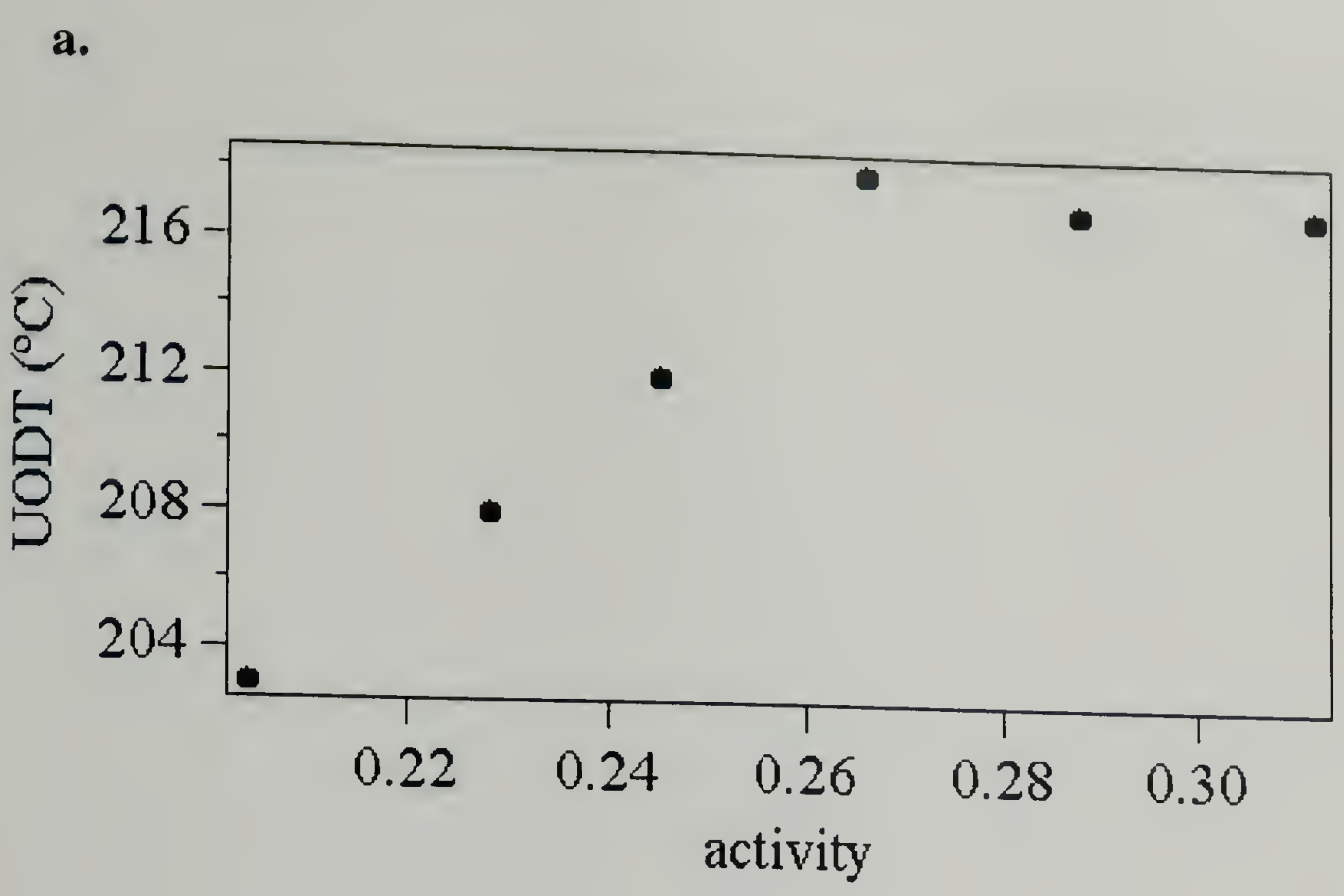

Figure 4.8: a. UODT as a function of CO_2 activity before hydrostatic pressure correction and b. UODT temperature after correction for hydrostatic pressure

The resulting UODT increase with CO_2 activity is linear, with one deviant data point at an activity of approximately 0.265. This was at the critical pressure of carbon dioxide. Since

the temperature was far above the carbon dioxide critical temperature this deviation was likely not due to critical phenomena, such as critical wetting which can result in enhanced fluid sorption. Instead, it is well known that activity calculations have increased error near the critical point. This error is the likely root of the deviation of that data point.

4.4.3 Compressible Regular Solution Theory Calculations

In Chapter 3 the closed-loop phase diagram was predicted using straightforward volumetric arguments, set forth by Ruzette *et al.*, in which regular solution theory was modified to account for component density changes as a result of thermal expansion[20, 21]. Carbon dioxide can be considered a differential diluent. As such, the free volume it imparts to the block copolymer segments can be evaluated using the same formalisms described previously to account for thermal expansion. If the closed-loop expansion was driven predominantly by volumetric differences, reduced density arguments should accurately capture this effect. The swelling data shown above were used to calculate the reduced density and solubility parameter of the PS and PnPMA blocks as a function of CO_2 temperature and pressure. The results are shown in Figures 4.11 and 4.12 below.

In Figure 4.11, the UODT temperature for 39.9K lamellar PS-*b*-PnPMA, as determined from birefringence measurements, is plotted as a function of carbon dioxide activity. In red is shown the prediction from the compressible regular solution theory arguments, in which differential dilation is shown to appreciably elevate the location of the UODT. The transition temperature location is unreasonably high, but the theory was successful at predicting the trends observed in the swelling experiments.

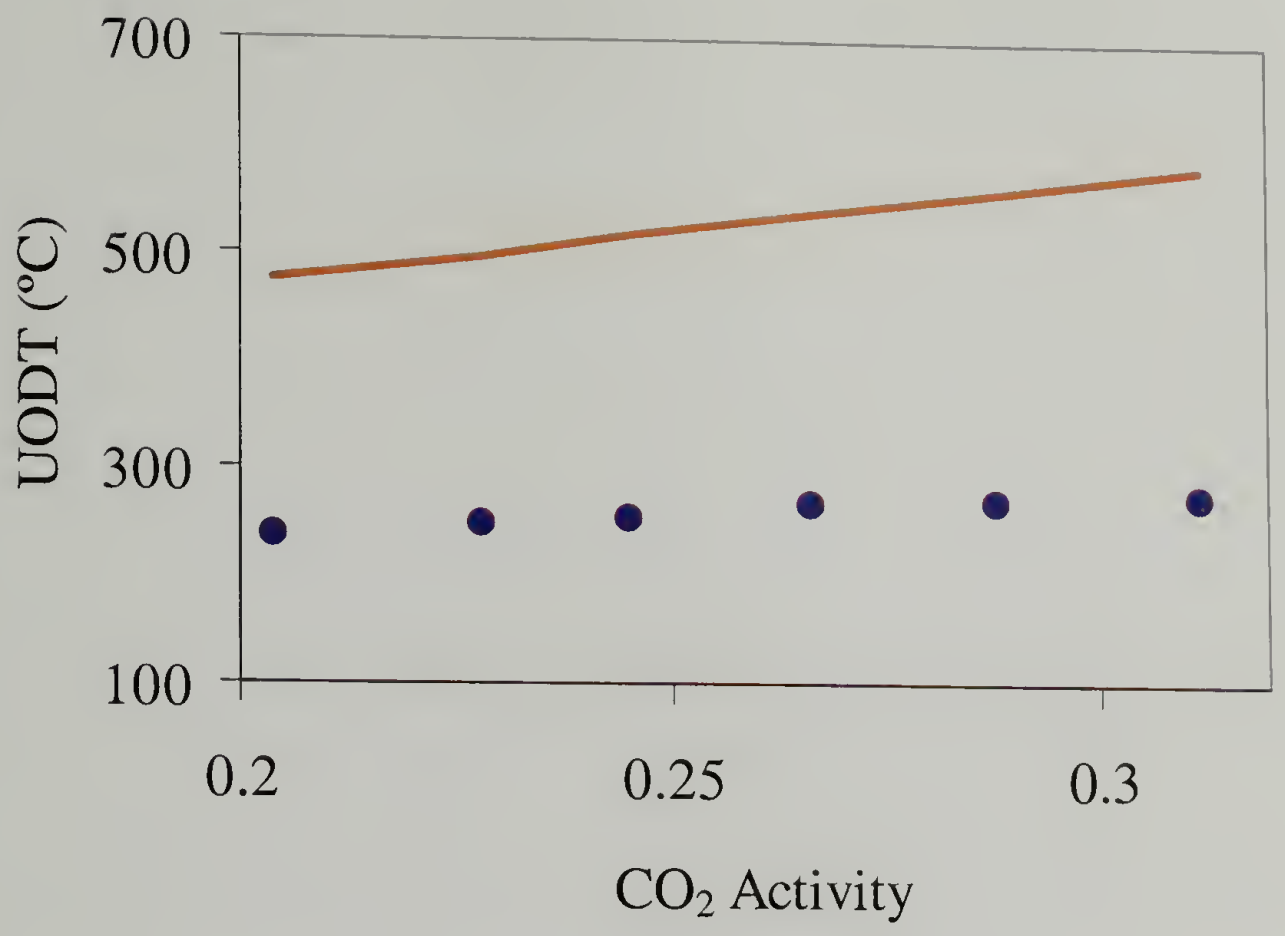

Figure 4.9: Effect of carbon dioxide dilation on the UODT in 39.9K PS-*b*-PnPMA from birefringence measurements (●) and cRST calculations (—)

The UODT underwent an elevation of 34˚C/0.1 activity unit, while the cRST predicted a rise of 67˚C/0.1 activity unit. While the cRST calculated the correct trend, the theory slightly overpredicted its magnitude. Even still, the theory was correct in showing that the carbon dioxide will significantly elevate the UODT, treating the fluid simply as a differential diluent with no enthalpic contribution to the system phase behavior. The influence of compressed carbon dioxide on the LDOT is shown in Figure 4.10, below, for the same block copolymer.

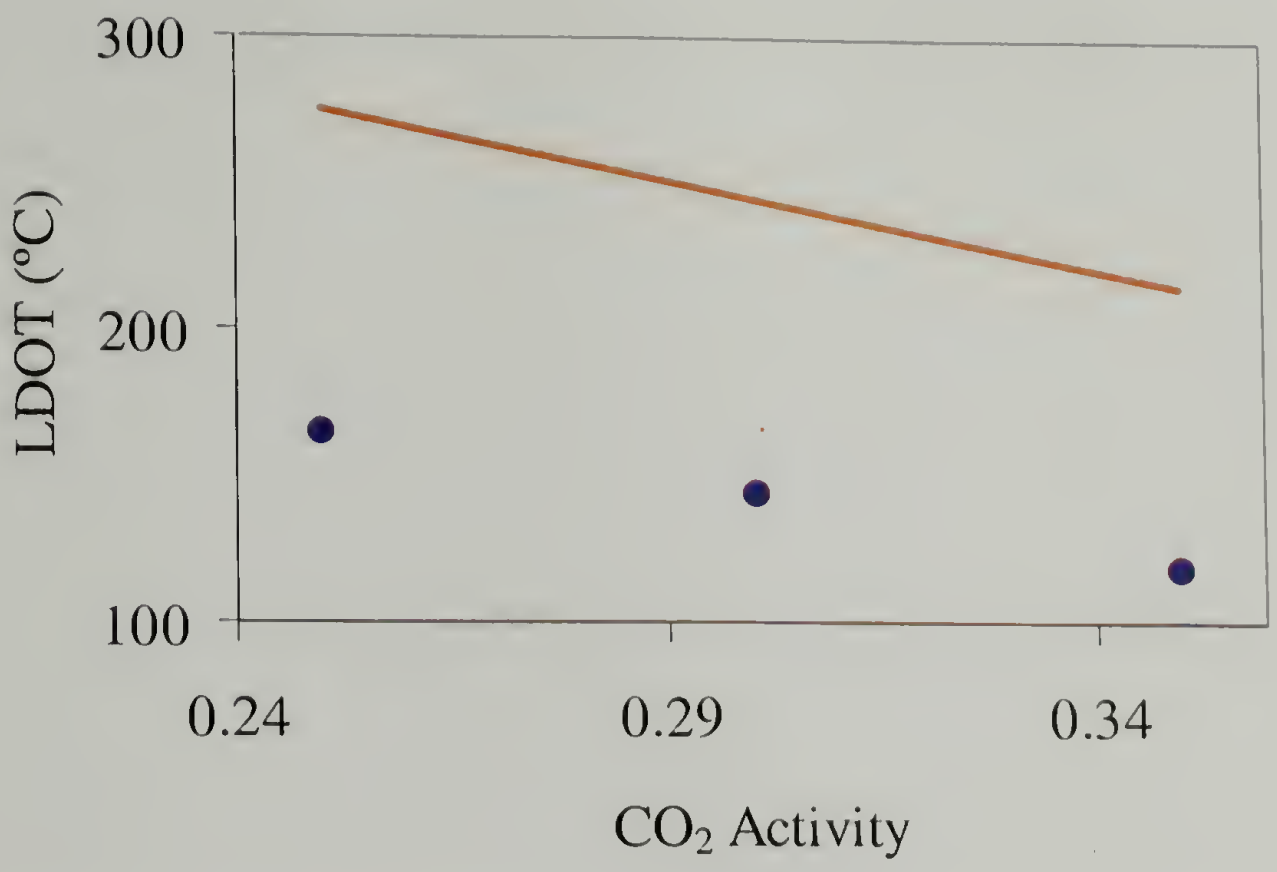

Figure 4.10: Effect of carbon dioxide dilation on the LDOT in 39.9K PS-*b*-PnPMA from birefringence measurements (●) and cRST calculations (—)

Experimentally, the LDOT undergoes a depression of 47°C/0.1 activity unit. The cRST predicts a depression of 60°C/0.1 activity unit. This prediction is very close to the experimentally determined LDOT depression, showing that the effect on the phase behavior can be accurately described using volumetric arguments. The enthalpic interaction between carbon dioxide and the block copolymer has little impact on the closed-loop phase diagram. Overall, the compressible regular solution theory is successful in predicting the proper thermodynamic trends of carbon dioxide dilation, but the specific temperatures from the calculations lack accuracy.

4.4.4 SANS Measurements

Small angle neutron scattering (SANS) has been shown to be a powerful technique[22] for extracting block copolymer thermodynamic information. While birefringence is sensitive to the location of the microphase separation transition temperature, SANS can be used to follow the peak location and shape to determine the degree of order or disorder, as well as the impact of CO_2 swelling on the domain spacing[23]. SANS experiments were performed at the National Center for Neutron Research at NIST on the NG-3 SANS beamline. The pressure cells used were the same as those used in the high-pressure birefringence experiments described above. The measurements were performed at constant density, ramping in temperature and pressure and allowing 15 minutes for equilibration between data acquisition runs. The neutron wavelength was 6 Å with a sample to detector distance of 5.3 m. A representative set of data is given in Figure 4.9, below, for 39K D_8PS-*b*-PnPMA, which is disordered over the complete temperature range at atmospheric pressure[24].

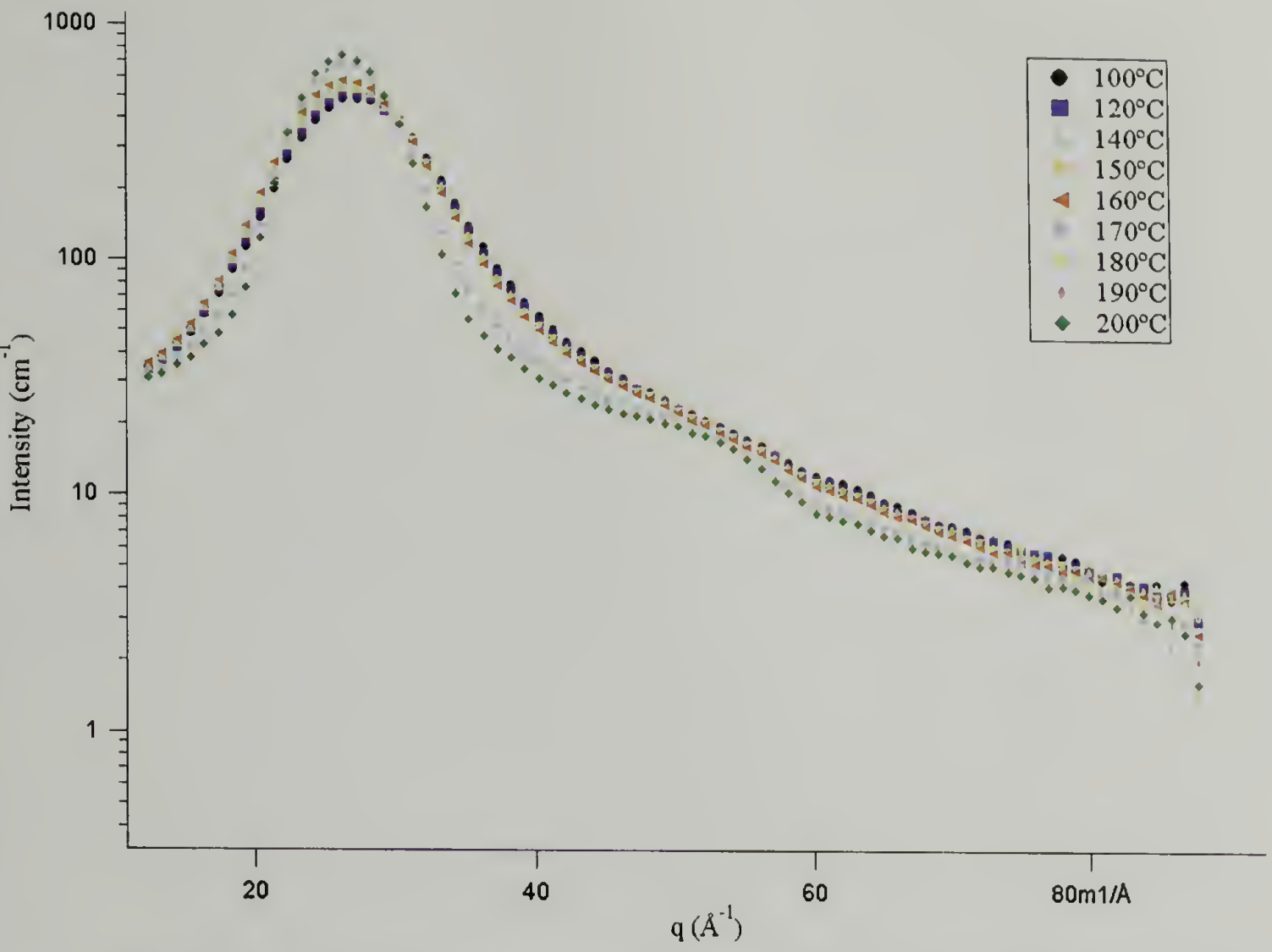

Figure 4.11: SANS of 39K 50/50 dPS-*b*-PnPMA at CO_2 density of 0.07 g/mL

At low temperatures, the SANS curves display only a broad, low intensity peak arising due to the connectivity of the blocks in the disordered state. This correlation hole scattering becomes a first-order scattering peak, increasing in intensity and sharpening in width between 160°C and 170°C as the BCP passed through the LDOT temperature. A second-order scattering peak was also easily identifiable, as well as hints of a third-order at high q. This is indicative of a high degree of long-range order in the microphase separated block copolymer, as well as high phase purity and narrow interfacial width[25].

In addition to changes in the peak shape, a shift in the peak position uncovers information on chain stretching in the copolymer. In general, PS-*b*-PnPMA block copolymers should display chain stretching on passing into the ordered state as the blocks

attempt to avoid unfavorable contacts at the microdomain interface. This should be identifiable by a decrease in q on ordering. Under CO_2, additional effects such as domain swelling and isothermal compressibility from hydrostatic pressure will impact the position of the primary scattering peak, q*. The peak position is plotted as a function of temperature at several CO_2 densities in Figure 4.10 below.

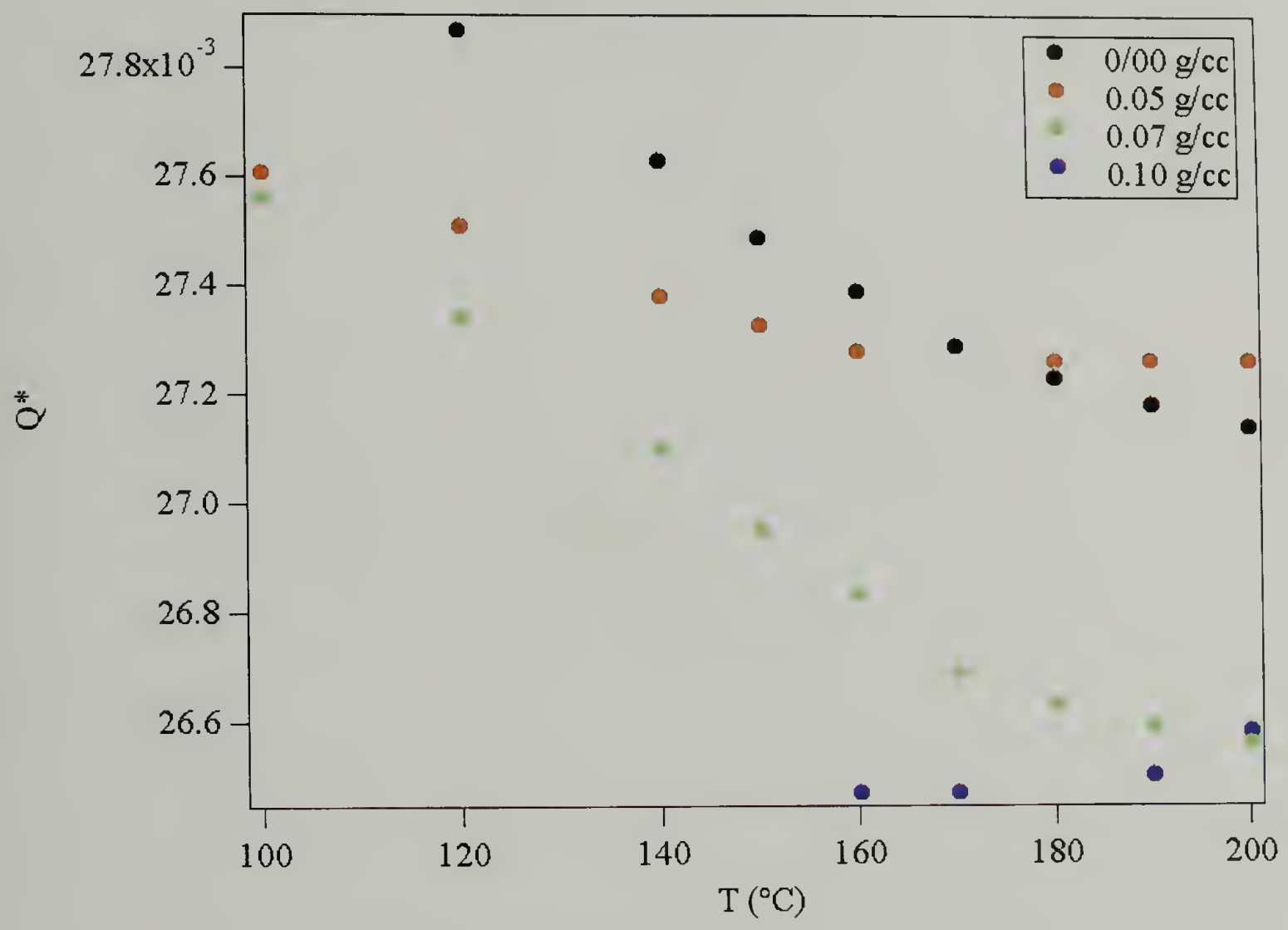

Figure 4.12: Q* as a function of temperature at various CO_2 densities

On first inspection there does not appear to be any identifiable trend in the Q* data. However, the effects of differential dilation, using the values determined from homopolymer swelling experiments, in addition to the hydrostatic pressure effects, which include isothermal compressibility of the blocks (dQ*/dP) and the pressure coefficient

(dT/dP) shift along the T axis, must be taken into account. This reduces the data onto the same pressure and swelling axis, so that thermodynamic trends in the data can be evaluated. If the data collapse onto the same curve then the system thermodynamics can be described by the simple evaluation of carbon dioxide as a differential diluent, and enthalpy has an insignificant effect on the LDOT region of the phase diagram. This collapsed data is shown in Figure 4.13.

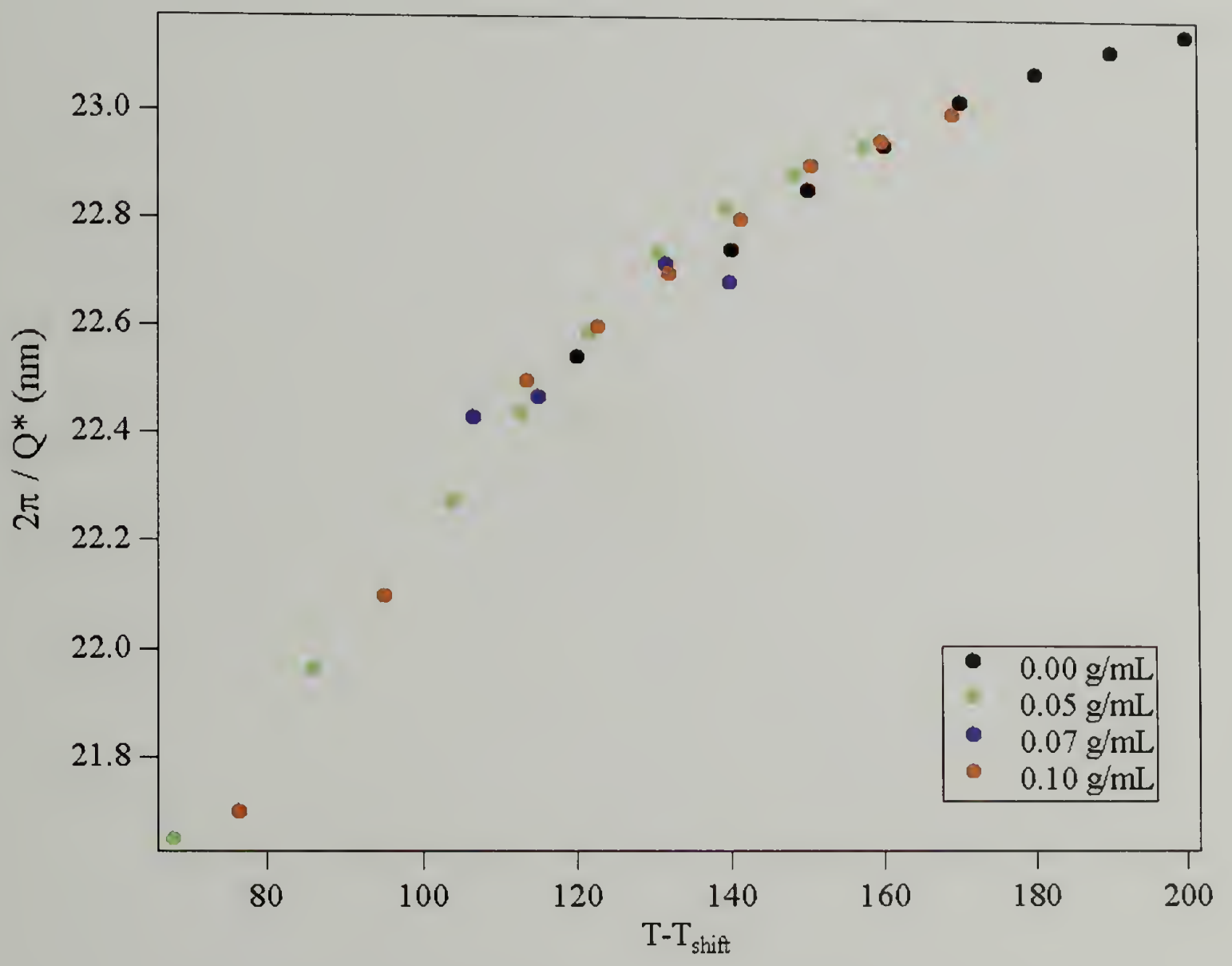

Figure 4.13: Q* from SANS on 39K PS-*b*-PnPMA corrected for hydrostatic pressure and differential dilation

As seen above, the data do collapse onto a continuous curve. This shows that the domain spacing under CO_2 dilation can be fully described by selective swelling and hydrostatic pressure effects. The increase and subsequent plateau in the 2π / Q* behavior is similar to that seen for all symmetric low molecular weight dPS-*b*-PnPMA copolymers, where the temperature at the center of the closed-loop is approximately 200°C. The effect of carbon dioxide on the system thermodynamics are not observable in the Q* data. These effects would be desirable only in the width and intensity of the scattering peak. However, fits of these data, such as those accomplished using the RPA theory in Chapter 3, are not straightforward and were not attempted here.

4.5 Conclusions

Compressible carbon dioxide was used as a means to explore the volumetric origins of the closed-loop phase behavior of PS-*b*-PnPMA block copolymers. CO_2 sorption served to differentially dilate the system, thus exacerbating volumetric disparity between the components. As a result, the closed-loop expanded appreciably with mild fluid sorption. The experimental results were compatible with predictions using compressible RST arguments treating CO_2 simply as a differential diluent. The phase behavior of CO_2-dilated PS-*b*-PnPMA was shown to be fully explained using hydrostatic pressure and dilation effects.

References

1. Lemmon, E.W., M.O. McLinden, and D.G. Friend, *Thermophysical Properties of Fluid Systems*, in *NIST Chemistry WebBook, NIST Standard Reference Database Number 69*, W.G. Mallard and P.J. Linstrom, Editors. 1998, National Institute of Standards and Technology: Gaithersburg MD, 20899. p. http://webbook.nist.gov.

2. McHugh, M.A. and V.J. Krukonis, *Supercritical Fluid Extraction: Principles and Practice*. 1986, Boston: Butterworths.

3. Watkins, J.J. and T.J. McCarthy, *Polymer/metal nanocomposite synthesis in supercritical co2*. Chemistry of Materials, 1991. **7**(11).

4. Shah, P.S., et al., *Steric Stabilization of Nanocrystals in Supercritical CO2 Using Fluorinated Ligands*. Journal of the American Chemical Society, 2000. **122**: p. 4245.

5. Sirard, S.M., et al., *Structure of End-Grafted Polymer Brushes in Liquid and Supercritical Carbon Dioxide: A Neutron Reflectivity Study*. Macro., 2003. **36**(9): p. 3365.

6. Blackburn, J.M., *Chemical Fluid Deposition: Reactive Deposition of Thin Metal Films from Supercritical Carbon Dioxide Solutions*, in *Chemical Engineering*. 2001, University of Massachusetts: Amherst, MA.

7. DeSimone, J.M., Z. Guan, and C.S. Elsbernd, *Synthesis of Fluoropolymers in Supercritical Carbon Dioxide*. Science, 1992. **257**: p. 945.

8. Sarbu, T., T. Styranec, and E.J. Beckman, *Non-fluorous polymers with very high solubility in supercritical CO2 down to low pressures*. Nature, 2000. **405**: p. 165.

9. McHugh, M.A. and V.J. Krukonis, in *Encyclopedia of Polymer Science and Engineering*, H.F. Mark, et al., Editors. 1989, John Wiley and Sons: New York.

10. Wissenger, R.G. and M.E. Paulaitis, *Glass Transitions in Polymer/CO2 Mixtures at Elevated Pressures*. Journal of Polymer Science: Polymer Physics, 1991. **29**: p. 631.

11. RamachandraRao, V.S. and J.J. Watkins, *Phase Separation in Polystyrene-Poly(vinyl methyl ether) Blends Dilated with Compressed Carbon Dioxide*. Macromolecules, 2000. **33**(14): p. 5143.

12. Vogt, B.D., et al., *Phase behavior of nearly symmetric polystyrene-block-polyisoprene copolymers in the presence of CO2 and ethane*. Macromolecules, 1999. **32**(23): p. 7907-7912.

13. Vogt, B.D., et al., *Phase Behavior of Polystyrene-block-poly(n-alkyl methacrylate)s Dilated with Carbon Dioxide.* Macro., 2003. **36**(11): p. 4029.

14. Hanley, K.J., T.P. Lodge, and C.-I. Huang, *Phase Behavior of a Block Copolymer in Solvents of Varying Selectivity.* Macromolecules, 2000. **33**(16): p. 5918-5931.

15. Lodge, T.P., et al., *Failure of the Dilution Approximation in Block Copolymer Solutions.* Journal of Polymer Science: Part B: Polymer Physics, 1995. **33**: p. 2289-2293.

16. Hanley, K.J. and T.P. Lodge, *Effect of Dilution on a Block Copolymer in the Complex Phase Window.* Journal of Polymer Science: Part B: Polymer Physics, 1998. **36**: p. 3101-3113.

17. Watkins, J.J., et al., *Phase Separation in Multi-Component Polymer Systems Induced by Compressible Solvents.* Macromolecules, 1999. **32**: p. 7737.

18. Vogt, B.D. and J.J. Watkins, *Phase Behavior of Diblock Copolymers Dilated with Light Alkanes:The Influence of Solvent Compressibility on Upper and Lower Ordering Transitions.* Macromolecules, 2002. **35**(10): p. 4056.

19. Kamiya, Y., K. Mizoguchi, and Y. Naito, *Sorption and partial molar volumes of inert gases in rubbery polymers.* Journal of Membrane Sciene, 1994. **93**: p. 45-52.

20. Ruzette, A.V. and A.M. Mayes, *A Simple Free Energy Model for Weakly Interacting Polymer Blends.* Macromolecules, 2001. **34**: p. 1894.

21. Ruzette, A.V., et al., *A Simple Model for Baroplastic Behavior in Block Copolymer Melts.* J. Chem. Phys., 2001. **114**: p. 8205.

22. Stein, R.S., et al., *Recent Small Angle Neutron Scattering Studies of Polymers in the Solid State.* Physica B, 1986. **137**: p. 194-203.

23. Hashimoto, T., et al., *Time-Resolved Small-Angle X-ray Scattering Studies on the Kinetics of the Order-Disorder Transition of Block Polymers 2. Concentration and Temperature Dependence.* Macromolecules, 1986. **19**: p. 754-762.

24. Sakamoto, N., et al., *Effect of Addition of a Neutral Solvent on the Order-Order and Order-Disorder Transitions in a Polystyrene-block-polyisoprene-block-polystyrene Copolymer.* Macromolecules, 1997. **30**: p. 5321-5330.

25. Russell, T.P., *Small-Angle Scattering*, in *Handbook on Synchrotron Radiation*, G.D. Brown and D.E. Moncton, Editors. 1991, Elsevier Science Publishers: Amsterdam.

CHAPTER 5

BLOCK COPOLYMER MORPHOLOGY UNDER COMPRESSED CO_2

5.1 Introduction

The properties of compressible fluids make them particularly useful in the polymer processing and nanostructure formation[1, 2]. As discussed previously, compressible fluids impart enhanced transport properties to swollen materials, able to depress T_g by as much as 75°C[3]. Additionally, carbon dioxide acts as a differential diluent for many block copolymers[4-6]. The consequences of this on the location of the volumetrically-driven LDOT and UODT transitions were shown in the previous chapter. This differential dilation, however, can have a profound impact on the equilibrium structures created during microphase separation. In this chapter I will discuss the effects of these properties on nanostructure formation in block copolymers, both in thin films and in the bulk.

5.2 Order-to-Order Transitions

A critical parameter in the determination of the equilibrium morphologies of block copolymers is the volume fraction of the component blocks. The equilibrium morphologies observed, such as lamellae, cylinders, and spheres, result from a balance of energy contributions from domain surface area, chain stretching, and the desire to keep the junction point near the domain interface[7, 8]. It is well known that the addition of liquid solvents to block copolymers can result in a shift in the phase boundary, not only between order and disorder but between ordered phases, depending on the selectivity of the solvent. Hanley and Lodge studied the phase diagram of PS-*b*-PI with solvents of varying

selectivity, such as di(n-butyl) phthalate (DBP), diethyl phthalate (DEP), and dimethyl phthalate (DMP)[9, 10]. They found that the complete range of morphologies in the phase cube could be explored by varying the solvent volume fraction. In general, the phases observed could be explained by knowing the melt phase behavior of the polymer, and applying knowledge of the effect of solvent partitioning on the interfacial curvature of the domains. OOT's were easily observed using a combination of birefringence and SAXS.

Carbon dioxide, as a differential diluent, can induce an OOT in a given block copolymer. For polystyrene-*block*-poly(n-alkyl methacrylate)s, that selectivity is slight. In addition, the degree of swelling is small with CO_2 volume fractions below 0.20. This limits the experimentally accessible region of the polymer phase cube. CO_2-induced OOT's are only observable if the copolymer volume fraction is near a morphological phase boundary, such that CO_2 pressurization changes the relative volume fraction enough to induce a morphological change. One such system was found to be 42.9K 41/59 PS-*b*-PnPMA. This material is fully disordered over the full temperature range at atmospheric pressure. From the component volume fraction the prediction is that this copolymer would exhibit lamellar morphology. High-pressure birefringence measurements were performed, and the results are shown in Figure 5.1.

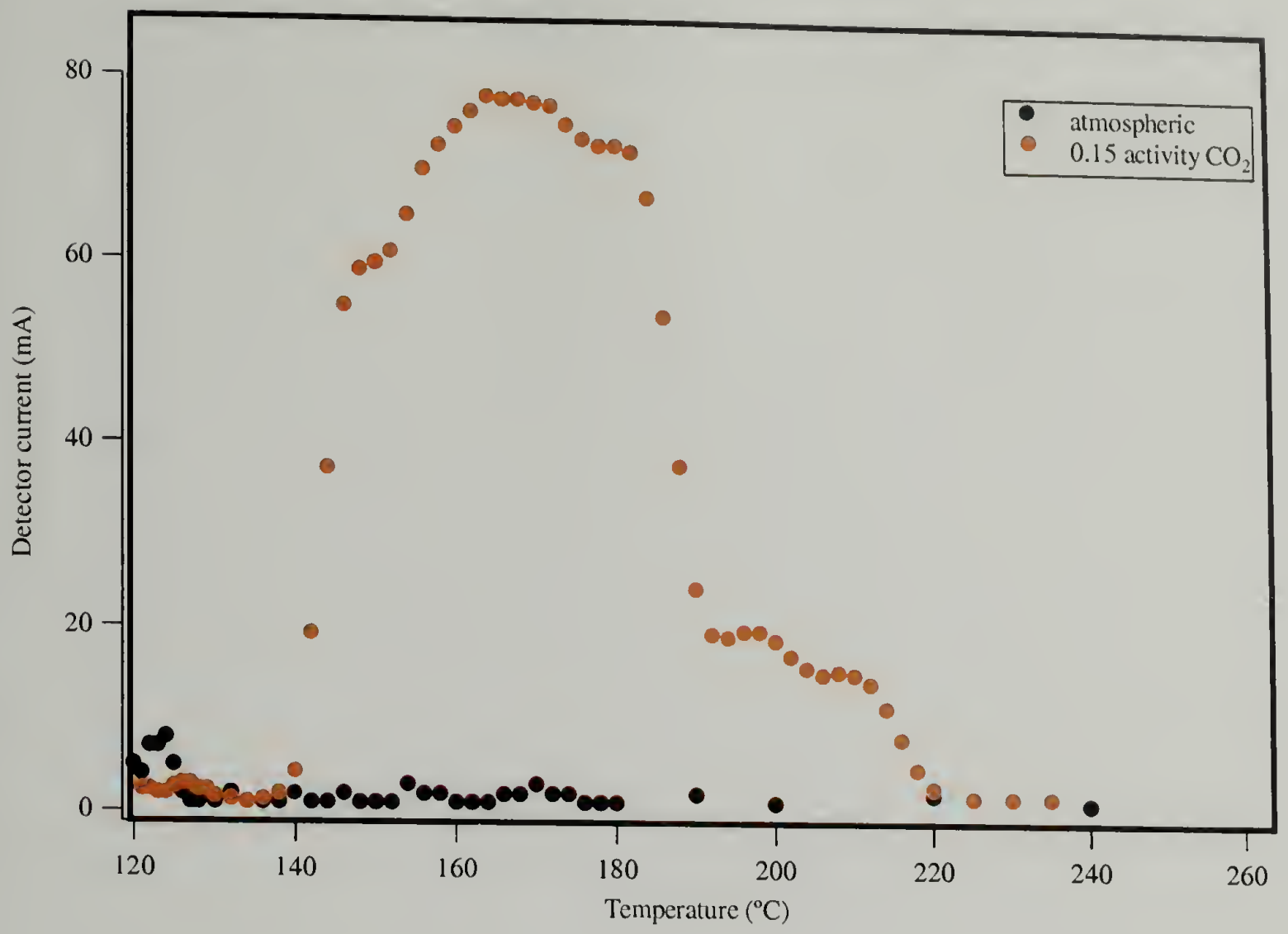

Figure 5.1: Birefringence traces for 42.9K PS-*b*-PnPMA, at atmospheric pressure and 0.15 CO_2 activity

At atmospheric pressure the block copolymer is disordered over the complete temperature range. This was as expected. With the application of a small amount of carbon dioxide, maintaining a constant activity of 0.15 at all temperatures, the copolymer was disordered at low temperatures, passed into the ordered state at approximately 140°C, and increased steadily in intensity, which is the result of grain ripening. At ~188°C the copolymer exhibited a drop in intensity, followed by a second plateau in intensity. At ~215°C the copolymer birefringence dropped to zero, resulting in nearly complete extinction of the light intensity. The two intensity regions were thought to be two different morphologies, with the transition at 188°C being an OOT between the two phases. The LDOT and UODT were at 140°C and 215°C, respectively.

SAXS was used in order to confirm the morphology of the block copolymer in the two regions. Since *in situ* measurements could not performed with the in house equipment the block copolymer microdomains needed to be frozen in while still under carbon dioxide pressure. This was accomplished using ultraviolet radiation, which served to crosslink the polystyrene domains. The radiation was passed through a sapphire window, which allowed ~75% transmittance. Crosslinking was carried out for approximately 15 minutes, after which the system was depressurized slowly over 48 hours. It is known that, in addition to crosslinking PS, UV radiation will degrade the alkyl methacylate block. This was considered inconsequential as this should not impact the morphology, and may in fact improve electron density contrast between the phases.

The morphology of this PS-*b*-PnPMA sample was investigated at a variety of temperatures and pressures. Two representative SAXS curves are given in Figures 5.2 and 5.3, below. The sample in Figure 5.2 was annealed at 140°C and 1200 psi CO_2 for 1 day. These are conditions that correspond to low-temperature plateau in Figure 5.1. The sample in Figure 5.3 was annealed at 220°C and 3000 psi for 1 day. This corresponds to the conditions of the second, higher temperature plateau in Figure 5.1. After the annealing time, both samples were exposed to UV radiation for 15 minutes, cooled to room temperature and depressurized slowly over the course of 48 hours. The copolymer samples were 1 mm thick. The incident x-ray radiation was CuKα with a wavelength of 1.54 Å from a tube x-ray source. The sample chamber and beam path were kept under vacuum.

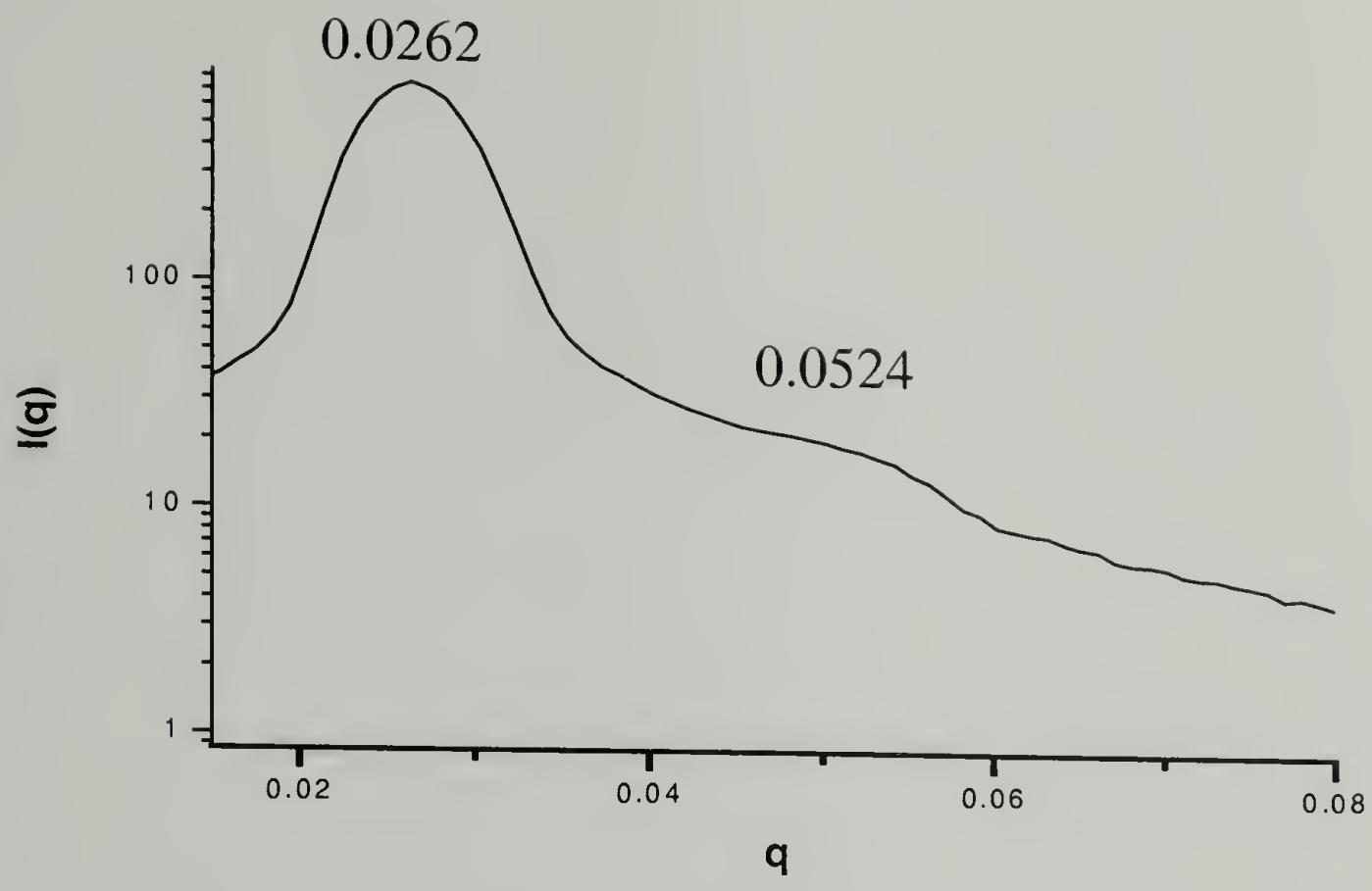

Figure 5.2: SAXS of 42.9K PS-*b*-PnPMA annealed at 140°C and 1200 psi for 1 day

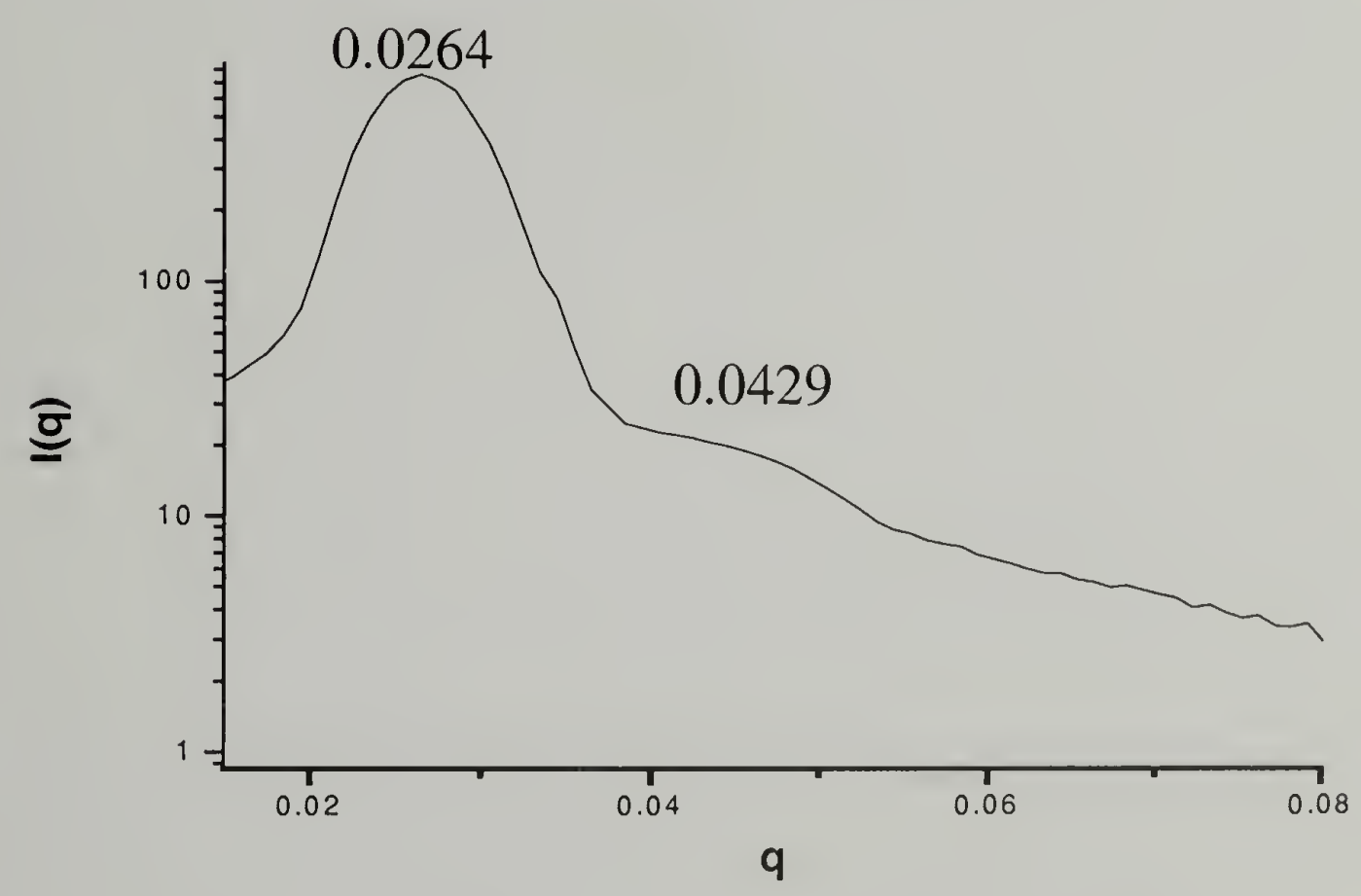

Figure 5.3: SAXS of PS-*b*-PnPMA annealed at 220°C and 3000 psi for 1 day

The SAXS trace in Figure 5.2 shows the first order scattering peak at 0.0262 $Å^{-1}$, corresponding to a block copolymer period of 23.9 nm. The second order peak at 0.0524 $Å^{-1}$ occurs at an approximate ratio of 1:2 with the first order peak, indicating the morphology is lamellar. The broadness of the second order peak is likely due to incomplete crosslinking of the block copolymer under UV. The sample was 1 micron thick, and the radiation may not have penetrated the entire film. In comparison, the SAXS trace in Figure 5.3 shows a first order peak at 0.0264 $Å^{-1}$, corresponding to a domain spacing of 23.8 nm. This was close to that observed in the lamellar sample. However, the second order peak was centered at 0.0429 $Å^{-1}$. This occurred at a ratio of $1:\sqrt{3}$ with the location of the first order peak. This was indicative of a hexagonally-packed cylindrical morphology. The low- and high-temperature plateaus in Figure 5.1 were, then, the lamellar and cylindrical phases of the block copolymer.

The location of the OOT was studied as a function of carbon dioxide activity. With an increase in carbon dioxide loading, the degree of differential dilation should change slightly leading to a shift in the OOT phase boundary. Since CO_2 in slightly preferential for the PnPMA block, and since that is the majority component, higher activities lead to a larger PnPMA volume fraction. This should tend to drive the system towards a cylindrical morphology. These observations are shown in Figure 5.4, where the order-to-order transition is plotted as a function of both activity and the corresponding swollen block copolymer volume fraction. The PnPMA volume fraction plotted is the volume fraction of the polymeric component, such that $\phi_{PS} + \phi_{PnPMA} = 1$.

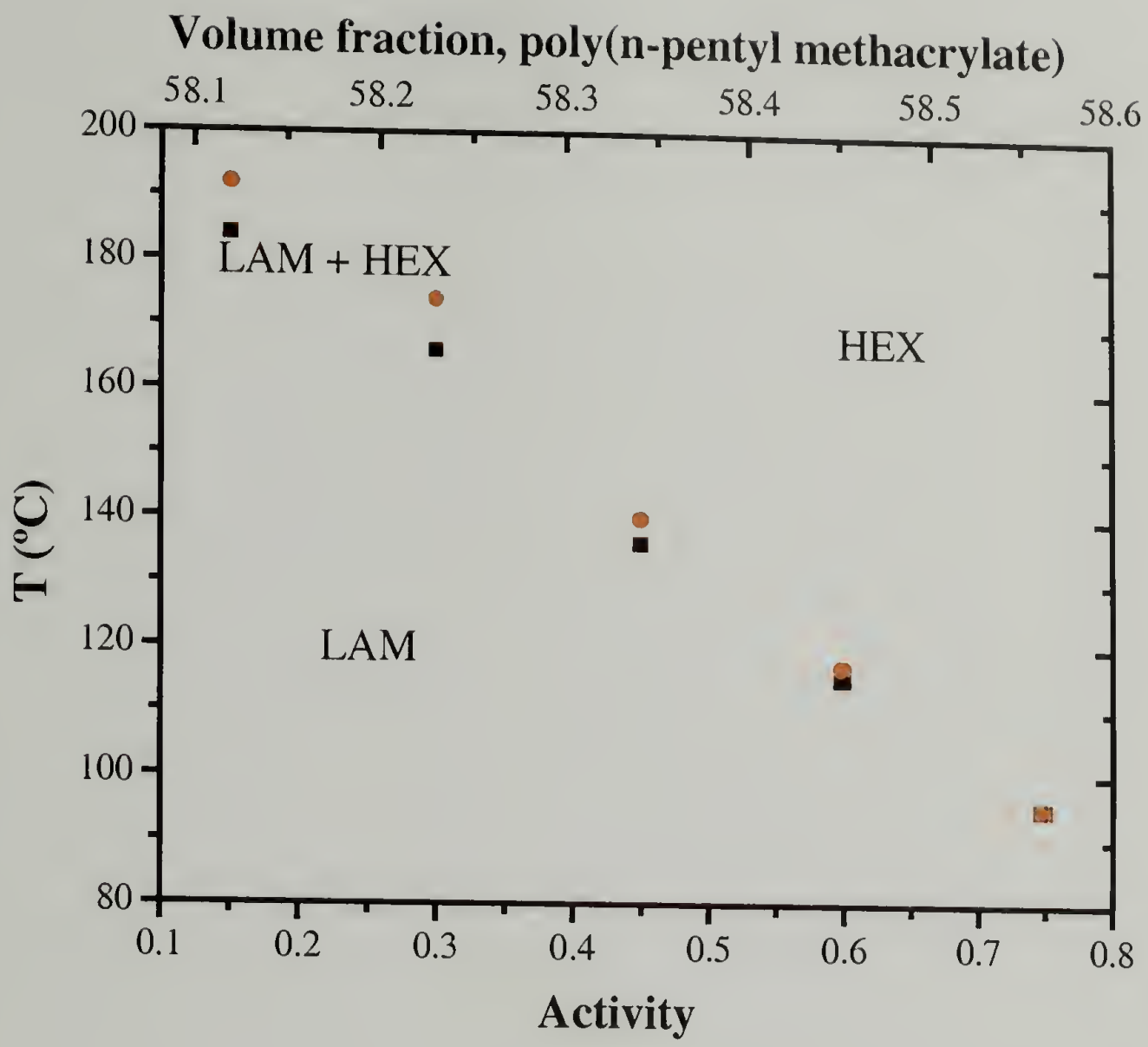

Figure 5.4: OOT temperature as a function of carbon dioxide activity and PnPMA swollen volume fraction on heating (●) and cooling (■)

With an increase in CO_2 swelling there is a systematic decrease in the location of the OOT. As a result of the preferential swelling of the PnPMA phase, the PnPMA volume fraction, relative to that of PS, increases, driving the system further into the cylindrical phase. Additionally, a hysteresis was observed on heating and cooling. This was fully reproducible, and decreased in magnitude at higher CO_2 activities until it completely disappeared at an activity of ~0.70. This was thought to be a region of coexistence between hexagonal and lamellar phases, although no direct experimental evidence of both

phases was observed in this range. The decrease in the size of this region with increased dilation was attributed to a corresponding increase in χ, which served to sharpen the phase boundary, thus improving phase segregation and decreasing the size of the region of metastability. While carbon dioxide strongly drives LDOT- and UODT-type block copolymers into the ordered state, there is clearly the consequence of changing the volume fractions of the blocks, leading to possible shifts in the block copolymer morphology.

5.3 Enhanced Ordering Kinetics Under CO_2 Dilation

The processing of polymers using carbon dioxide dilation has the distinct advantage of imparting enhanced flow properties to the swollen material[11, 12]. The glass transition temperature can be significantly depressed[3], and the extent of plasticization can be directly controlled by altering the CO_2 pressure[13]. This has been used to great advantage in polymer processing and welding[14]. Through the use of isotopic labeing one can directly observe the self-diffusion of polymer chains directly using neutron scattering techniques. In terms of block copolymer ordering kinetics, however, the effects of CO_2 dilation have not been studied in great detail. Specifically in high molecular weight copolyerms, for which large degrees of chain entanglement hinder the microphase separation process, the impact of CO_2 dilation on the ability to create equilibrium structures has not been quantified. In this section I will describe experiments studying the impact of enhanced kinetics on copolymer thin film ordering.

5.3.1 Lamellar Block Copolymer Thin Films

Block copolymer ordering in thin films has long been a focus of research as a means to create nanoscale templates and scaffolds for the creation of structures on the size scale of 50 nm or less[15]. In lamellar block copolymers, where the volume fraction ratios of the component blocks are nearly 50/50, structures normal to a surface have been created with potential application as nanowires, gratings, and nanoscale templates. Structures parallel to the substrate result in the formation of lamellar stacks, where the lower surface energy component segregates to the free surface and the component with stronger interaction with the substrate segregates to the substrate interface. Russell and coworkers observed this in dPS-*b*-PMMA films, using neutron reflectivity as a means to nondestructively study the copolymer ordering as a function of film depth[16-18]. The ability to deuterium-label the polystyrene component makes this a particularly attractive technique for studying thin film morphology as a function of depth.

One of the most promising applications of parallel lamellar stacks is in the fabrication of 1-dimensional photonic bandgap materials. However, for block copolymers to be useful in this regard the lamellar domain spacing must approach $\lambda / 4n$ where λ is the wavelength of light and n is the refractive index contrast between layers[19, 20]. This leads to lamellar spacings on the tenth-micron size scale. Since domain spacing for lamellae in the strong segregation limit scales as molecular weight to the 2/3 power, high molecular weight copolymers are required to obtain structures on this size scale. For instance, 300 KDa PS-*b*-PMMA yields a d-spacing of ~85 nm, but in order to achieve a d-spacing above 100 nm the molecular weight must be increased to near 500 KDa. Unfortunately, copolymers of such high molecular weight suffer from entanglements which make thermal

annealing insufficient to order these materials. RamachandraRao *et al.* performed a simple study where 301K dPS-*b*-PMMA films spin coated onto silicon wafers[21]. The as cast film, thermally-annealed, and CO_2-annealed films were observed under an optical microscope in reflectance mode. The edge of the film was observed in order to check for terracing of the parallel-aligned copolymer domains, as indicated by sharp color changes in reflectance micrograph. Terracing at the edge of the spin-coated film would indicate a microphase separated structure. The results are shown in Figure 5.5.

a.

b.

c.

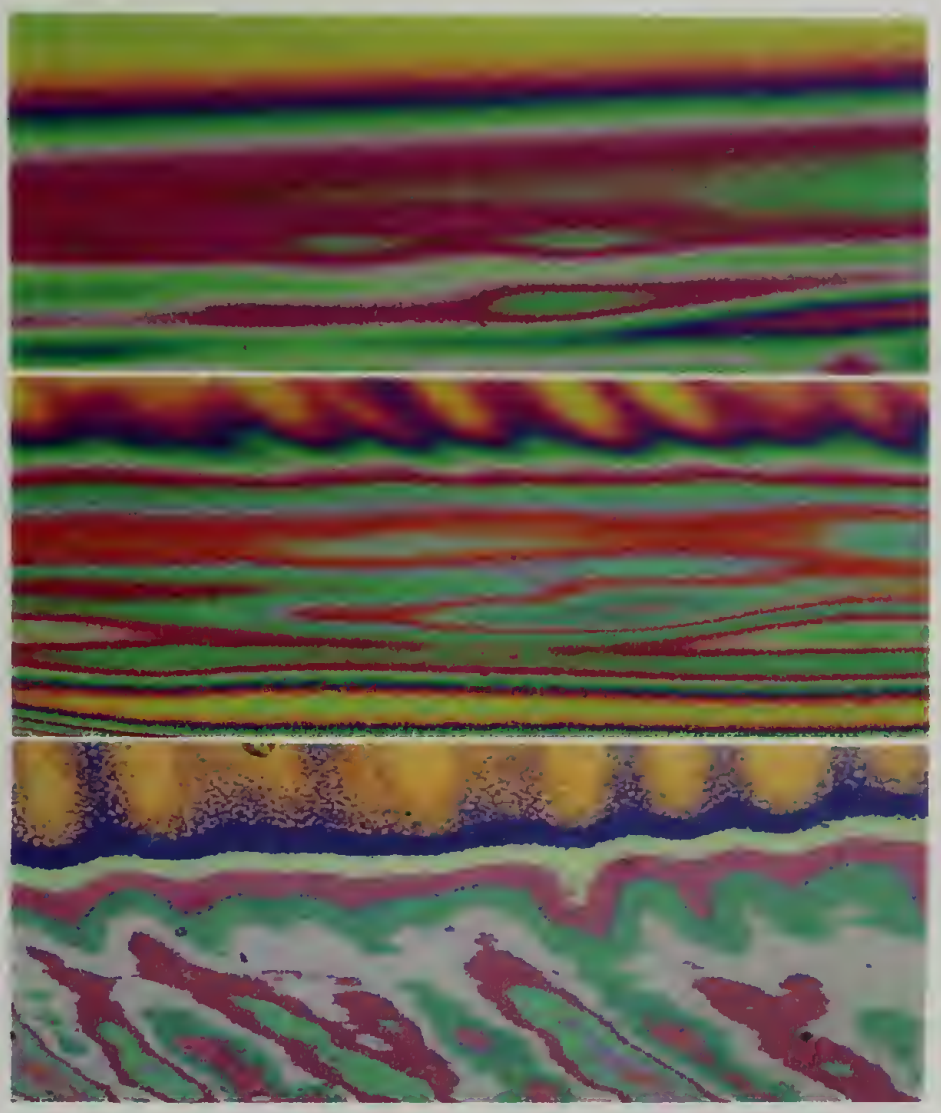

Figure 5.5: Reflectance optical micrograph of 301K dPS-*b*-PMMA on Si/SiO_x a. as cast, b. vacuum annealed at 175 ° C for 240 hours and c. at 175 ° C under 346 bar CO_2 for 48 hours[21]

Figure 5.5a shows the as cast film. The variation in color is gradual, as expected for a disordered film. Figure 5.5b shows the thermally annealed film, which also shows a gradual color change, showing that chain entanglements hindered the kinetics enough to prevent ordering on this time scale. The CO_2–annealed film, shown in Figure 5.5c, showed discrete color changes as indicative of a parallel-aligned microphase separated block copolymer film. Despite this promising observation, quantitative investigation of the ordering in these films, nor the kinetics of ordering under carbon dioxide plasticization, were investigated.

Neutron reflectivity studies were undertaken in order to investigate the internal thin film structure of 301K and 500K dPS-*b*-PMMA, annealed both thermally and under carbon dioxide pressurization. The experiments were carried out at Los Alamos National Laboratory at the Lujan Neutron Scattering Center. The SPEAR reflectometer, under the guidance of Dr. Gregory Smith, was used to obtain the specular reflectivity from a series of block copolymer films. The Lujan Center is a spallation neutron source, thus SPEAR is a time-of-flight reflectometer. Therefore, the sample was held at fixed angle and packets of neutrons of varying energies, or wavelengths, were reflected off the surface. The different wavelengths were binned by the detector according to their time of flight, and converted to $k_{z,0}$ by the relation $\frac{2\pi}{\lambda}\sin\left(\frac{\theta}{2}\right)$. Two representative reflectivity plots are given in Figures 5.6 and 5.7. In both figures the background-subtracted intensity was normalized such that total external reflection had a reflectivity of 1. The x-axis is $k_{z,0}$, which is the neutron momentum transfer under vacuum in the direction normal to the film.

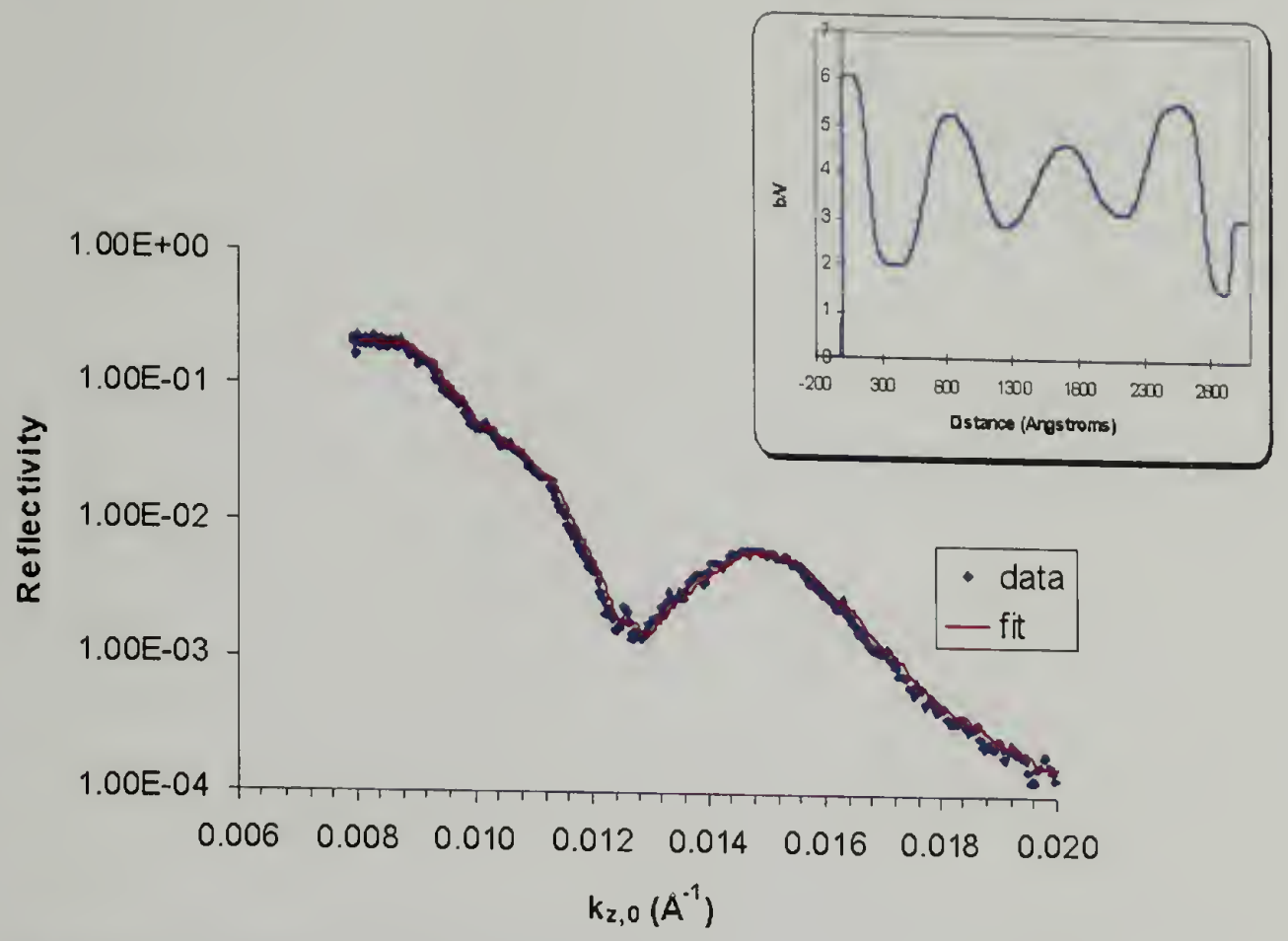

Figure 5.6: 301K dPS-*b*-PMMA vacuum-annealed at 160˚C for 3 days

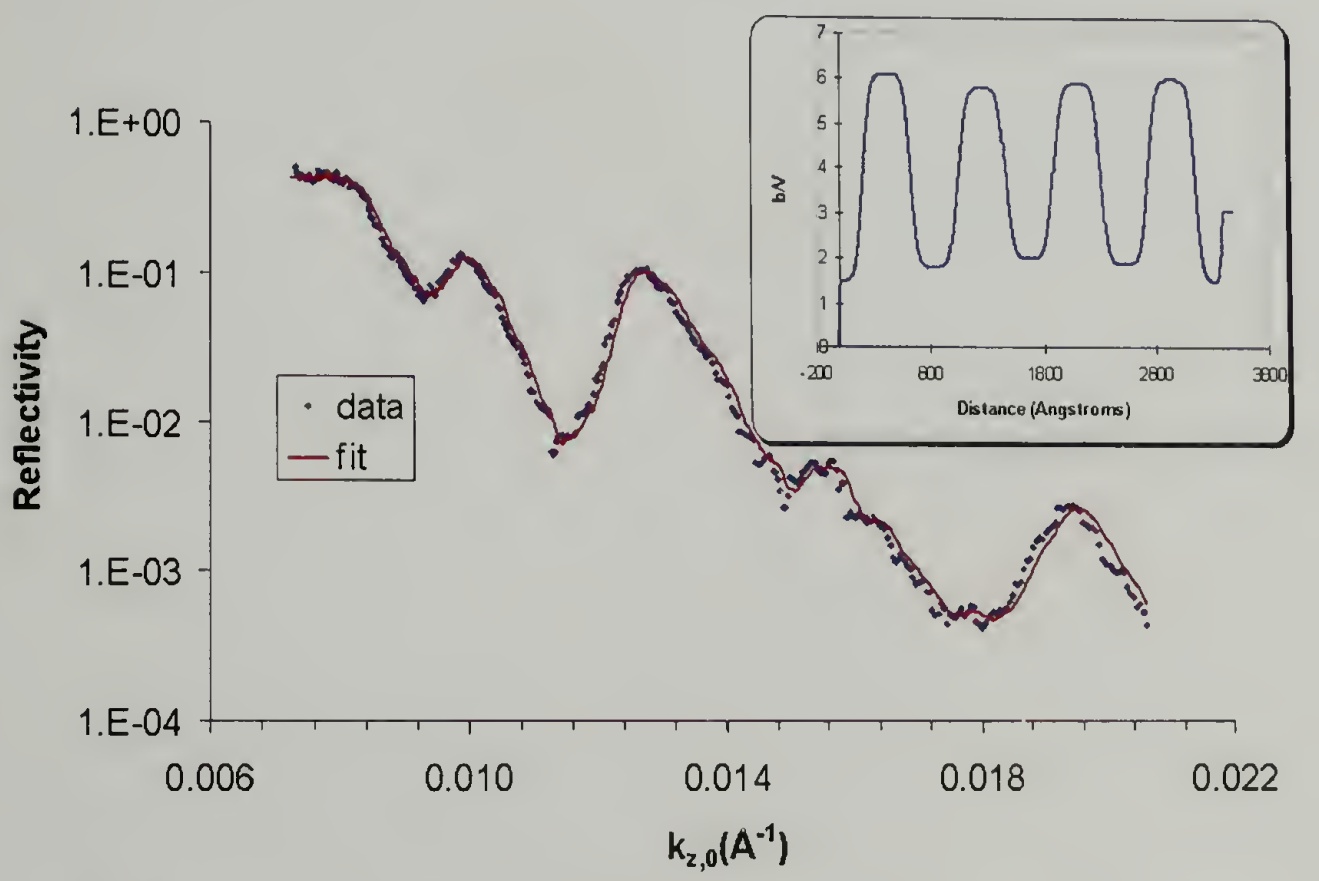

Figure 5.7: 301K dPS-*b*-PMMA annealed under CO_2 at 160˚C and 4000 psi for 3 days

The reflectivity curve in Figure 5.6 shows one broad peak. This is indicative of the presence of a characteristic layer spacing in the film. However, that characteristic distance was poorly defined and with broad interfacial roughness. Fits to the scattering data were performed using a FORTRAN fit routine modified from the MLAYER3 program developed by Anastasiadis and Menelle at IBM Almaden. The program used is given in Appendix A. It assumed an exponential decay function for the copolymer domain interfaces. This sample had PS at the free surface, as determined from X-ray Photoelectron Spectroscopy (XPS), and was assumed to have PMMA at the Si/SiO_x interface. The film thickness was determined both by elipsometry and AFM. The inset in Figure 5.6 shows the scattering length density, (b/V), as a function of film depth determined from the fit to the data. The deuterium-labeled polystyrene has a scattering length density of ~6.1, so a pure dPS later will have this value for the b/V. PMMA has a scattering length density of ~1.8, so, likewise, layers with this b/V value are pure PMMA. According to the fit to the thermally annealed sample there is surface-induced ordering at both the free surface and the silicon substrate. This order quickly decays in the interior of the film. This was due to chain entanglements in the high molecular weight copolymer film.

Figure 5.7 shows a reflectivity curve from a 301K dPS-*b*-PMMA film annealed for only 2 days under 4000 psi carbon dioxide at 160°C. The degree of order in the film is striking in comparison to the thermally-annealed sample. There is a high degree of phase purity throughout the film, as evidenced by the alternating plateaus of values 6.1 and 1.8 in b/V. It is interesting to note that instead of dPS being at the free surface, as was the case in the vacuum-annealed sample, PMMA is now at the free surface. This was thought

to be a combination of a preferential interaction of PMMA with the CO_2 atmosphere and the lowered surface energy due to slightly preferential swelling. PMMA was verified to be at the free surface using XPS. In addition to the phase purity, the interfaces between the microdomains were quite narrow. The interfacial roughness was 15 nm, compared to 35 nm for the vacuum-annealed sample. It is shown, then, that carbon dioxide plasticization has a profound impact on the ordering in diblock copolymer thin films. 300K block copolymers, in which ordering is kinetically hindered, can be induced to order by swelling with carbon dioxide.

Ideally, the lamellar domain spacing for use in photonic applications should approach 100 nm. 300K dPS-*b*-PMMA, while well ordered, only had a domain spacing of ~80 nm. Additionally, the order will have to propagate throughout several lamellar layers, depending the degree of refractive index contrast. In order to test these limits, a symmetric 500K dPS-*b*-PMMA block copolymer was investigated at various film thicknesses. This copolymer had a domain spacing near a tenth-micron, so if ordering of this sample could be directed though several layers there existed the possibility that the resulting structure could be used as a template for a photonic bandgap material. The samples were annealed at 170°C at 4000 psi for 4 days. Scattering length density profiles for 230 nm and 480 nm thick films are shown in Figure 5.8. The copolymer is symmetrically wetting, with the first sample having a two-period thick film. The second represents a four-period thick film.

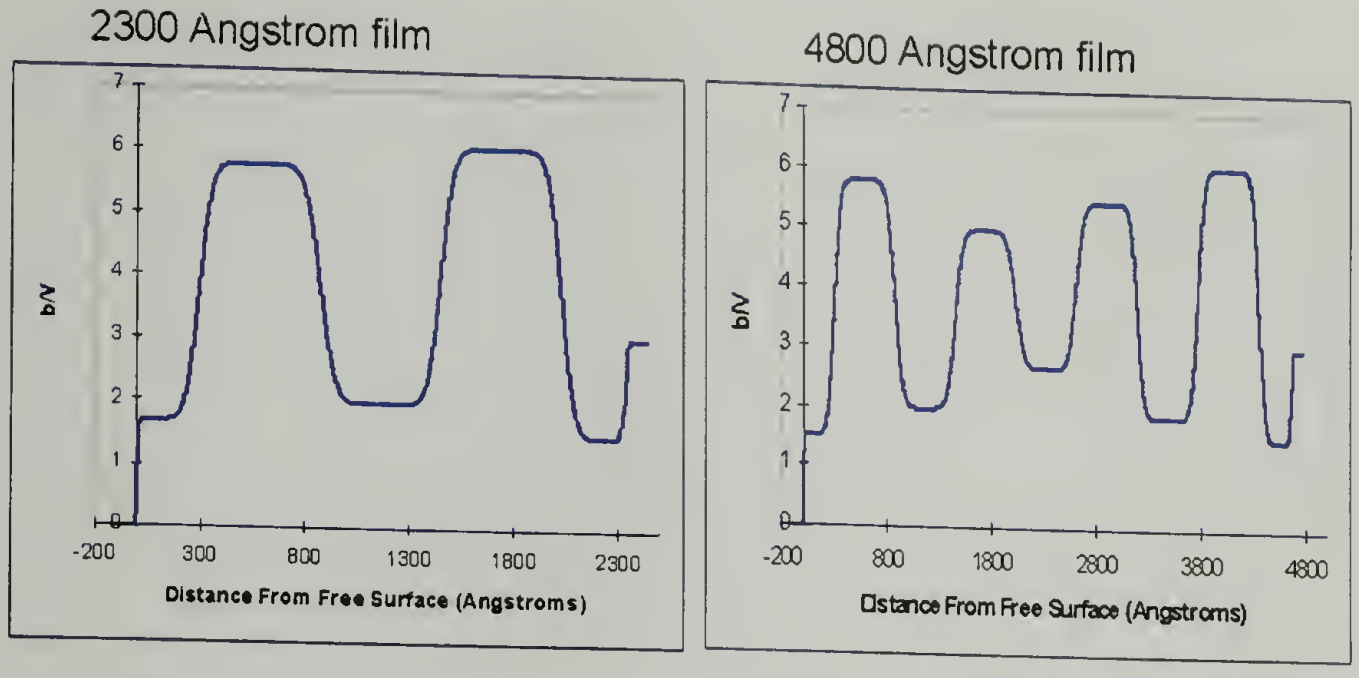

Figure 5.8: Scattering length density profiles for 500K dPS-*b*-PMMA films of different thicknesses annealed at 170˚C and 4000 psi CO_2

The results were slightly disappointing. The 2-period film remained well ordered throughout the entire film. This was likely aided by surface segregation effects, with CO_2 pasticization imparting sufficient mobility to the polymer chains to organize at the interfaces. Order in the four period film was significantly worse. While order at the interfaces remained strong, the phase purity decreased significantly on the interior of the film. Interfacial broadening was also evident on the interior of the film. The entangled copoylmer chains retarded propagation of order to the film interior. Films thicker that 4 periods showed considerably worse degrees of order. This led to the conclusion that strong surface forces were necessary to drive order in very high molecular weight block copolymers. Additionally, 500K presented a limit to the degree to which carbon dioxide could impart mobility to PS-*b*-PMMA copolymers.

5.3.2 Cylindrical Block Copolymer Thin Films

Asymmetric block copolymers with a component volume fraction of roughly 70/30 self-assemble in the ordered phase into hexagonally-packed cylinders. This has proven to be particularly useful in a variety of applications, including the fabrication of nanoporous films for low-k dielectric materials[22], highly lateral-ordered cylinders[16, 23-25] for high-density magnetic storage, and channels for charge transfer in fuel cells or batteries. A number of techniques have evolved in the improvement of the spatial arrangement of these cylinders, whether normal or parallel to the substrate[15, 26-28]. In all of these cases an important consideration is the thermal stability of the copolymer used. While many copolymers, including PS-*b*-PnAMA's, PS-*b*-P2VP, and PS-*b*-PEO are stable at temperatures up to 250°C, others possess sensitive functional groups or linkages which initiate crosslinking, chain cleavage, or functional group deprotection upon heating to such temperatures. Annealing such systems, while ensuring their stability, can be a challenge. One means of circumventing this is through the depression of T_g through the use of carbon dioxide plasticization.

One block copolymer that is particularly sensitive to elevated temperatures is that of PS and PMMA linked by a [4π + 4 π] photocleavable anthracene bridge. This copolymer was synthesized by Dr. James Goldbach as part of his Ph.D. thesis work under the tutelage of Profs. Jacques Penelle and Thomas Russell at UMass[29, 30]. The anthracene linkage was designed to separate upon UV irradiation at 280 nm, leading to PMMA domains dispersed in a polystyrene matrix. This was designed to be a possible route towards creating gradient films of increasing PMMA domain size. It was found, however, that the linkage separated at 120°C, leading to block separation before microphase

separation of the block copolymer could take place. To circumvent this issue, the copolymer was ordered at low temperatures ordering using CO_2 swelling as a means to depress T_g. 30 nm thick films were annealed at 80°C under 2000 psi CO_2. The film thickness was near to one block copolymer period in order to obtain perpendicularly oriented cylindrical domains. The films were spun on to untreated silicon wafers. AFM phase and height images are given in Figure 5.9.

Figure 5.9: AFM phase (left) and height (right) images of PS-AA-PMMA annealed at 80°C and 2000 psi CO_2[29, 30]

Typically, a neutral surface for both blocks is required in order to achieve a perpendicular cylindrical copolymer film. This is often achieved through the use of an anchored neutral brush layer, or through passivation of the silicon substrate surface using a dilute hydrofluoric acid etch. However, carbon dioxide swelling mediates the PS and PMMA surface energies leading to a large proportion of perpendicularly-aligned cylinders. One item of note is observed in the phase image. The PMMA minority component appears darker than the PS matrix, which is indicative of a lower modulus material. However, PMMA is harder than PS at room temperature, and as such should appear lighter in color. This effect may be explained by preferential swelling of the PMMA phase during CO_2 annealing. The density of PMMA relative to that of PS decreases, and the modulus, likewise, decreases. The voids in the polymer left by CO_2 upon depressurization became

locked in to the final structure when the system was dropped below T_g. This hypothesis was tested by raising the sample in Figure 5.9 above T_g. The resulting surface is given in Figure 5.10, below.

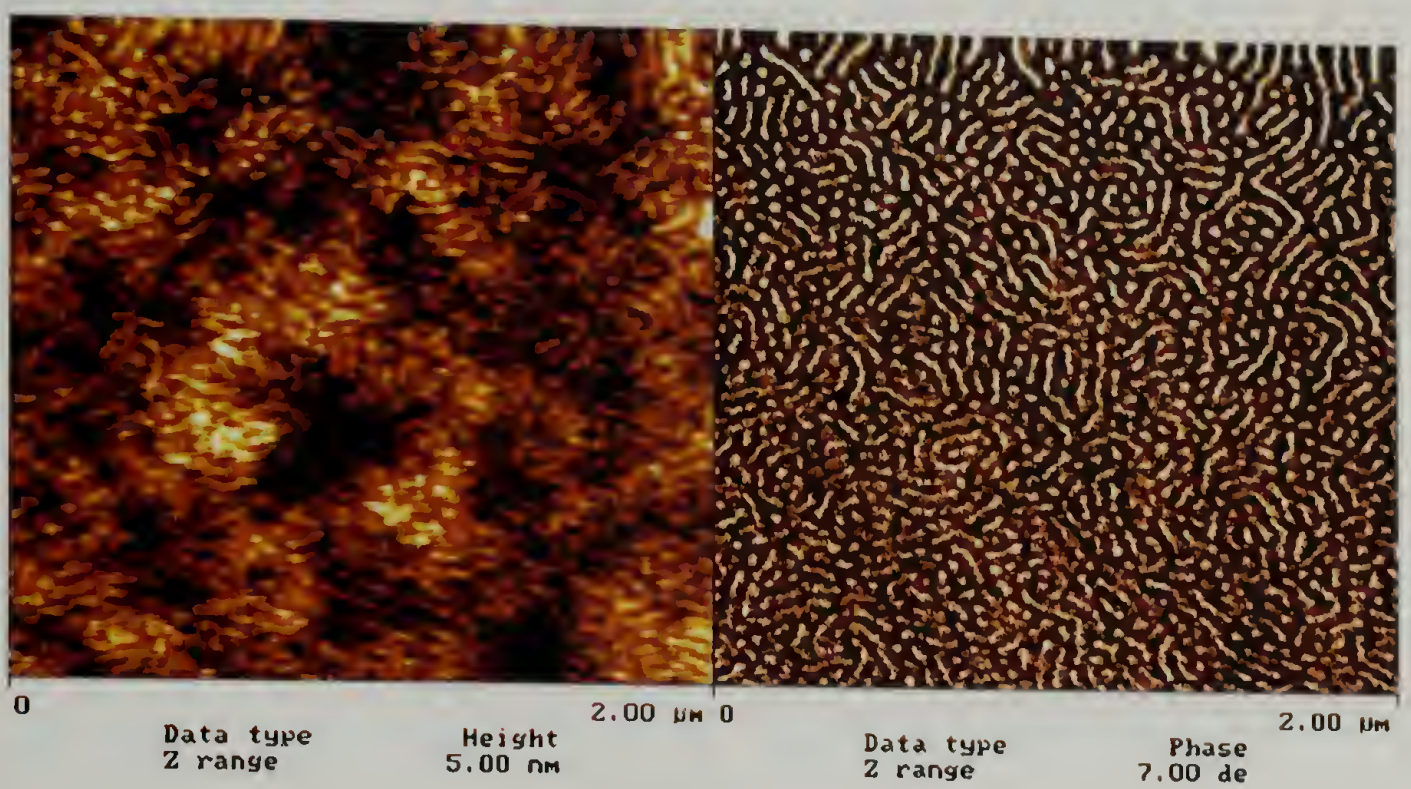

Figure 5.10: CO_2 annealed PS-AA-PMMA after 10 minutes at 160°C[30]

The phase image flipped to what is typically observed in thermally annealed PS-*b*-PMMA samples. PMMA appears lighter than the PS matrix in the phase image, indicating that the domains have relaxed, densified, and possess a larger modulus than the PS matrix. Carbon dioxide, then, is successful at imparting sufficient mobility to the PS-AA-PMMA copolymer to allow ordering below the cleavage temperature, while preserving the cylindrical morphology and promoting the orientation of cylinders normal to the substrate.

5.4 Conclusions

Carbon dioxide can have a profound influence on the observed morphology of block copolymer thin films. The T_g depression imparted through carbon dioxide dilation affords the opportunity to obtain structures otherwise unattainable, both through the disentanglement of high molecular weight copolymers and the low-temperature processing of lower molecular weight copolymers. As a differential diluent, CO_2 can induce OOT's, thus allowing additional control over the observed block copolymer morphology.

References

1. McHugh, M.A. and V.J. Krukonis, *Supercritical Fluid Extraction: Principles and Practice*. 1986, Boston: Butterworths.

2. Knutson, B.L., et al., *Kinetics of a Diels-Alder Reaction in Supercritical Propane*, in *Innovations in Supercritical Fluids*, K.W. Hutchenson and N.R. Foster, Editors. 1995, American Chemical Society: Washington. p. 166.

3. Wissenger, R.G. and M.E. Paulaitis, *Glass Transitions in Polymer/CO2 Mixtures at Elevated Pressures.* Journal of Polymer Science: Polymer Physics, 1991. **29**: p. 631.

4. Vogt, B.D., et al., *Phase behavior of nearly symmetric polystyrene-block-polyisoprene copolymers in the presence of CO2 and ethane.* Macromolecules, 1999. **32**(23): p. 7907-7912.

5. Vogt, B.D., et al., *Phase Behavior of Polystyrene-block-poly(n-alkyl methacrylate)s Dilated with Carbon Dioxide.* Macro., 2003. **36**(11): p. 4029.

6. RamachandraRao, V.S. and J.J. Watkins, *Phase Separation in Polystyrene-Poly(vinyl methyl ether) Blends Dilated with Compressed Carbon Dioxide.* Macromolecules, 2000. **33**(14): p. 5143.

7. Helfand, E. and Z.R. Wasserman, *Microdomain structure and the interface in block copolymers*, in *Developments in block copolymers*, I. Goodman, Editor. 1982, Applied Science: London. p. 99.

8. Helfand, E., *Block Copolymer Theory. III. Statistical Mechanics of the Microdomain Structure.* Macromolecules, 1975. **8**(4): p. 552.

9. Hanley, K.J. and T.P. Lodge, *Effect of Dilution on a Block Copolymer in the Complex Phase Window.* Journal of Polymer Science: Part B: Polymer Physics, 1998. **36**: p. 3101-3113.

10. Hanley, K.J., T.P. Lodge, and C.-I. Huang, *Phase Behavior of a Block Copolymer in Solvents of Varying Selectivity.* Macromolecules, 2000. **33**(16): p. 5918-5931.

11. Gupta, R.R., V.S. RamachandraRao, and J.J. Watkins, *Measurement of Probe Diffusion in CO2-Swollen Polystyrene using in situ Fluorescence Nonradiative Energy Transfer.* Macromolecules, 2000. **submitted**.

12. Gupta, R.R., et al., *Self-diffusion of polystyrene in a CO2-swollen polystyrene matrix: A real time study using neutron reflectivity.* Macromolecules, 2002: p. submitted.

13. Wissenger, R.G. and M.E. Paulaitis, *Swelling and Sorption in Polymer-CO2 Mixtures at Elevated Pressures.* Journal of Polymer Science: Polymer Physics, 1987. **25**: p. 2497.

14. Wang, W.-C.V., E.J. Kramer, and W.H. Sachse, *Effects of High-Pressure CO2 on the Glass Transition Temperature and Mechanical Properties of Polystyrene.* Journal of Polymer Science: Part B: Polymer Physics, 1982. **20**: p. 1371-1384.

15. Thurn-Albrecht, T., et al., *Nanoscopic templates from oriented block copolymer films.* Advanced Materials, 2000. **12**(11): p. 787-791.

16. Mansky, P., et al., *Phase Coherence and Microphase Separation Transitions in Diblock Copolymer Thin Films.* Macromolecules, 1999. **32**(15): p. 4832.

17. Anastasiadis, S.H., et al., *Neutron Reflectivity Studies of the Surface-Induced Ordering of Diblock Copolymer Films.* Physical Review Letters, 1989. **62**(16): p. 1852.

18. Menelle, A., et al., *Ordering of thin diblock copolymer films.* Physical Review Letters, 1992. **68**(1): p. 67.

19. Urbas, A.M., et al., *Tunable Block Copolymer/Homopolymer Photonic Crystals.* Advanced Materials, 2000. **12**(11): p. 812.

20. Maldovan, M. and E.L. Thomas, *Diamond-Structured Photonic Crystals.* Nat. Mat., 2004. **3**(9): p. 593.

21. RamachandraRao, V.S., et al., *Enhancement of Diblock Copolymer Ordering Kinetics by Supercritical Carbon Dioxide Annealing.* Macromolecules, 2001. **34**(23): p. 7923.

22. Pai, R.A., et al., *Mesoporous Silicates Prepared Using Preorganized Templates in Supercritical Fluids.* Science, 2004. **303**(5657): p. 507.

23. Huang, E., et al., *Nanodomain control in copolymer thin films.* Nature, 1998. **395**: p. 757.

24. Mansky, P., P.M. Chaikin, and E.L. Thomas, *Monolayer Films of Diblock Copolymer Microdomains For nanolithographic Applications.* J. Mat. Sci., 1995. **30**: p. 1987.

25. Mansky, P., et al., *Large-Area Domain Alignment in Block Copolymer Thin Fields Using Electric Fields.* Macromolecules, 1998. **31**: p. 4399.

26. Thurn-Albrecht, T., et al., *Pathways toward Electric Field Induced Alignment of Block Copolymer.* Macromolecules, 2002.

27. Kim, H.-C. and T.P. Russell, *Ordering in Thin Films of Asymmetric Diblock Copolymers.* Journal of Polymer Science:Part B:Polymer Physics, 2001. **39**: p. 663.

28. Kim, S.H., M.J. Misner, and T.P. Russell, *Solvent-Induced Ordering in Thin Film Diblock Copolymer/Homopolymer Mixtures.* Advanced Materials, 2004. **16**(23): p. 2119.

29. Goldbach, J.T., T.P. Russell, and J. Penelle, *Synthesis and Thin Film Characterization of Poly(styrene-block-methyl methacrylate) Containing an Anthracene Dimer Photocleavable Junction Point.* Macro., 2002. **35**(11): p. 4271.

30. Goldbach, J.T., et al., *Nano- to Macro-Sized Heterogeneities Using Cleavable Diblock Copolymers.* Macro., 2004. **37**(25): p. 9639.

CHAPTER 6

CONCLUSIONS AND RECOMMENDED FUTURE WORK

6.1 Conclusions

In this thesis I have addressed the importance of monomer free volume in determination of the phase behavior and morphology of block copolymers. This concept was best illustrated in the study of the origins of the closed-loop phase behavior of polystyrene-*block*-poly(n-pentyl methacrylate) block copolymers. In order to understand the origins of the closed-loop the use of pressure was employed, both as hydrostatic pressure and through carbon dioxide dilation. The lower disorder-to-order transition (LDOT), the lower bound of the closed-loop, was known to be driven by volumetic disparity between blocks. The upper order-to-disorder transition (UODT), however, had never been observed. This work found that its origins were due to combinatorial entropy, which dominates the phase behavior at high temperatures. However, side-chain expansion along the PnPMA backbone may be the source of the unusual thermal expansion behavior that allows this transition to be observed at experimentally accessible temperatures.

The use of carbon dioxide swelling was another means of investigating the volumetric origins of the closed-loop. CO_2 was a differential diluent, being slightly preferential for the PnPMA block. This served to exacerbate volumetric disparity between the blocks. Therefore, with an increase in CO_2 activity the size of closed-loop increased appreciably. In addition to its impact on the LDOT and UODT temperatures, carbon dioxide dilation can have a profound impact on the resulting morphology of the ordered state. Copolymers possessing a volume fraction near the morphological boundary may

undergo an order-to-order transition (OOT) as a result of differential dilation. Additionally, the glass transition depression imparted by carbon dioxide swelling allows the ordering of high molecular weight copolymers, which are otherwise kinetically hindered, and the low temperature ordering of heat-sensitive copolymers. CO_2 provided both a means of studying block copolymer thermodynamics and of creating nanostructures otherwise unattainable.

6.2 Recommended Future Work

The series of polystyrene-*block*-poly(n-alkyl methacrylate)s have proven to be an interesting model system for the study of block copolymer phase transitions. By simply altering the alkyl sidechain length the thermodynamic compatibility of the system changes dramatically. Alkyl methacrylates of intermediate sidechain length ($2 \leq n \leq 5$) show the greatest compatibility with PS. As such, volumetric consideration become important an LDOT- and UODT-type transitions are observed. Shorter ($n = 1$) and longer ($n \geq 6$) sidechains show only enthalpically-driven order-to-disorder transitions. These trends are well understood, with the exception of the PS-*b*-PnHMA ($n = 6$) copolymers. Thorough studies of the pressure coefficients of the PS-*b*-PnAMA series have been undertaken, and the trends in this particular block copolymer remain a mystery. It possesses a negative volume change on mixing, and as such its pressure coefficient is negative. However, its magnitude is -60°C/kbar, which is larger than any other ODT-type system studied to date. Additionally, unlike PS-*b*-PnOMA, the pressure coefficient does not decrease in magnitude with the application of large hydrostatic pressure. Recent investigations have revealed an unusual temperature dependence of Q* on passing through the ODT. SANS

measurements show the copolymer chains stretch on passing into the disordered state, despite a negative volume change on mixing. This system remains poorly understood, and may provide the key to a fully unified understanding of block copolymer phase behavior.

As was discussed in Chapter 5, the conformation of the n-alkyl methacrylate sidechain has an important role in the subtle volumetric changes observed in PS-*b*-PnPMA copolymers. Better methods must be developed in order to observe these changes more directly. If the sidechain can be deuterium-labeled, SANS would provide this information. Also, high temperature NMR measurements would be useful to monitor the changes in the sidechain carbon atoms' chemical environments, which could be correlated to conformational changes. If these techniques can developed further the unusual volumetric behavior of PS-*b*-PnPMA and PS-*b*-PnHMA copolymers can be better understood.

High pressure SANS measurements on PS-*b*-PnPMA copolymers in the disordered state may be explained by a better understanding of the PnPMA side chain conformation. It was noted in Chapter 3 that the temperature of maximum SANS intensity at a given pressure shifts with increasing pressure. This shift to higher temperatures is shown in Figures 6.1 and 6.2, below.

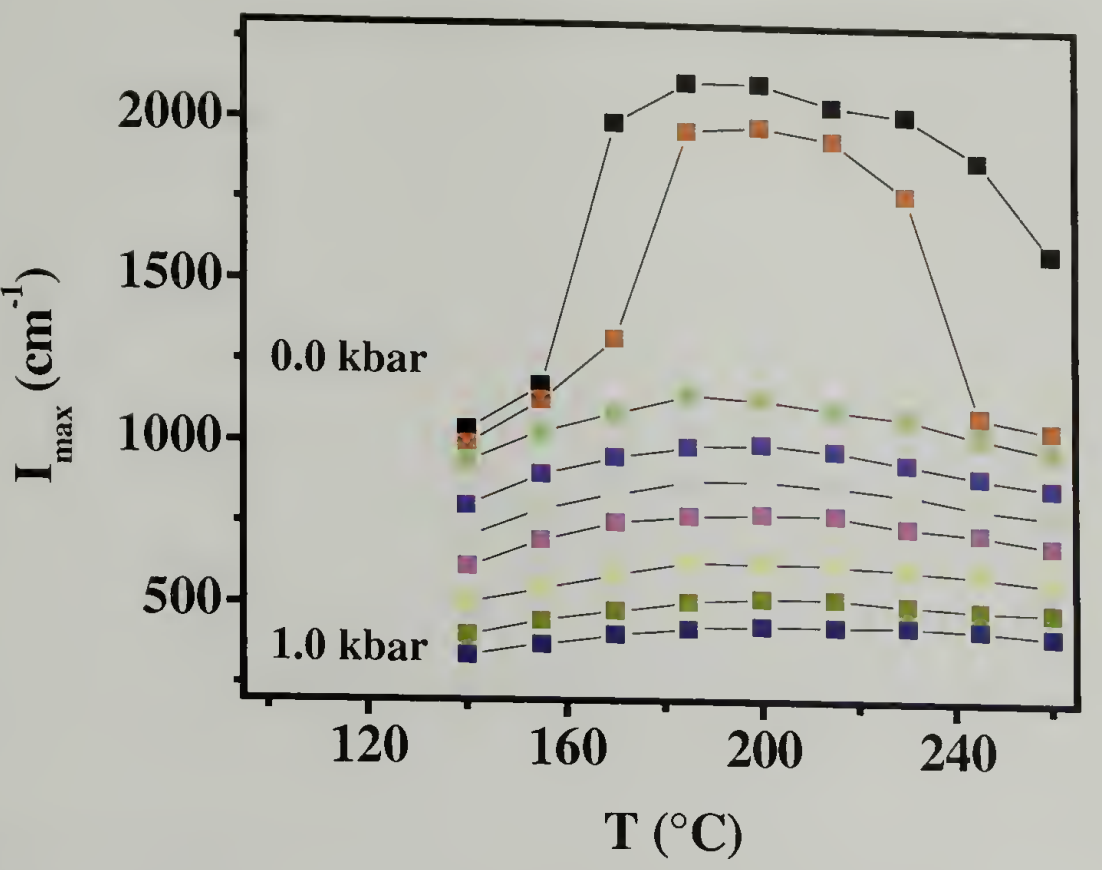

Figure 6.1 SANS maximum intensity as a function of pressure for 50/50 50K dPS-*b*-PnPMA

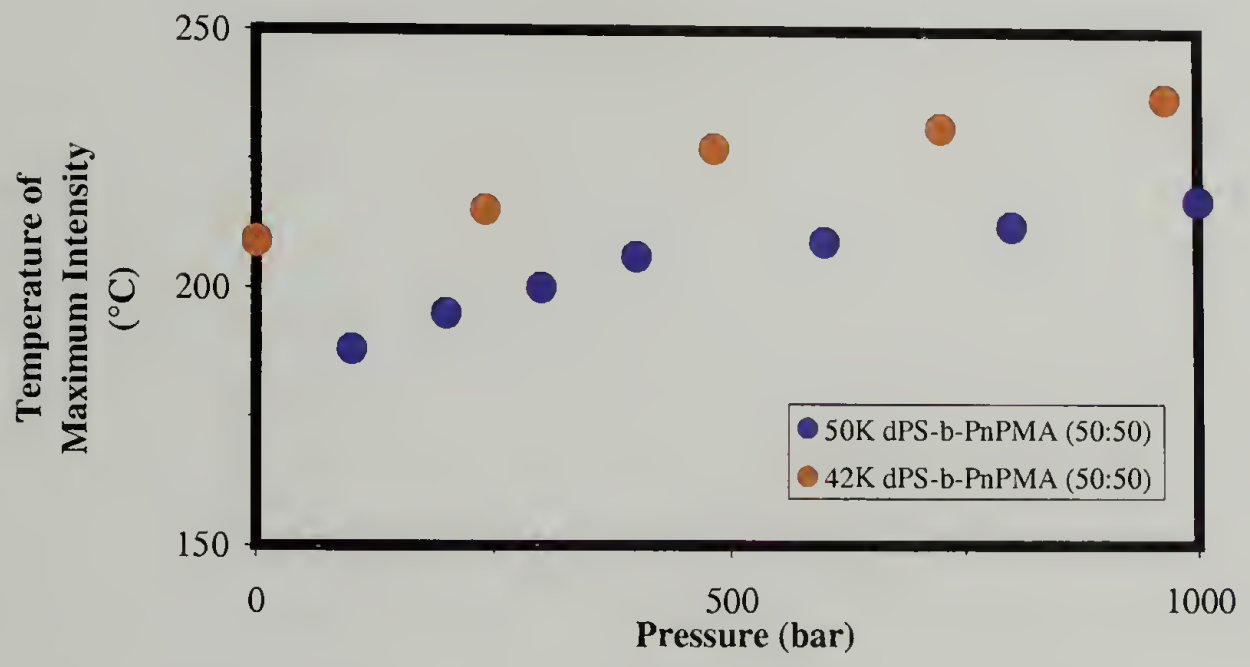

Figure 6.2 Temperature of maximum SANS intensity as a function of pressure for disordered symmetric dPS-*b*-PnPMA copolymers

One explanation for the phenomena is that once free volume is squeezed out of the copolymer, driving it fully into the disordered state, the side chain conformation becomes effected by increased pressure. This can force out any effects of the side chain on the thermal expansion coefficient, making the system thermodynamics more like a typical LDOT-type system. This observed by an increase in the center of the residual closed-loop. Direct observation of the side chain via SANS would allow examination of this effect.

APPENDIX

FORTRAN CODE FOR REFLECTIVITY CALCULATIONS

```
C ***************************************************************
C     PROGRAM: dps-pnbma lamellar                                *
C     Purpose: for fitting reflectivity data from a generic      *
C              lamellar multilayer. Can specify layer asymmetry, *
C              identity of block at substrate, and symmetric or  *
C              antisymmetric boundary conditions.                *
C                                                                *
C     REPROGRAMMED BY KRIS LAVERY                                *
C                                                                *
C                                                                *
C     Inspired by MLAYER3 (Spiros Anastasiadis and Alain Menelle)*
C     A modified version of Peter Lambooy's program F.  The      *
C     modifications are a change in the parameterization and the *
C     addition of a routine to calculate an appropriate b/V      *
C     profile.                                                   *
C                                                                *
C     Meaning of:                                                *
C      FA  = 0 parameter fixed                                   *
C      FA  = 1 parameter to be varied                            *
C      There are NO SLAVE PARAMETERS. FA=1,0 only.               *
C                                                                *
C      Parameterization of profile:  (all distances in angstroms)*
C                                                                *
C     a(1) = multiplier                                          *
C     a(2) = dlambda/lambda                                      *
C     a(3) = dtheta/theta                                        *
C     a(4) = lamellar period, angstroms                          *
C     a(5) = number of lamellae                                  *
C     *****  NOTE: A is ALWAYS defined as the component  **********
C     *****  at the air surface.(ie. dps is A in this program)  ****
C     a(6) = volume fraction of A component                      *
C     a(7) = b/V for A component                                 *
C     a(8) = b/V for B component                                 *
C     a(9) = A/B interfacial width                               *
C     a(10) = roughness at top (air) surface                     *
C     a(11) = roughness at polymer/SiOx interface                *
C     a(12) = SiOx thickness                                     *
C     a(13) = SiOx/Si surface roughness                          *
C     a(14) = decay length from Si                               *
C     a(15) = decay length from Air                              *
C     a(16) = the excess fraction of dps in the air substrate    *
C     a(17) = the excess fraction of dps in the siox substrate   *
C ***************************************************************
      PROGRAM dpsnbma
      IMPLICIT NONE
      INTEGER DMAX,PMAX,MMAX
      PARAMETER (DMAX = 1000)
      PARAMETER (PMAX = 500)
      PARAMETER (MMAX = 40)
      REAL CHIMIN
      PARAMETER (CHIMIN = 0.1)
      REAL X(DMAX),Y(DMAX),SIG(DMAX),R(DMAX)
```

```
      REAL A(PMAX),AMIN(PMAX),AMAX(PMAX),ASTEP(PMAX),A_NEW,A_UP,ADOWN
      REAL K0,NOL,CHISQ,OLDCHISQ,STORE,BGR
      INTEGER I,J,K,N,NDATA,LISTA(MMAX),MFIT,FA(PMAX),MAXITT,ITT
      REAL XMIN,XMAX, DTHICK, zlayr(330)
      REAL POS(20000),BV(20000),POSMAX
      LOGICAL MODIFIED, DONE
      CHARACTER*45 ADESC(pmax)
      COMPLEX BOVERV(330)


C NAME OF THE THEORETICAL FUNCTION: TESTF

      EXTERNAL REFL
C
C Read model parameters
C
      open(unit=7,file='paramin.txt')
      open(unit=10,file='jcount.txt')
      read(7,*) xmin, xmax, maxitt
      read(7,*) k0, nol, BGR
C read parameters: starting value, fit flag, min, max, step
      write (*,*) 'xmin'
      do i=1,19,1
      read(7,*) A(i), FA(i),AMIN(i),AMAX(i),ASTEP(i), ADESC(i)
      enddo
      close(unit=7)
      nol=2*a(5)+4


C Read experimental data
C Only data with Xmin < X < Xmax is selected

      open(unit=4,file='DIBLOCK_03.txt')
      I=1
 100  READ (4,*,END=110,ERR=110) X(I),Y(I),SIG(I)
      IF ((X(I).ge.Xmin).and.(X(I).le.Xmax)) I=I+1
      GOTO 100
 110  NDATA=I-1
      WRITE (*,*) 'NR OF DATA POINTS READ IN :',NDATA
      close(unit=4)

C prepare parameters for the fitting:
C make list of fit parameters
      MFIT=0
      DO I=1, 19
        IF (FA(I).EQ.1) THEN
          MFIT=MFIT+1
          LISTA(MFIT) = I
        ENDIF
      ENDDO
      WRITE (*,*) 'NR OF PARAMETERS TO BE FIT:',MFIT

C Calculate initial reflectivity
C
      CALL REFL(X,A,R,NDATA,K0,NOL,Y,SIG,OLDCHISQ,BGR,DONE)
      open(unit=2,file='paramout.txt')
      WRITE (2,*) 'Initial ChiSquared: ', OLDCHISQ
C
C Vary parameters
C
```

```
      IF (MFIT.EQ.0) GOTO 300
      DO ITT=1, MAXITT
        MODIFIED = .FALSE.
        DO J=1, MFIT
          I = LISTA(J)
          A_NEW = A(I)
          A_UP  = A(I)+ASTEP(I)
          ADOWN = A(I)-ASTEP(I)
C try A+ASTEP
          IF (A_UP.LE.AMAX(I)) THEN
            A(I) = A_UP
C         make slaves equal to their masters
            DO K=1, 3*INT(nol)+3
              IF (FA(K).GT.1) A(K)=A(FA(K))
            ENDDO
            CALL REFL(X,A,R,NDATA,K0,NOL,Y,SIG,CHISQ,BGR,DONE)
            IF (CHISQ.LT.OLDCHISQ) THEN
              MODIFIED = .TRUE.
              OLDCHISQ = CHISQ
              A_NEW = A_UP
            ENDIF
          ENDIF
C try A-ASTEP
          IF (ADOWN.GE.AMIN(I)) THEN
            A(I)=ADOWN
C         make slaves equal to their masters
            DO K=1, 3*INT(nol)+3
              IF (FA(K).GT.1) A(K)=A(FA(K))
            ENDDO
            CALL REFL(X,A,R,NDATA,K0,NOL,Y,SIG,CHISQ,BGR,DONE)
            IF (CHISQ.LT.OLDCHISQ) THEN
              MODIFIED = .TRUE.
              OLDCHISQ = CHISQ
              A_NEW = ADOWN
            ENDIF
          ENDIF
          A(I) = A_NEW
        ENDDO
C Save intermediate results
c       write (8,*) 'Itteration', ITT, 'Chi-Squared =', CHISQ
c         write (8,*) A(1), A(2), A(3)
c       DO I=1, INT(NOL)
c         write (8,*) A(3*I+1), A(3*I+2), A(3*I+3)
c       ENDDO

        IF (.NOT.MODIFIED) GOTO 300
      ENDDO
C
C Write final result
C
300   WRITE (2,*) ' '
      write (*,*) 'ndata= ',ndata
      open(unit=3,file='reflectivityout.txt')
      DO I=1, NDATA
        WRITE (3,*) X(I), R(I), R(I)
      ENDDO
      close(unit=3)
      write (2,*) 'Itteration', ITT, 'Chi-Squared =', CHISQ
      DO I=1, 19, 1
         write (2,50) fa(i), a(I), '=', adesc(i)
```

```
      ENDDO

50    format (i5, f12.6, A4, A45)

      write (2,*) 'Final ChiSquared: ', CHISQ
      close(unit=2)
C
C Write b/V profile
C
      done = .true.
      call REFL(X,A,R,NDATA,K0,NOL,Y,SIG,CHISQ,BGR,DONE)

      END

C ***************************************************************
C     SUBROUTINE REFL
C
C
C     THIS PROGRAM CALCULATES THE REFLECTIVITIES FOR
C
C     A SEQUENCE OF LAYERS. THE INTERFACES MAY BE ROUGH.
C
C Written by P. Lambooy to fit Reflectivity data from NIST and Argonne
C to an N layer model, after the example of MLAYER3 by A. Menelle
C
C Meaning of the parameters:
C
C ***************************************************************

      SUBROUTINE  REFL(X,A,R,NDATA,K0,NOL,Y,SIG,CHISQ,BGR,DONE)
      IMPLICIT NONE
      INTEGER DMAX,PMAX
      PARAMETER (DMAX = 300)
      PARAMETER (PMAX = 500)
      INTEGER I,NDATA
      REAL X(DMAX),A(PMAX),R(DMAX),Y(DMAX),SIG(DMAX),NOL,CHISQ
      REAL C,K0,DLALA,DTHETA,TKS(330),RGS(330),BGR
      COMPLEX BOVERV(330)
      LOGICAL DONE

      C      = A(1)
      DLALA  = A(2)
      DTHETA = A(3)

      call lamel(a,boverv,tks,rgs,nol,done)

      call layers(X,R,NDATA,k0,C,dlala,dtheta,nol,BoverV,tks,rgs)
      CHISQ=0.0
      DO I=1, NDATA
        R(I)  = R(I)  + BGR
        CHISQ = CHISQ + ((Y(I)-R(I))/SIG(I))**2
      ENDDO
      RETURN
      END

C***************************************************************
STY00010
C
STY00020
```

```
C    SUBROUTINE LAMEL  - Paul Mansky, Oct. 1995, IBM Almaden
STY00030
C
STY00040
C    This routine generates composition and b/V profiles for lamellar
diSTY00050
C    copolymer films containing a few percent deuterated material at
theSTY00060
C    PMMA chain ends.
STY00070
C
STY00080
C*****************************************************************
STY00090

STY00100
      SUBROUTINE LAMEL(a,boverv,tks,rgs,nol,done)
STY00110
      IMPLICIT NONE
STY00130
      INTEGER  PMAX
      PARAMETER (PMAX=500)
      REAL a(pmax), tks(330),rgs(330)
STY00140
      COMPLEX BOVERV(330)
      REAL BVPSH, BVPSD, BVPBMAH, BVPBMAD, BVAIR, BVSIO,nol,bvsi
      REAL phia, phis,totalt,dthick,pi,average
      REAL jcount(330),jcount2(300),jcount1(300)
      REAL phistot(100), phimtot(100),phimh(100),phisd(100),zlayr(100)
      REAL JM1,fromsi(330), fromair(330),air(330)
      INTEGER NINTFS, i, j, k, l, m, n
STY00170
      parameter (bvpsd=6.2)
STY00230
      parameter (bvpbmah=0.5)
STY00240
      parameter (bvpbmad=4.8)
STY00250
      parameter (bvsio=3.07)
STY00260
      parameter (pi=3.1415927)
      parameter (bvsi=2.1)
STY00270
      logical done

      average=a(7)*a(6)+a(8)*(1-a(6))
c     boverv(1)=bvpsd*a(18)+bvpbmah*(1-a(18))
c      tks(1)=a(4)/4
c      rgs(1)=a(10)

c      tks(2)= a(4)/2
c      rgs(2)=a(9)
        do i=1,nol-2,1
         jcount1(i)=(a(16))*exp(real(-(i-2)/a(14)))*cos(pi*(i+1))
c        jcount1(i)=jcount1(i)*a(7)+(1-jcount1(i))*a(8)
c        write(*,*) 'ok'
         jcount2(i)=(a(17))*exp(real(-(nol-2-i)/a(15)))
     1  *cos(pi*(nol-i))
          enddo
c     jcount1(1) = -a(6)
```

```
c       jcount1(nol-2)= a(16)*exp(real(-(nol-3)/a(14)))
c       jcount2(1) = a(17)*exp(real(-(nol-3)/a(15)))
c       jcount2(nol-2)=-a(6)
c      jcount2(i)=jcount2(i)*a(7)+(1-jcount2(i))*a(8)
c        do k = 1,nol-2,1
c      write(*,*) jcount1(k), jcount2(k)
c       enddo
       do j = 1,nol-2,1
       if (abs(jcount1(j)).ge.abs(jcount2(j))) then
           boverv(j)= (jcount1(j)+a(6))*a(7)+(1-jcount1(j)-a(6))*a(8)
        else
           boverv(j)= (jcount2(j)+a(6))*a(7)+(1-jcount2(j)-a(6))*a(8)
       endif
        if ((j*0.5).eq.int(j*0.5)) then

          tks(j)= a(6)*a(4)

        else
           tks(j)=(1-a(6))*a(4)
          endif

       rgs(j)=a(9)
       write(10,*) j, jcount1(j), jcount2(j), real(boverv(j))
         enddo
c        rgs(2)=a(9)/2
c        rgs(nol-2)=a(9)/2
         tks(1)= (1-a(6))*a(4)/2
         tks(nol-2) = (1-a(6))*a(4)/2
      rgs(1)= a(10)
      tks(nol-1)=a(12)
      boverv(nol-1) = bvsio
      rgs(nol-1) = a(11)
      boverv(nol)=bvsi
STY01070
      tks(nol)=10000.0
STY01080
      rgs(nol)=a(13)

       if (done) call profile(nol,a,boverv,tks,rgs,phistot,phimtot,
     1   phimh,phisd,zlayr)

      do i=1,nol,1
         boverv(i)=boverv(i)*1e-06
      enddo
STY01120

      return
STY01130
      end


C ***************************************************************
C * SUBROUTINE LAYERS
C *
C * Convolutes the theoretical reflectivity with the
C * instrumental resolution G  (k), where G is a normalised Gaussian
C * with HWHM = dk.          dk
C *
C * Integration is from -5 dk to 5 dk in steps of di:
C *
```

```
C *
C *     di = min( dk/2 , ____pi____ )
C *                      4 dmax
C *
C *
C * with dmax the largest thickness in the model.
C *
C ***************************************************************

      SUBROUTINE LAYERS(Kexp,R,NDATA,k0,C,dlala,dtheta,nol,BoverV,t,rg)

      IMPLICIT NONE

      INTEGER I,J,NDATA
      INTEGER DM
      PARAMETER (DM=300)
      REAL C,dlala,dtheta,nol,k0,dmax
      REAL t(330),rg(330),GAUSS,FRESNEL
      REAL Kexp(NDATA),R(NDATA),di(DM),dk(DM),dk1,dk2
      REAL Kgrid(6000),Rgrid(6000),pi
      COMPLEX BoverV(330)
      PARAMETER (pi=3.1415927)

C
C Calculate the resolution dk and the integration step di
C
      dmax = t(1)
      DO I=2, INT(nol)
        IF (t(I).gt.dmax) dmax = t(I)
      ENDDO
      IF (dmax.eq.0.0) dmax = 1.0
      DO I=1, NDATA
C       dk(I) = Kexp(I)*dlala + k0*dtheta
        dk1   = Kexp(I)*dlala
        dk2   = k0*dtheta
        dk(I) = SQRT(dk1*dk1 + dk2*dk2)
        di(I) = min(dk(I)/2,0.25*pi/dmax)
      ENDDO
C
C Create a grid with Kgrid and Rgrid values
C
      Kgrid(1) = Kexp(1) - 5*dk(1)
      Rgrid(1) = FRESNEL(Kgrid(1),nol,BoverV,t,rg)
      J = 1
      DO I=1, NDATA
        DO WHILE (Kgrid(J).LT.(Kexp(I)/2 + Kexp(I+1)/2))
          J = J + 1
          Kgrid(J) = Kgrid(J-1) + di(I)
          Rgrid(J) = FRESNEL(Kgrid(J),nol,BoverV,t,rg)
        ENDDO
      ENDDO
      DO WHILE (Kgrid(J).LT.(Kexp(NDATA) + 5*dk(NDATA)))
        J = J+1
        Kgrid(J) = Kgrid(J-1) + di(NDATA)
        Rgrid(J) = FRESNEL(Kgrid(J),nol,BoverV,t,rg)
      ENDDO
C
C Perform the convolution
C
      DO I=1, NDATA
```

```
          R(I) = 0.0
          J=1
          DO WHILE (Kgrid(J).LT.(Kexp(I) - 5*dk(I)))
            J = J+1
          ENDDO
          DO WHILE (Kgrid(J).LT.(Kexp(I) + 5*dk(I)))
            R(I) = R(I) + Rgrid(J) *
     1             GAUSS(dk(I),Kexp(I)-Kgrid(J)) * (Kgrid(J)-Kgrid(J-1))
            J=J+1
          ENDDO
          R(I) = C * R(I)
        ENDDO
        RETURN
        END

C ***************************************************************
C     REAL FUNCTION GAUSS: Normalised Gaussian
C ***************************************************************
        REAL FUNCTION GAUSS(dk,k)

        IMPLICIT NONE
        REAL dk,k,pi
        PARAMETER (pi=3.1415927)
          GAUSS = EXP(-log(2.0)*(k/dk)**2) * SQRT(log(2.0)/pi) / dk
        RETURN
        END

C ***************************************************************
C *
C *  FUNCTION FRESN
C *
C *  This routine calculates optical reflection of neutrons of a
C *  thin-film/substrate system.
C *  Input parameters are wavelength, angle of incidence, film
C *  thickness and complex refractive indices of the three media.
C *
C *  Multiple reflection and interference effects are taken into
C *  account using Fresnel coefficients for a multiple layer system.
C *
C *  Formulas are adapted from
C *  T. Russell, Materials Science Reports 5 (1990) 171-271
C *  S. Anastasiadis e.a. Phys.Rev.Lett. 62, 1855 (1989)
C *
C *  Definitions:
C *
C *  optical density:       2
C *                    lambda       b
C *          N = 1 - --------- * ---
C *                     2 pi        V
C *
C *  wave vector transfer:
C *
C *       K = K  SIN(theta)
C *            O
C *
C *  NB: in data file and SRS program : K = 2 K SIN(theta)
C *                                          O
C *
C *
C *  critical wave vector K is approximated by:
```

```
C *                              C
C *                                                  b
C *          K * K   = 2 (1 - N) = 4 pi ---
C *           C   C                                  V
C *
C *
C *
C *
C * Version 15 jan 1992 Peter Lambooy
C *
C * Parameterisation:
C *
C *
C *                  SIGMA(nol)       SIGMA(nol-1)  ......      SIGMA(1)
C *
C *          SUBSTR    |     d (nol-1)   |     d (nol-2)  ......  |   AIR
C *                    |                 |                        |
C *           b        |     b           |     b                  |
C *          ---(nol)  |    ---(nol-1)   |    ---(nol-2)  ......  |
C *           V        |     V           |     V                  |
C *
C                                                  Z ---->
C *
C * SIGMA (S) is HWHM of a Gaussian smearing
C *
C * G (Z) = exp(-Z*Z/(2*S*S))/SQRT(2*pi)/S
C *  S
C *
C ***************************************************************

      REAL FUNCTION FRESNEL(k,nol,BoverV,d,SIGMA)

      IMPLICIT NONE

      REAL pi
      PARAMETER (pi =3.1415927)
      COMPLEX i
      PARAMETER (i = (0,1))

      INTEGER j
      REAL    k,nol,d(330),SIGMA(330),gexp
      COMPLEX kvec(0:330),Ampl,r(330),gcexp
      COMPLEX BoverV(330)
      kvec(0) = k

C SNELLIUS' LAW
C FRESNEL REFLECTION COEFFICIENTS
C N.B. SIGMA(j) DENOTES THE GAUSSIAN HALFWIDTH BETWEEN
C THE jth and (j-1)th LAYERS


      DO j = 1, INT(nol)
        kvec(j) = SQRT( kvec(0)*kvec(0) - 4.0*pi*BoverV(j))
        gexp = EXP(-2.0*kvec(j-1)*kvec(j)*SIGMA(j)*SIGMA(j))
        r(j) = gexp * (kvec(j-1) - kvec(j)) / (kvec(j-1) + kvec(j))
      ENDDO

      Ampl = r(nol)
      DO j = INT(nol)-1, 1, -1
        gcexp = CEXP(2.0*i*kvec(j)*d(j))
```

```
        Ampl = ( r(j) + Ampl*gcexp ) / ( 1 + r(j)*Ampl*gcexp )
      ENDDO

      FRESNEL = CABS(Ampl)**2

      RETURN
      END

C ***************************************************************
C * SUBROUTINE PROFILE
C *
C * Purpose: to calculate b/V profile for a stack of slabs
C *
C * Author: P. Lambooy
C ***************************************************************
      SUBROUTINE PROFILE(nol,A,boverv,tks,rgs,phistot,phimtot,
     1   phimh,phisd,zlayr)

      IMPLICIT NONE

      INTEGER I,J,K
      REAL A(500),H(330),Z(330),POS(20000),BV(20000)
      REAL phistot(500),phimtot(500),phimh(500),phisd(500),zlayr(500)
      REAL nol,erfc(10000),tks(330),rgs(330),POSMAX,AR,X,Y,rboverv(330)

      complex boverv(330)

      do i=1, int(nol), 1
         rboverv(i)=real(boverv(i))
      enddo

C Build a series of step functions from the slabs
      Z(1) = 0
      H(1) = rboverv(1)
      DO I=2, int(nol)
        Z(I) = Z(I-1) + tks(I-1)
        H(I) = rboverv(I) - rboverv(I-1)
      ENDDO

C Make the Profile
      POSMAX = int(Z(int(nol)))+200
      POS(1) = -100
      BV(1)  = 0.0
      POS(2) = -99
      BV(2)  = 0.0
      K = 2
      DO I=3, POSMAX
        X = I - 100
        Y = 0
        DO J = 1, int(nol), 1
C         write (*,*) rgs(j)
          AR = 0.7071*(X-Z(J))/RGS(J)
          IF (AR.LT.10.0) Y = Y + H(J)*(1-0.5*ERFC(AR))
          IF (AR.GE.10.0) Y = Y + H(J)
        ENDDO
C check for redundancy
        IF ((Y.EQ.BV(K)).AND.(BV(K).EQ.BV(K-1))) THEN
          POS(K) = X
        ELSE
          K = K + 1
```

```
          POS(K) = X
          BV(K)  = Y
        ENDIF
      ENDDO

      POSMAX = K

      open(unit=1,file='bovervout.txt')
      do i=1, POSMAX
         write (1,900) pos(i), bv(i)
      enddo
      close(unit=1)

      open(unit=10,file='what.txt')
      do i=1, nol-2
         write(10,910) zlayr(i), phistot(i), phimtot(i), phimh(i),
     1         phisd(i)
      enddo
      close(unit=10)

900   format(f8.1,f8.3)
910   format(f8.1,4(f8.3))

      RETURN
      END
```

BIBLIOGRAPHY

Allen, R.D., T.E. Long, and J.E. McGrath, Preparation of High-Purity, Anionic-Polymerization Grade Alkyl Methacrylate Monomer. Polym. Bul., 1986. 15: p. 127.

Almdal, K., J.H. Roseldale, and F.S. Bates, Order-Disorder Transition in Binary Mixtures of nearly Symmetric Diblock Copolymers. Macro., 1992. 23: p. 4336.

Anastasiadis, S.H., et al., Neutron Reflectivity Studies of the Surface-Induced Ordering of Diblock Copolymer Films. Physical Review Letters, 1989. 62(16): p. 1852.

Bates, F.S. and G.H. Fredrickson, Block Copolymer Thermodynamics: Theory and Experiment. Annual Review of Physical Chemistry, 1990. 41: p. 525.

Bates, F.S. and G.H. Fredrickson, Block Copolymers - Designer Soft Materials. Physics Today, 1999: p. 32.

Bates, F.S., et al., Fluctuations, Conformational Asymmetry and Block Copolymer Phase Behavior. Faraday Discuss., 1994. 98: p. 7.

Bates, F.S., J.H. Rosedale, and G.H. Fredrickson, Fluctuation effects in a symmetric diblock copolymer near the order-disorder transition. Macromolecules, 1990. 92(10): p. 6255.

Beecroft, L.L. and C.K. Ober, Nanocomposite Materials for Optical Applications. Chemistry of Materials, 1997. 9: p. 1302.

Beiner, M. and H. Huth, Nanophase separation and hindered glass transition in side-chain polymers. Nat. Mat., 2003. 2(9): p. 595.

Blackburn, J.M., Chemical Fluid Deposition: Reactive Deposition of Thin Metal Films from Supercritical Carbon Dioxide Solutions, in Chemical Engineering. 2001, University of Massachusetts: Amherst, MA.

Born, M. and E. Wolf, Principles of Optics. 1980, Oxford: Pergamon Press.

de Gennes, P.-G., Scaling Concepts in Polymer Physics. 1979, Ithaca: Cornell University Press.

DeSimone, J.M., Z. Guan, and C.S. Elsbernd, Synthesis of Fluoropolymers in Supercritical Carbon Dioxide. Science, 1992. 257: p. 945.

Dormidontova, E.E., Role of Competitive PEO-Water and Water-Water Hydrogen Bonding in Aqueous Solution PEO Behavior. Macro., 2002. 35(3): p. 987.

Dudowicz, J. and K.F. Freed, Effect of Monomer Struture and Compressibility on the Properties of Multicomponent Polymer Blends and Solutions: 1. Lattice Cluster Theory of Compressible Systems. Macromolecules, 1991. 24: p. 5076.

Dudowicz, J. and K.F. Freed, Explanation for the Unusual Phase Behavior of Polystyrene-b-poly(n-alkyl methacrylate) Diblock Copolymers: Specific Interactions. Macromolecules, 2000. 33: p. 5292.

Dudowicz, J. and K.F. Freed, Relation of Effective Interaction Parameters for Binary Blends and Diblock Copolymers: Lattice Cluster Theory Predictions and Comparisons with Experiment. Macromolecules, 1993. 26: p. 213-220.

Encyclopedia of Polymer Science and Engineering. 1987, New York: John Wiley & Sons.

Felcher, G.P., et al., Rev. Sci. Instr., 1987. 58: p. 609.

Flory, P.J., Principles of Polymer Chemistry. 1953, Ithaca, NY: Cornell University Press.

Flory, P.J., Thermodynamics of High Polymer Solutions. Journal of Chemical Physics, 1941. 9: p. 660.

Frielinghaus, H., et al., Composition Fluctuations and Coil Conformation in a Poly(ethylene-propylene)-Poly(ethylethylene) Diblock Copolymer as a Function of Temperature and Pressure. Macromolecules, 1996. 29: p. 3263.

Goldbach, J.T., et al., Nano- to Macro-Sized Heterogeneities Using Cleavable Diblock Copolymers. Macro., 2004. 37(25): p. 9639.

Goldbach, J.T., T.P. Russell, and J. Penelle, Synthesis and Thin Film Characterization of Poly(styrene-block-methyl methacrylate) Containing an Anthracene Dimer Photocleavable Junction Point. Macro., 2002. 35(11): p. 4271.

Gonzalez-Leon, J.A., et al., Low-Temperature Processing of 'Baroplastics' by Pressure-Induced Flow. Nature, 2003. 426: p. 424.

Gupta, R.R., et al., Self-diffusion of polystyrene in a CO2-swollen polystyrene matrix: A real time study using neutron reflectivity. Macromolecules, 2002: p. submitted.

Gupta, R.R., V.S. RamachandraRao, and J.J. Watkins, Measurement of Probe Diffusion in CO2-Swollen Polystyrene using in situ Fluorescence Nonradiative Energy Transfer. Macromolecules, 2000. submitted.

Hajduk, D.A., et al., High-Pressure Effects on the Disordered Phase of Block Copolymer Melts. Macromolecules, 1995. 28: p. 7148-7156.

Hajduk, D.A., et al., High-Pressure Effects on the Order-Disorder Transition in Block Copolymer Melts. Macromolecules, 1996. 29: p. 1473-1481.

Hamley, I.W., The Physics of Block Copolymers. 1998, Oxford: Oxford University Press.

Hammouda, B. and B.J. Bauer, Compressibility of Two Polymer Blend Mixtures. Macromolecules, 1995. 28: p. 4505-4508.

Hanley, K.J. and T.P. Lodge, Effect of Dilution on a Block Copolymer in the Complex Phase Window. Journal of Polymer Science: Part B: Polymer Physics, 1998. 36: p. 3101-3113.

Hanley, K.J., T.P. Lodge, and C.-I. Huang, Phase Behavior of a Block Copolymer in Solvents of Varying Selectivity. Macromolecules, 2000. 33(16): p. 5918-5931.

Hashimoto, T., et al., Domain Boundary Structure of Styrene-isoprene Block Copolymer Films Cast from Toluene Solutions. Macromolecules, 1974. 7: p. 364.

Hashimoto, T., et al., Ordered Structure in Blends of Block Copolymers .1. Miscibility Criterion for Lamellar Block Copolymers. Macro., 1993. 26: p. 2895.

Hashimoto, T., et al., Time-Resolved Small-Angle X-ray Scattering Studies on the Kinetics of the Order-Disorder Transition of Block Polymers 2. Concentration and Temperature Dependence. Macromolecules, 1986. 19: p. 754-762.

Hashimoto, T., M. Shibayama, and H. Kawai, Ordered Structure in Block Polymer Solutions. 4. Scaling Rules on Size of Fluctuations with Block Molecular Weight, Concentration, and Temperature in Segregation and Homogeneous Regimes. Macromolecules, 1983. 16: p. 1093-1101.

Helfand, E. and Z.R. Wasserman, Microdomain structure and the interface in block copolymers, in Developments in block copolymers, I. Goodman, Editor. 1982, Applied Science: London. p. 99.

Helfand, E., Block Copolymer Theory. III. Statistical Mechanics of the Microdomain Structure. Macromolecules, 1975. 8(4): p. 552.

Huang, E., et al., Nanodomain control in copolymer thin films. Nature, 1998. 395: p. 757.

Huggins, M.L., Solutions of Long Chain Compounds. Journal of Chemical Physics, 1941. 9: p. 440.

Janssen, S., et al., Pressure Dependence of the Flory-Huggins Interaction Parameter in Polymer Blends: A SANS Study and a Comparison to the Flory-Orwoll-Vrij Equation of State. Macro., 1993. 26: p. 5587.

Kamiya, Y., K. Mizoguchi, and Y. Naito, Sorption and partial molar volumes of inert gases in rubbery polymers. Journal of Membrane Sciene, 1994. 93: p. 45-52.

Karis, T.E., et al., Rheology of the Lower Critical Ordering Transition. Macromolecules, 1995. 28: p. 1129.

Kasten, H. and B. Stuhn, Density Discontinuity at the Microphase Separation Transition of a Symmetric Diblock Copolymer. Macro., 1995. 28: p. 4777.

Kim, H.-C. and T.P. Russell, Ordering in Thin Films of Asymmetric Diblock Copolymers. Journal of Polymer Science:Part B:Polymer Physics, 2001. 39: p. 663.

Kim, S.H., M.J. Misner, and T.P. Russell, Solvent-Induced Ordering in Thin Film Diblock Copolymer/Homopolymer Mixtures. Advanced Materials, 2004. 16(23): p. 2119.

Knutson, B.L., et al., Kinetics of a Diels-Alder Reaction in Supercritical Propane, in Innovations in Supercritical Fluids, K.W. Hutchenson and N.R. Foster, Editors. 1995, American Chemical Society: Washington. p. 166.

Leibler, L., Theory of Microphase Separation in Block Copolymers. Macromolecules, 1980. 13: p. 1602-1617.

Lemmon, E.W., M.O. McLinden, and D.G. Friend, Thermophysical Properties of Fluid Systems, in NIST Chemistry WebBook, NIST Standard Reference Database Number 69, W.G. Mallard and P.J. Linstrom, Editors. 1998, National Institute of Standards and Technology: Gaithersburg MD, 20899. p. http://webbook.nist.gov.

Lodge, T.P. and G.H. Fredrickson, Optical Anisotropy of Tethered Chains. Macromolecules, 1992. 25: p. 5643-5650.

Lodge, T.P., et al., Failure of the Dilution Approximation in Block Copolymer Solutions. Journal of Polymer Science: Part B: Polymer Physics, 1995. 33: p. 2289-2293.

Maldovan, M. and E.L. Thomas, Diamond-Structured Photonic Crystals. Nat. Mat., 2004. 3(9): p. 593.

Mansky, P., et al., Large-Area Domain Alignment in Block Copolymer Thin Fields Using Electric Fields. Macromolecules, 1998. 31: p. 4399.

Mansky, P., et al., Phase Coherence and Microphase Separation Transitions in Diblock Copolymer Thin Films. Macromolecules, 1999. 32(15): p. 4832.

Mansky, P., P.M. Chaikin, and E.L. Thomas, Monolayer Films of Diblock Copolymer Microdomains For nanolithographic Applications. J. Mat. Sci., 1995. 30: p. 1987.

McHugh, M.A. and V.J. Krukonis, in Encyclopedia of Polymer Science and Engineering, H.F. Mark, et al., Editors. 1989, John Wiley and Sons: New York.

McHugh, M.A. and V.J. Krukonis, Supercritical Fluid Extraction: Principles and Practice. 1986, Boston: Butterworths.

Menelle, A., et al., Ordering of thin diblock copolymer films. Physical Review Letters, 1992. 68(1): p. 67.

Pai, R.A., et al., Mesoporous Silicates Prepared Using Preorganized Templates in Supercritical Fluids. Science, 2004. 303(5657): p. 507.

Park, C., C. De Rosa, and E.L. Thomas, Large Area Orientation of Block Copolymer Microdomains in Thin Films via Directional Crystallization of a Solvent. Macromolecules, 2001. 34: p. 2602.

Pollard, M., et al., Some Thermodynamic Considerations of the Lower Disorder to Order Transition of Diblock Copolymers, in Scattering from Polymers, ACS Symposium Series, B.S. Hsiao, D.J. Lohse, and P. Cebe, Editors. 2000, American Chemical Society. p. 261.

Pollard, M., et al., The Effect of Hydrostatic Pressure on Lower Critical Ordering Transition in Diblock Copolymers. Macromolecules, 1998. 31(19): p. 6493-6498.

Quirk, R.P. and M. Morton, Research on Anionic Triblock Copolymers, in Thermoplastic Elastomers, G. Holden, et al., Editors. 1996: Munich.

RamachandraRao, V.S. and J.J. Watkins, Phase Separation in Polystyrene-Poly(vinyl methyl ether) Blends Dilated with Compressed Carbon Dioxide. Macromolecules, 2000. 33(14): p. 5143.

RamachandraRao, V.S., et al., Enhancement of Diblock Copolymer Ordering Kinetics by Supercritical Carbon Dioxide Annealing. Macromolecules, 2001. 34(23): p. 7923.

Rockford, L., et al., Polymers on Nanoperiodic, Heterogeneous Surfaces. Physical Review Letters, 1999. 82(12): p. 2602.

Russell, T.P., et al., A lower critical ordering transition in a diblock copolymer melt. Nature, 1994. 368: p. 729-731.

Russell, T.P., R.P. Hjelm, and P.A. Seeger, Temperature Dependence of the Interaction Parameter of Polystrene and Poly(methyl methacrylate). Macromolecules, 1990. 23: p. 890-893.

Russell, T.P., Small-Angle Scattering, in Handbook on Synchrotron Radiation, G.D. Brown and D.E. Moncton, Editors. 1991, Elsevier Science Publishers: Amsterdam.

Russell, T.P., X-ray and neutron reflectivity for the investigation of polymers. Materials Science Reports, 1990. 5: p. 171.

Ruzette, A.V. and A.M. Mayes, A Simple Free Energy Model for Weakly Interacting Polymer Blends. Macromolecules, 2001. 34: p. 1894.

Ruzette, A.V., et al., A Simple Model for Baroplastic Behavior in Block Copolymer Melts. J. Chem. Phys., 2001. 114: p. 8205.

Ruzette, A.V., et al., Pressure Effects on the Phase Behavior of Styrene/n-Alkyl Methacrylate Block Copolymers. Macro., 2003. 36(9): p. 3351-3356.

Ruzette, A.-V.G., et al., Phase Behavior of Diblock Copolymers between Styrene and n-Alkyl Methacrylates. Macromolecules, 1998. 31(24): p. 8509-8516.

Ryu, D.Y., et al., Closed-loop phase behaviour in block copolymers. Nat Mat, 2002. 1(2): p. 114.

Ryu, D.Y., et al., Effect of Hydrostatic Pressure on Closed-Loop Phase Behavior of Block Copolymers. Physical Review Letters, 2003. 90: p. 235501.

Sakamoto, N., et al., Effect of Addition of a Neutral Solvent on the Order-Order and Order-Disorder Transitions in a Polystyrene-block-polyisoprene-block-polystyrene Copolymer. Macromolecules, 1997. 30: p. 5321-5330.

Sanchez, I.C. and C.G. Panayiotou, Equation of State Thermodynamics of Polymer and Related Solutions, in Models for Thermodynamic and Phase Equilibria Calculations. 1994, Marcel Dekker, Inc.: New York. p. 187.

Sarbu, T., T. Styranec, and E.J. Beckman, Non-fluorous polymers with very high solubility in supercritical CO2 down to low pressures. Nature, 2000. 405: p. 165.

Schwahn, D., et al., Temperature and Pressure Dependence of the Order Parameter Fluctuations, Conformational Compressibility, and the Phase Diagram of the PEP-PDMS Diblock Copolymer. Physical Review Letters, 1996. 77(15): p. 3153.

Shah, P.S., et al., Steric Stabilization of Nanocrystals in Supercritical CO2 Using Fluorinated Ligands. Journal of the American Chemical Society, 2000. 122: p. 4245.

Sirard, S.M., et al., Structure of End-Grafted Polymer Brushes in Liquid and Supercritical Carbon Dioxide: A Neutron Reflectivity Study. Macro., 2003. 36(9): p. 3365.

Stein, R.S., et al., Recent Small Angle Neutron Scattering Studies of Polymers in the Solid State. Physica B, 1986. 137: p. 194-203.

Stuhn, B., The Relation Between the Microphase Separation Transition and the Glass Transition in Diblock Copolymers. Journal of Polymer Science:Part B:Polymer Physics, 1992. 30: p. 1013.

Thurn-Albrecht, T., et al., Nanoscopic templates from oriented block copolymer films. Advanced Materials, 2000. 12(11): p. 787-791.

Thurn-Albrecht, T., et al., Pathways toward Electric Field Induced Alignment of Block Copolymer. Macromolecules, 2002.

Urbas, A.M., et al., Tunable Block Copolymer/Homopolymer Photonic Crystals. Advanced Materials, 2000. 12(11): p. 812.

Utracki, L.A., Polymer Alloys and Blends. 1990.

van Krevelen, D.W. and P.J. Hoftyzer, Preperties of Polymers. Correlation with Chemical Structure. 1972, New York: Elsevie Publishing Co.

Vogt, B.D. and J.J. Watkins, Phase Behavior of Diblock Copolymers Dilated with Light Alkanes:The Influence of Solvent Compressibility on Upper and Lower Ordering Transitions. Macromolecules, 2002. 35(10): p. 4056.

Vogt, B.D., et al., Phase behavior of nearly symmetric polystyrene-block- polyisoprene copolymers in the presence of CO2 and ethane. Macromolecules, 1999. 32(23): p. 7907-7912.

Vogt, B.D., et al., Phase Behavior of Polystyrene-block-poly(n-alkyl methacrylate)s Dilated with Carbon Dioxide. Macro., 2003. 36(11): p. 4029.

Wang, W.-C.V., E.J. Kramer, and W.H. Sachse, Effects of High-Pressure CO2 on the Glass Transition Temperature and Mechanical Properties of Polystyrene. Journal of Polymer Science: Part B: Polymer Physics, 1982. 20: p. 1371-1384.

Watkins, J.J. and T.J. McCarthy, Polymer/metal nanocomposite synthesis in supercritical co2. Chemistry of Materials, 1991. 7(11).

Watkins, J.J., et al., Phase Separation in Multi-Component Polymer Systems Induced by Compressible Solvents. Macromolecules, 1999. 32: p. 7737.

Winey, K.I., et al., Compositional Dependence of the Order-Disorder Transition in Diblock Copolymers. Macromolecules, 1994. 27: p. 2392-2397.

Wissenger, R.G. and M.E. Paulaitis, Glass Transitions in Polymer/CO2 Mixtures at Elevated Pressures. Journal of Polymer Science: Polymer Physics, 1991. 29: p. 631.

Wissenger, R.G. and M.E. Paulaitis, Swelling and Sorption in Polymer-CO2 Mixtures at Elevated Pressures. Journal of Polymer Science: Polymer Physics, 1987. 25: p. 2497.